



TECHNISCHE
UNIVERSITÄT
WIEN

Dissertation

Synthesis and Characterisation of PCP Pincer Complexes with non-Precious Metals

ausgeführt zum Zwecke der Erlangung des akademischen Grades eines
Doktors der technischen Wissenschaften unter der Leitung von

Ao. Univ. Prof. Dr. Karl Kirchner

Institut für Angewandte Synthesechemie E163
Getreidemarkt 9/163, A-1060 Wien

eingereicht an der Technischen Universität Wien
Fakultät für Technische Chemie

von

Dipl.-Ing. Daniel Himmelbauer

Matr. Nr. 1225398
Seitenberggasse 63, A-1160 Wien

Wien, am _____



Die approbierte gedruckte Originalversion dieser Dissertation ist an der TU Wien Bibliothek verfügbar.
The approved original version of this doctoral thesis is available in print at TU Wien Bibliothek.

Declaration

Ich habe zur Kenntnis genommen, dass ich zur Drucklegung meiner Arbeit unter der Bezeichnung

Dissertation

nur mit Bewilligung der Prüfungskommission berechtigt bin. Ich erkläre weiters Eides statt, dass ich meine Dissertation nach den anerkannten Grundsätzen für wissenschaftliche Abhandlungen selbstständig ausgeführt habe und alle verwendeten Hilfsmittel, insbesondere die zugrunde gelegte Literature, genannt habe. Weiters erkläre ich, dass ich diese Dissertation bisher weder im In- noch Ausland (einer Beurteilerin/einem Beurteiler zur Begutachtung) in irgendeiner Form als Prüfungsarbeit vorgelegt habe und dass diese Arbeit mit der vom Begutachter beurteilten Arbeit übereinstimmt.

This work was performed at the Vienna University of Technology, Institute for Applied Synthetic Chemistry, in the research group of Prof. Karl Kirchner, Organometallic Chemistry and Catalysis and financed by the Austrian Science Fund (FWF, project No.: P 29584 and P 32570).

Acknowledgement

I wish to express my sincere appreciation to my supervisor, Prof. Karl Kirchner, who gave me the wonderful opportunity to work in his awesome research group. During this time, he has given me convincing guidance and support, while at the same time allowing me plenty of freedom in carrying out this project. In addition, I would like to acknowledge the great opportunities he offered me to participate in several conferences, which allowed me to gain experience in communicating and presenting scientific information. Especially the conference in Poland with the six hour drive was splendid and memorable, including the one passing manoeuvre. Thank you very much for the great time.

I want to thank the Institute of Applied Synthetic Chemistry of the Vienna University of Technology for realisation and the Austrian Science Fund (FWF) for funding this work.

Special thanks to Dr Berthold Stöger for introducing me to X-ray crystallography and providing support for the single crystal structure analysis as well as for the funny hours in which we enjoyed Crianza wines from Rioja and the Asian cuisine.

I wish to express my deepest gratitude to Dr Marc Pignitter for the electron spin resonance measurements and the pleasant time during the Chemical Days in Linz as well as Dr Ernst Pittenauer and Peter Unteregger for the numerous ESI-MS measurements. I would also like to thank Prof. Luis Veiros for supporting this work with DFT calculations.

Furthermore, I want to thank all my former and current lab-colleagues for the amazing time and who have become close friends over the years. Dr Matthias Mastalir for the great support during the first month of my thesis and the memorable vacation days we spent together in Corsica and Lower Austria. DI Gerald Tomsu for providing crucial input to my work and the best inappropriate jokes. Dr Mathias Glatz for his briefing on the technical background of inert working and the introduction to the wonderful world of fried cuisine. DI Wolfgang Eder for the extensive and exposed discussions about my work. Julian Brünig M.Sc. for the numerous small talks during the workday and the familiarisation of unique German words. DI Stefan Weber for his help in catalytic issues and support during the beer tour through Vienna. Dr. Nikolaus Gorgas for his comments to my work and the nice evenings where a cold beer was enjoyed. DI Jan Pecak for introducing me to EPR spectroscopy and showing me the basic concept of DFT calculations. Dr Sara R. M. M. de Aguiar for her honest and brutal opinions. Dr Zita Csendes for the nice time.

In addition I want to thank all students who concluded their Bachelor/Master thesis or internship in this research group for the great time and contributions to my work: Markus Rotter, Heiko Schratzberger, Matthias Käfer, Inga Lelievre, Flora Jessl, Alex Rosner, Claudia Rabijasz, Ines Blaha, Daniel Zobernig, Dina Iebed and Michael Weisner.

Advice and comments given by Dr Sven Barth has been a great help for my work and I want to thank him for that. On an other note I want to thank all the co-workers from other institutes with whom I also had a good time: DI Alexander Viernstein, DI Philipp Winkler, Dr Klaus Dobrezberger, Dr Philipp Hans, Dr Leonie Deilmann, Dr Alexey Cherevan, Dr Jia Wang, Dr Esther Knittl and Dr Roland Bittner.

I also want to show my gratitude to the colleagues DI Marco Seifried, DI Willi Zeni, Dr Danny Müller, Georg Gravogel M.Sc. and Dr Christian Knoll in the research group of Dr Peter Weinberger for sharing and providing certain chemical equipment and reagents.

Finally I want to thank my family and partner Melanie Kalina for their great love and support during this time.

Abstract

A steadily increasing number of research topics focuses on the development of catalytic systems featuring earth abundant transition metal complexes. In this context, so called pincer complexes play an important role in the activation of transition metals. Therefore, this work focused on the development, synthesis and characterisation of PCP pincer complexes, in respect to first row transition elements as well as their chemical properties and possible catalytic applications. It could be demonstrated that by developing new pincer ligands featuring a halogen at the *ipso*-carbon position the oxidative reaction pathway when treated with metal carbonyl precursors ($\text{Fe}(\text{CO})_5$, $\text{Fe}_2(\text{CO})_9$, $\text{Mn}_2(\text{CO})_{10}$ and $\text{M}(\text{CO})_6$ ($\text{M} = \text{Cr}, \text{Mo}, \text{W}$)) under solvothermal conditions is enhanced. With this method the first manganese and chromium PCP pincer complexes could be synthesised along with a series of uncommon paramagnetic high spin ($S = 2$) borohydride and low-spin ($S = 1/2$) nitrosyl chromium PCP pincer complexes. Several iron PCP pincer complexes in different oxidation states were synthesised and studied by the means of DFT calculations. Furthermore, an alkyl chromium pincer complex was synthesised that catalyses the transformation of ketones to alcohols at room temperature within one hour, utilising hydrosilanes as hydrogen source. Changing the alkyl moieties at the phosphine donors of the pincer ligands had a major impact on the outcome of the solvothermal reaction and different iron, chromium and molybdenum complexes were obtained. With the latter a completely unusual coordination mode in one of the molecular structures was observed where a CO ligand is bridged between the *ipso*-carbon of the benzene moiety and the metal center with an intact $\text{C}_{ipso}\text{-Mo}$ σ -bond. This work provided a new synthetic approach for the formation of PCP pincer complexes along with insights of their chemical and structural properties.

Kurzfassung

Eine stetig wachsende Zahl von Forschungsthemen konzentriert sich auf die Entwicklung von katalytischen Systemen mit nachhaltigen Metallkomplexen. In diesem Zusammenhang spielen sogenannte Pincer-Komplexe eine wichtige Rolle bei der Aktivierung von Übergangsmetallen. Daher konzentrierte sich diese Arbeit auf die Entwicklung, Synthese und Charakterisierung von PCP-Pincer-Komplexen in Bezug auf die Übergangselemente der ersten Reihe sowie deren chemische Eigenschaften und mögliche katalytische Anwendungen. Es konnte gezeigt werden, dass durch die Entwicklung neuer Pincer-Liganden, die ein Halogen an der *ipso*-Kohlenstoff Position aufweisen, der oxidative Reaktionsweg mit Metallcarbonylen ($\text{Fe}(\text{CO})_5$, $\text{Fe}_2(\text{CO})_9$, $\text{Mn}_2(\text{CO})_{10}$ and $\text{M}(\text{CO})_6$ ($\text{M} = \text{Cr}, \text{Mo}, \text{W}$)) unter solvothermalen Bedingungen verbessert wird. Mit dieser Methode konnten die ersten Mangan und Chrom PCP-Pincer-Komplexe zusammen mit einer Reihe von ungewöhnlichen paramagnetischen High-Spin ($S = 2$) Borohydrid- und Low-Spin ($S = 1/2$) Nitrosyl-Chrom-PCP-Pincer-Komplexen synthetisiert werden. Mehrere Eisen PCP-Pincer-Komplexe in verschiedenen Oxidationsstufen wurden synthetisiert und mittels DFT-Berechnungen untersucht. Weiterhin wurde ein Alkyl-Chrom-Pincer-Komplex synthetisiert, der die Umwandlung von Ketonen in Alkohole bei Raumtemperatur innerhalb einer Stunde unter Verwendung von Hydrosilanen als Wasserstoffquelle katalysiert. Die Änderung der Alkylreste an den Phosphin-Donoren der Pincer-Liganden hatte einen großen Einfluss auf das Ergebnis der solvothermalen Reaktion und es wurden verschiedene Eisen-, Chrom- und Molybdänkomplexe erhalten. Bei letzterem wurde ein völlig ungewöhnlicher Koordinationsmodus in einer der Kristallstrukturen beobachtet, bei dem ein CO-Ligand zwischen dem *ipso*-Kohlenstoff des Liganden und dem Metallzentrum gebunden ist und die $\text{C}_{ipso}\text{-M}$ σ -Bindung komplett intakt ist. Diese Arbeit lieferte einen neuen synthetischen Ansatz für die Bildung von PCP-Pincer-Komplexen sowie Erkenntnisse über deren chemische und strukturelle Eigenschaften.

List of Abbreviations

***n*-BuLi** *n*-butyllithium.

bipy 2,2'-bipyridine.

br broad.

CW continuous wave.

DFT density functional theory.

dme dimethoxyethane.

dmpe 1,2-bis(dimethylphosphino)ethan.

EPR electron paramagnetic resonance.

eq. equivalent.

ESI-MS electrospray ionisation mass spectrometry.

EtOAc ethyl acetate.

F-TEDA 1-chlormethyl-4-fluor-1,4-diazonia bicyclo[2.2.2]octanebis(tetrafluorborat).

HBpin pinacolborane.

HSQC heteronuclear single quantum coherence.

IR infra red.

KHMDS potassium bis(trimethylsilyl)amide.

LUMO lowest unoccupied molecular orbital.

MeCN acetonitrile.

MeOH methanol.

MS mass spectrometry.

n.d. not determined.

NMR nuclear magnetic resonance.

no. number.

PTFE polytetrafluoroethylene.

rt room temperature.

SOMO singly occupied molecular orbital.

TLC thin layer chromatography.

TMEDA N,N,N',N'-tetramethylethane-1,2-diamine.

UV ultra violet.

Table of Content

1	Introduction	1
1.1	PCP Pincer Complexes in the Literature	2
1.2	Carbon Monoxide	7
1.3	Nitrosyl a Non-Innocent Ligand	9
1.4	Phosphines in Pincer Chemistry	10
1.5	Metal Hydrides	11
1.6	Spectroscopic Methods for Paramagnetic Complexes	12
2	Results and Discussion	19
2.1	Synthesis of PCP and POCOP Ligands	20
2.2	Iron PCP Pincer Complexes	21
2.3	Manganese PCP Pincer Complexes	26
2.4	Chromium PCP Pincer Complexes	29
2.5	Molybdenum and Tungsten PCP pincer complexes	38
3	Conclusion	47
4	Experimental	49
4.1	Synthesis of PCP Ligands	49
4.2	Synthesis of Fe PCP Pincer Complexes	53
4.3	Synthesis of Mn PCP Pincer Complexes	55
4.4	Synthesis of Cr PCP Pincer Complexes	56
4.5	Synthesis of Mo PCP Pincer Complexes	58
4.6	Synthesis of W PCP Pincer Complexes	60
5	References	61
6	Appendix	67
6.1	NMR Spectra	67
6.2	Crystallographic Data	88
7	Curriculum Vitae	91

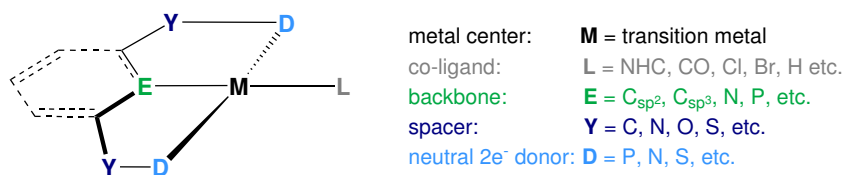


Die approbierte gedruckte Originalversion dieser Dissertation ist an der TU Wien Bibliothek verfügbar.
The approved original version of this doctoral thesis is available in print at TU Wien Bibliothek.

Chapter 1

Introduction

Formation of new chemical bonds by activation of inert starting materials using highly tuned transition metal complexes is one of the fundamental research topics in applied synthetic chemistry. In this context, synthetic transformations that are metal catalysed have to be efficient, selective and sustainable. The latter can be achieved by using earth-abundant transition metals like nickel, iron or manganese, considering that most catalytic reactions utilize precious metals from the second or third row transition elements as catalysts. Furthermore, high stability and variability is required of such complexes to easily change the stereoelectronic properties and tune the catalysts for the respective reactions. This can be achieved by changing the ligand system coordinated to the metal center which is in most cases composed of one or more different organic frameworks. So called pincer ligands are excellent candidates to fulfil these purposes. These are tridentates that coordinate in a coplanar fashion to the metal center adopting a meridional geometry (Scheme 1.1). Because of the chelating effect pincer complexes are very stable and the ligand framework can be easily modified to change the electronic properties of the metal center in a controlled manner without changing the coordination geometry. In general pincer ligands consists of an aromatic or aliphatic backbone which can be either neutral or anionic with two bulky electron donor atoms connected to this backbone by a variety of different spacers. Over the last decades a great number of different pincer ligands and complexes have been reported in the literature with a broad range of catalytic applications.¹⁻⁹

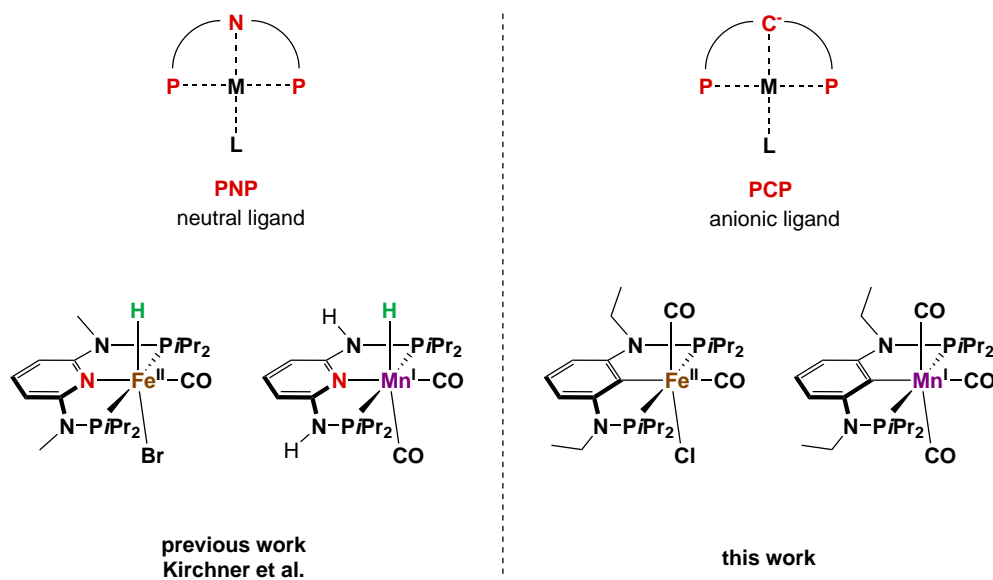


Scheme 1.1: Generalised schematic representation of pincer complexes.

Aim of This Work

This work focused on the development and characterisation of new, so called **PCP** pincer complexes with regards of iron, manganese as well as the group six (Cr, Mo and W) transition metals. The nomenclature derives from the three coordinating groups which are in this case one carbon and two phosphine atoms with a benzene moiety as backbone and nitrogen or oxygen as linkers. The motivation for this work originated partially from the related isoelectronic iron and manganese PNP systems which showed excellent catalytic properties for chemoselective hydrogenation reactions using molecular hydrogen which

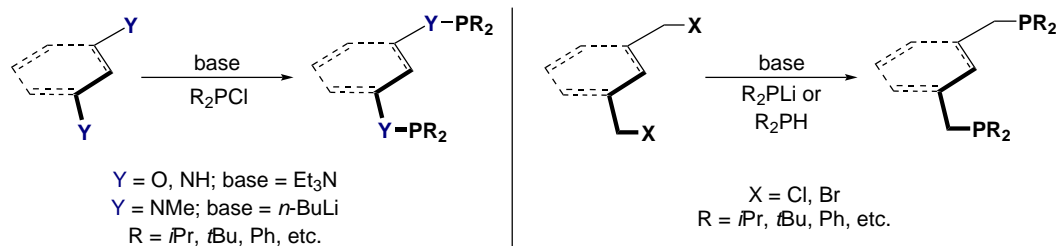
provide an efficient and green reduction of carbonyl compounds.^{9–11} The main difference between the PNP and PCP ligands is that the latter is anionic with an sp^2 carbon metal σ -bond and the former coordinates neutral with the nitrogen lone pair donated to the metal center (Scheme 1.2). This provides a completely different stereoelectronic environment for the metal center and could open new chemical properties. Another motivation for this work derived from developing a simple synthetic approach for iron, manganese and chromium PCP pincer complexes which were at this point scarce to non existing in the literature and contribute at least further knowledge to the field of pincer chemistry.



Scheme 1.2: Selected overview and comparison of previous work featuring PNP pincer complexes by Kirchner *et al.*^{9–11} and this work with PCP pincer complexes.^{12,13}

1.1 PCP Pincer Complexes in the Literature

The first reported pincer complexes were composed of an anionic ligand with an aromatic backbone and two bulky phosphine donors coordinated in a χ^3 -P,C $_{sp^2}$,P fashion to a single nickel atom. At this time, the interest for such species was partially derived from organometallic complexes that feature at least one carbon metal σ -bond.^{14,15} Meanwhile, transition metal mediated C-H bond activation is one of the main research areas of this century. Most reactions utilise precious metals as catalyst but the contribution of non-precious metals has increased significantly over the last years.^{16,17} In general, the carbon metal σ -bond slightly enhances the stability of the complexes when compared to the related PNP counterparts. On the other hand, many simple metal salts, in respect to the first row transition elements, fail to cleave the C-H bond of the aliphatic or aromatic moiety of the PCP pincer ligand and/or the resulting hydride complex is thermodynamically not stable. Thus, the chemistry of PNP pincer complexes have been studied very well over the last decades while iron, manganese and group six transition metals PCP pincer complexes are exceedingly rare. In contrast, the chemistry of nickel PCP pincer complexes is already quite comprehensive. In terms of both ligands, one of their most significant advantages are that the two bulky phosphine donors stabilise a high variety of transition metals in different oxidation states and the stereoelectronic properties of these complexes can be easily influenced by changing the phosphine alkyl or aryl moieties.^{1,3}

Scheme 1.3: Generalised schematic synthesis of PCP pincer complexes with different spacers.^{18–24}

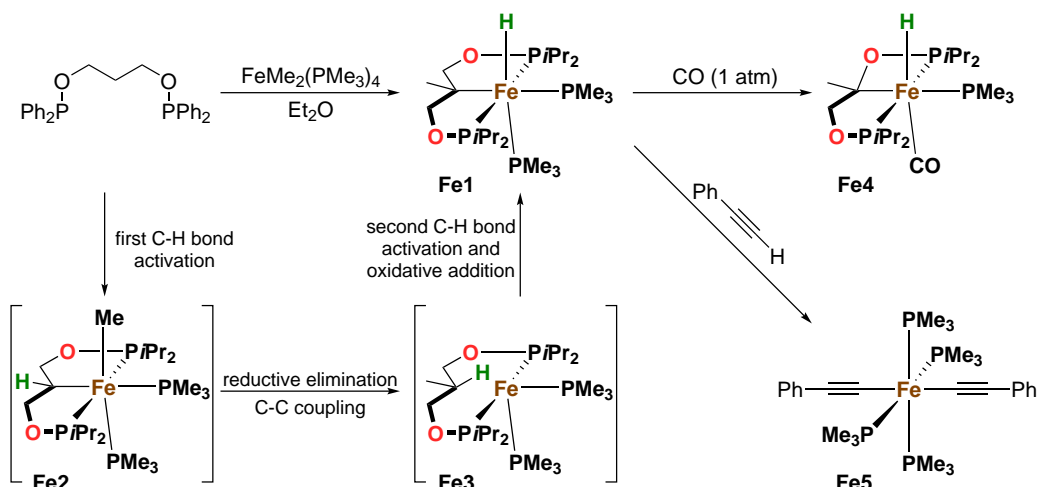
Depending on which spacer is used, the synthesis of these ligands is easy and straight forward (Scheme 1.3). In the case of the oxygen and nitrogen spacer, resorcinol or 1,3-propanediol and 1,3-diaminobenzol or *N,N'*-dimethylethane-1,2-diamine is treated with a chlorophosphine and base yielding the aromatic or aliphatic species, respectively.^{18–21} For the carbon linker, 1,3-bis(bromomethyl)benzene or dibromopentane can be treated with lithiumphosphine to yield the aromatic or aliphatic pincer ligand, respectively.^{22–24} Most of these chemicals are commercially available and particular complexes can even be synthesised in a one pot synthesis where the ligand precursor, the phosphine and the metal salt are added into one reaction vessel.^{25,26}

Fe PCP Pincer Complexes

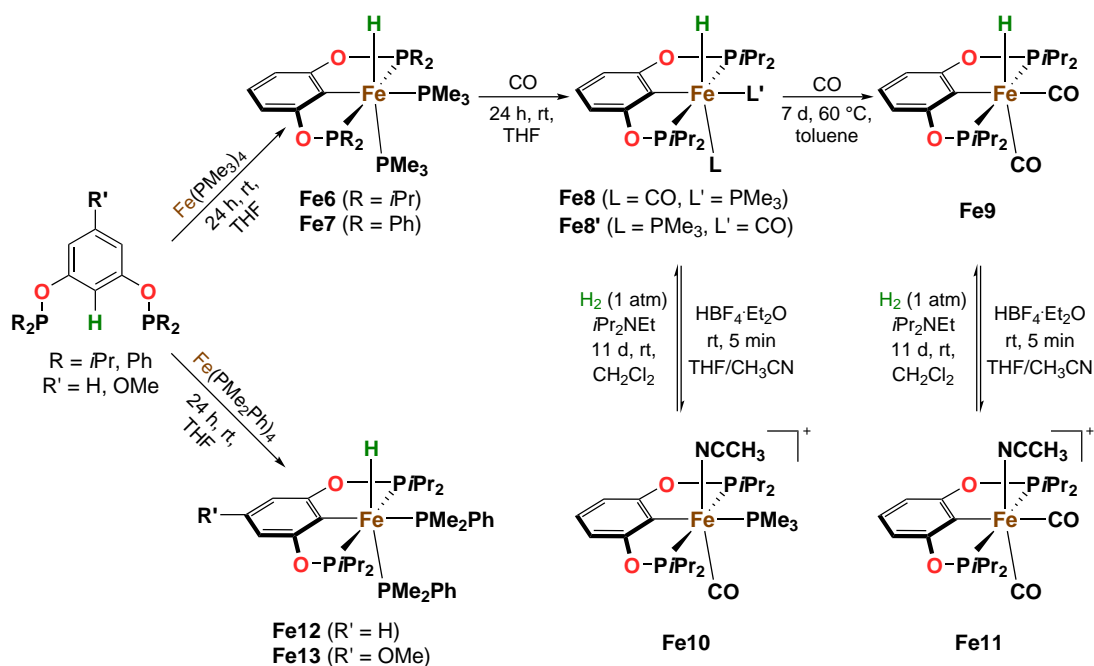
In this context, Li *et al.* reported in 2009 the synthesis of the first iron POC_{sp³}OP pincer complex [Fe(POCOP)(PMe₃)₂H] (**Fe1**) by treating the ligand (Ph₂POCH₂)₂CH₂ with the metal precursor FeMe₂(PMe₃)₄ in Et₂O (Scheme 1.4).²⁷ Particularly interesting about this complex is the proposed reaction mechanism. First, substitution of two phosphine groups and elimination of methane by a formal one electron oxidation reaction of the metal center to Fe(I) through C-H bond activation leads to the intermediate **Fe2**. Subsequent reductive elimination occurs with the formation of a new C-C σ-bond between the methyl group and the *ipso*-carbon of the ligand moiety. This leads to a four coordinated Fe(0) species **Fe3** as intermediate with a new ligand backbone. Followed by a second sp³ C-H bond activation and oxidative addition, which finally yields the product **Fe1**.²⁷ While this reaction pathway can be described as unusual, van Koten reported a similar C-C coupling between the sp² *ipso*-carbon of the arene moiety and the sp³ carbon of a methyl group by treating a platinum NCN pincer complex with methyl iodide.²⁸ Furthermore Li *et al.* could show that treatment of **Fe1** with CO and phenylacetylene resulted in ligand substitution and dissociation, forming the complexes **Fe4** and **Fe5**, respectively (Scheme 1.4).²⁷

Later on, Guan *et al.* reported the first iron hydride PC_{sp²}P pincer complex with an aromatic backbone.²⁹ Treatment of a 1,3-bis(phosphinite)benzol pincer ligand with the metal precursor Fe(PMe₃)₄ yielded [Fe(POCOP-R)(PMe₃)₂H] (**Fe6**, R = *i*Pr; **Fe7**, R = Ph) as yellow solid. No conversion could be achieved with the *t*Bu ligand. Exposure of **Fe6** to carbon monoxide gas at ambient temperature resulted in the ligand exchange of PMe₃ (*trans* to the hydride ligand) with CO (Scheme 1.5). Interestingly, nearly no ligand substitution proceeded with complex **Fe7** upon treatment with CO gas, even at elevated temperatures. Furthermore, due to the noticeable *trans* effect of the hydride ligand, in the molecular structures of complexes **Fe6** and **Fe1** the bond distance Fe-P_{*trans*} is 2.2583(7) and 2.2560(8) Å, which is, besides very similar to each other, also significantly longer compared to Fe-P_{*cis*} bond with 2.2167(7) and 2.2301(7) Å.^{27,29} Isomerisation of **Fe8** can be achieved at increased temperatures and the species with the carbonyl ligand in *cis* position with respect to the hydride ligand **Fe8'** can be isolated. If this reaction is carried

out again under a carbon monoxide atmosphere the substitution of the remaining PMe_3 ligand occurs forming the dicarbonyl iron complex *cis*- $[\text{Fe}(\text{POCOP-R})(\text{CO})_2\text{H}]$ (**Fe9**).²⁹



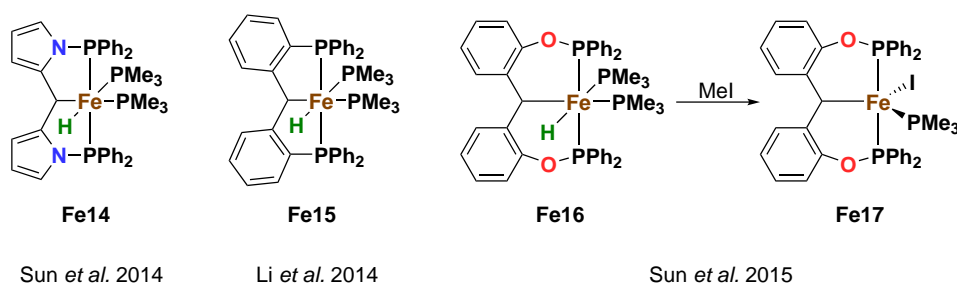
Scheme 1.4: Synthesis of the first iron PCP pincer complex and proposed formation mechanism.²⁷



Scheme 1.5: Synthesis of various neutral hydride and cationic mono- and dicarbonyl Fe PCP pincer complexes.^{29–31}

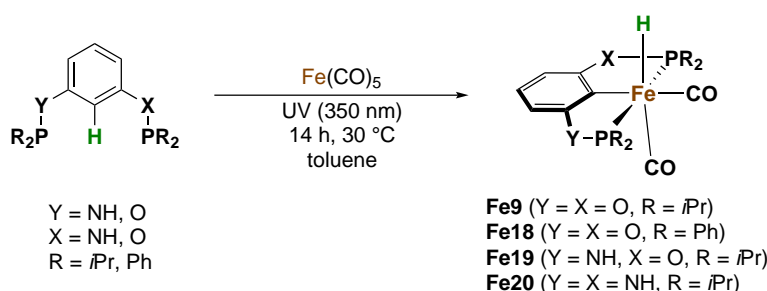
Protonation of the neutral iron complexes **Fe8** and **Fe9** with $\text{HBF}_4 \cdot \text{Et}_2\text{O}$ resulted in the formation of the cationic iron pincer species $[\text{Fe}(\text{POCOP-}i\text{Pr})(\text{MeCN})(\text{PMe}_3)(\text{CO})]$ (**Fe10**) and $[\text{Fe}(\text{POCOP-}i\text{Pr})(\text{MeCN})(\text{CO})_2]$ (**Fe11**) with 85% and 82% isolated yield. Independent of which isomer of the mono carbonyl complexes (**Fe8** and **Fe8'**) is used for the protonation reaction only the *trans* CO isomer **Fe10** is formed. Thus, two reaction mechanisms were proposed where either a distorted trigonal-bipyramidal or a square-pyramidal intermediate is formed during the reaction with the latter being the more probable one.³⁰ Kirchner *et al.* reported similar observations where the abstraction of a halogen from both *cis* and

trans isomers of a monocarbonyl halide iron(II) PNP pincer complex, with AgBF_4 under a CO atmosphere, led only to the *trans*- $[\text{Fe}(\text{PNP}^{\text{NH-}i\text{Pr}})(\text{CO})_2\text{X}]$ ($\text{X} = \text{Cl}, \text{Br}$) complex.³² The protonation reaction is reversible by adding $i\text{Pr}_2\text{NEt}$ under H_2 atmosphere whereby both isomers (**Fe8** and **Fe8'**) were obtained in the relative ratio 3:2. Complexes **Fe12** and **Fe13** were synthesised in a similar fashion to complex **Fe6** with the metal precursor $\text{Fe}(\text{PMe}_2\text{Ph})_4$ (Scheme 1.5). All three complexes (**Fe6**, **Fe12** and **Fe13**) show catalytic activity towards the dehydrogenation of ammonia borane with increased reactivity as listed in the parenthesis.³¹ Furthermore, the chemical transformation of aldehydes and ketones to alcohols *via* hydrosilylation reactions were comprehensively investigated utilising **Fe6** as catalyst.²⁹



Scheme 1.6: Variuos hydride Fe $\text{PC}_{\text{sp}^3}\text{P}$ pincer complexes.³³⁻³⁵

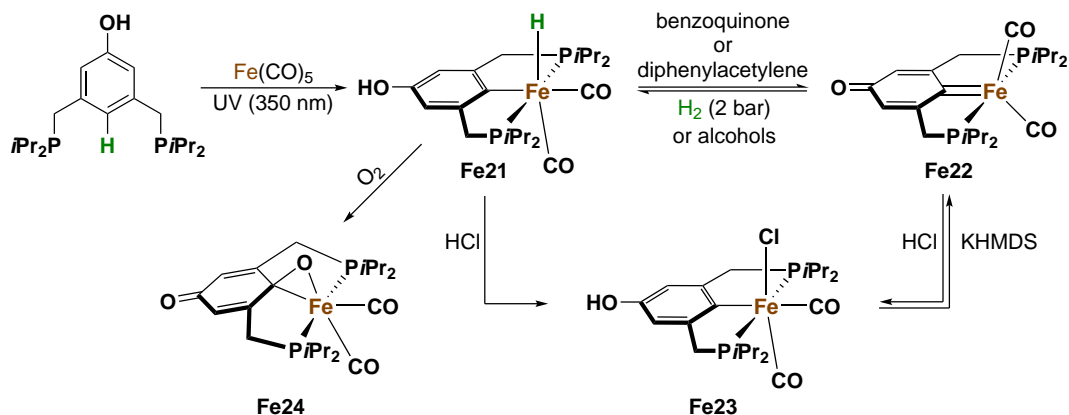
Contemporaneously, Li and Sun *et al.* further investigated the synthesis of iron PCP pincer complexes featuring a benzylbenzene and a dipyrrole backbone with a sp^3 carbon. Three different iron hydride pincer complexes (**Fe14** - **Fe16**) were reported and synthesised similarly to **Fe1** using $\text{Fe}(\text{PMe}_3)_4$ as metallizing agent (Scheme 1.6). In terms of catalytic applications, complexes **Fe15** and **Fe16** bring forth the reduction of different aldehydes and ketones to alcohols using $(\text{EtO})_3\text{SiH}$ as hydrogen source, while complex **Fe14** showed no activity towards hydrosilylation reactions. Other silanes such as Ph_3SiH or Et_3SiH were not converted. Furthermore, by treating complex **Fe16** with MeI the five coordinated iron species **Fe17** can be isolated upon losing one methane and PMe_3 molecule (Scheme 1.6). This coordinatively unsaturated complex has two unpaired electrons and thus is a paramagnetic d^6 high spin ($S = 1$) species adopting a trigonal bipyramidal coordination geometry around the metal center.³³⁻³⁵



Scheme 1.7: Synthesis of different hydride iron(II) PCP pincer complexes using $\text{Fe}(\text{CO})_5$ as metal precursor.³⁶

Sortais *et al.* reported the metalation of different pincer ligands bearing an aromatic backbone with nitrogen and oxygen spacers connected to different phosphine moieties (Scheme 1.7). Here, $\text{Fe}(\text{CO})_5$ was utilised under ultra violet (UV) radiation (350 nm) and treated with the corresponding ligand to yield the hydride iron(II) dicarbonyl PCP pincer

complexes **Fe9** and **Fe18 - Fe20**. They reported that it was necessary to submit the ligands in small excess to suppress the formation of unwanted side products. With the *t*Bu ligand no conversion occurred. Complex **Fe9** and **Fe20** showed catalytic activity towards the dehydrogenative borylation of styrene with pinacoleborane (HBpin) under UV radiation and both have very similar selectivity with the formation of styrylboronate as the clearly favoured product.³⁶



Scheme 1.8: Synthesis of ferraquinone and ferraquinone.³⁷

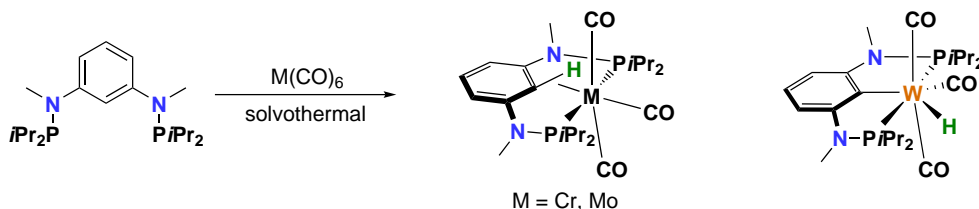
In 2017 Milstein *et al.* reported a series of different ferraquinone and ferraquinone PCP pincer complexes and investigated their chemical properties. By stirring 3,5-bis(diisopropylphosphinomethylene)phenol with $\text{Fe}(\text{CO})_5$ in THF under UV radiation the hydride iron dicarbonyl complex **Fe21** was isolated as green solid (Scheme 1.8),³⁷ in a similar fashion as reported by Sortais and co-workers.³⁶ The ferraquinone species **Fe22** can be obtained by dehydrogenation of **Fe21** with benzoquinone or an excess of (di)phenylacetylene as hydrogen acceptor. With the latter, the formation of a 3:1 mixture of (*Z*) and (*E*)-stilbene and a 15:1 mixture of styrene and ethylbenzene is observed, respectively. On the other hand, **Fe22** can be protonated using molecular hydrogen or an alcohol as hydrogen source. Furthermore, treatment of **Fe22** or **Fe21** with an aqueous hydrochloric acid solution yields the chloride dicarbonyl iron complex **Fe23** which reacts back to the former with potassium bis(trimethylsilyl)amide (KHMDS). Moreover, it was demonstrated that addition of Br_2 to the five coordinated ferraquinone complex **Fe22** resulted in a hydrogen-halogen exchange which is common for organic quinones. Exposure of the hydride ferraquinone species **Fe21** to air yielded an interesting oxyferraquinone complex (**Fe24**) where the oxygen atom is bridged by the *ipso*-carbon of the ligand and the metal center.³⁷

Mn PCP Pincer Complexes

Manganese and iron are both earth abundant transition metals and are considered to have a low to non environmental impact. Both received a lot of attention in the last years in regards to pincer chemistry and in respect to the first row transition elements. While iron was studied quite well over the last decades, the chemical properties of low-valent manganese pincer complexes have been noticed just recently. This could be attributed to the required metal precursors for manganese pincer complexes, which are often in low oxidation states, are very expensive.^{38–43} Though the related PNP systems were reported recently,^{9,44–49} in this thesis, to the best of my knowledge, the first reported manganese PCP pincer complex is presented and discussed in chapter 2.3.¹³

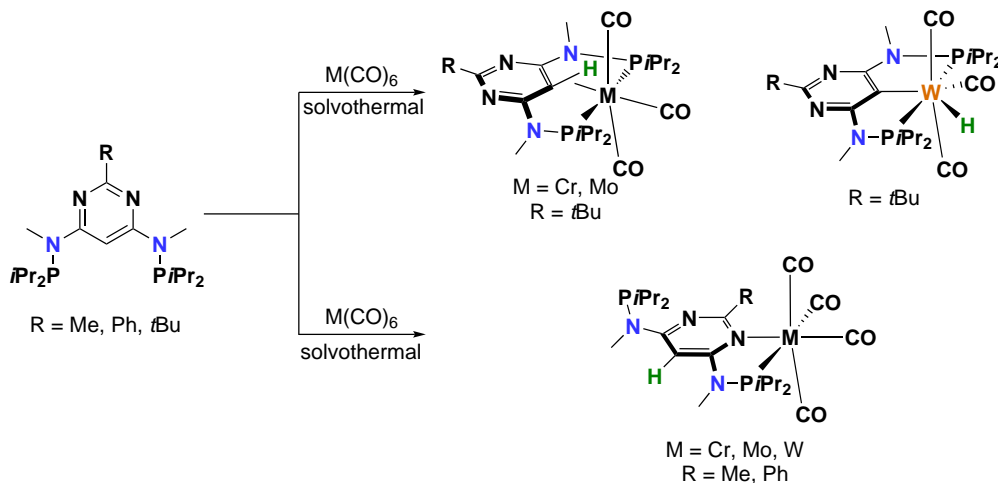
Group Six (Cr, Mo and W) PCP Pincer Complexes

In the previous work of Kirchner *et al.* the reaction of chromium, molybdenum and tungsten hexacarbonyl metal precursors with the PCP pincer ligand *N,N'*-(diisopropylphosphino)-*N,N'*-dimethyl-1,3-diaminobenzene under solvothermal condition were reported. In the case of chromium and molybdenum the agostic species with an η^2 -C_{ipso}-H coordination mode were isolated and characterised. Tungsten on the other hand mediated a C-H bond activation and formed a hydride complex (Scheme 1.9).⁵⁰



Scheme 1.9: Synthesis of agostic chromium, molybdenum and hydride tungsten PCP complexes with a benzene backbone⁵⁰

Later he published analogous results using a similar PCP ligand system with a pyrimidine backbone instead of benzene. The aim was to use an electron deficient system to increase the probability to cleave the C-H bond by the metal precursors. Here bulky alkyl groups like *t*Bu had to be in the *para* position to the *ipso*-carbon to prevent the χ^2 -P,N coordination mode. In the end, similar results were observed as before by isolating the agostic intermediates for molybdenum and chromium and the hydride complex for tungsten (Scheme 1.10).⁵¹



Scheme 1.10: Synthesis of agostic chromium, molybdenum and hydride tungsten PCP complexes with a pyrimidine backbone, plus the χ^2 -P,N coordination mode.⁵¹

1.2 Carbon Monoxide

The coordination of carbon monoxide (CO) to a metal centre has been very well studied both practically and theoretically over the past centuries. In general, when CO is engaging into a carbonyl metal bond, the free electron lone pair, located on the carbon atom, is donated into an empty d_σ frontier orbital, raising the electron count of the metal complex by two. Concurrent, metal electrons from the d_π orbital are contributed into the antibonding

π^* orbital of the CO *via* back bonding. Carbon monoxide is an excellent π acceptor with the π^* orbital being the lowest unoccupied molecular orbital (LUMO) that is polarised towards the carbon atom. This leads to a very strong carbon metal bond and can change the bond orders between M-C and C-O, depending on the strength of the back bonding as shown in Figure 1.1. As a consequence, strong metal carbon bonds polarise and weaken the C-O bond which is reflected in the IR spectroscopy and X-ray structure of the complex by increased intensity and decreased wave numbers of the CO stretching band and lengthening of the C-O bonds, in respect to free CO ($\nu = 2143 \text{ cm}^{-1}$, $r = 1.1282 \text{ \AA}$).^{52,53}

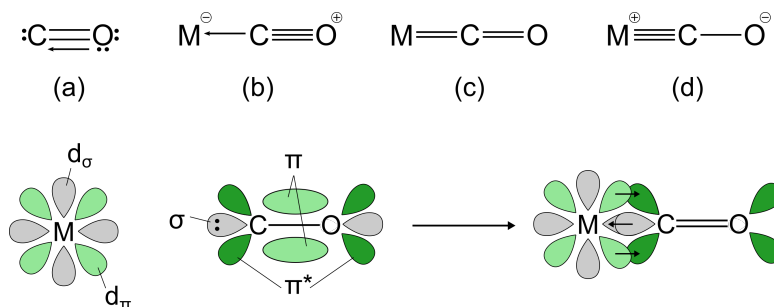
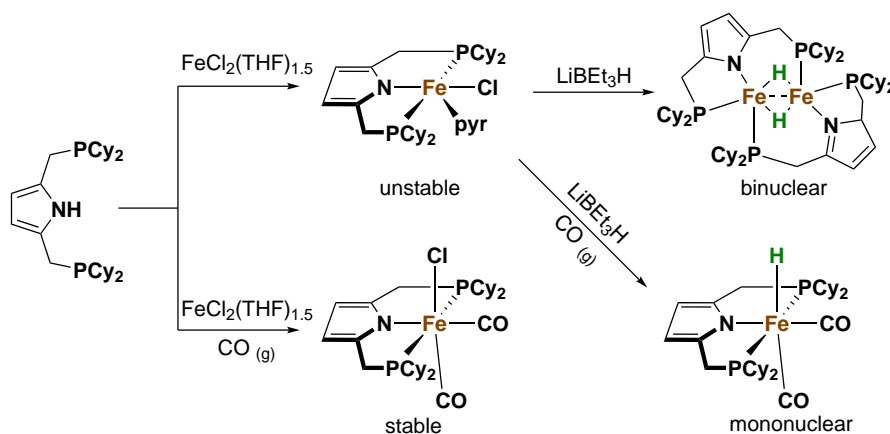


Figure 1.1: (top) Valence scheme of free CO (a), CO as pure σ donor and no backbonding (b), medium backbonding (c) and very strong backbonding where π_x^* and π_y^* are engaged (d). (bottom) Simplified picture of the orbital interaction between a CO molecule that coordinates to a metal atom.

That makes CO an ideal high field co-ligand in stabilizing a variety of different (pincer) complexes. Furthermore, organometallic complexes that feature both carbonyl and alkyl ligands can perform migratory insertion reactions. Here the CO inserts in the alkyl metal bond, forming an acyl complex with a new vacant coordination site. This reaction is well known⁵⁴ and finds application mostly in hydroformylation reaction and the production of acetic acid by carbonylation of methanol^{55,56} as well as, the recently reported, hydrogenation of nitriles.⁵⁷



Scheme 1.11: Synthesis of different iron pyrrole based PNP pincer complexes with and without carbonyl ligands.

On the other hand, profuse back bonding decreases the electron density of the metal center often making the complex less reactive as catalyst for chemical transformation. For example, Tonzentich *et al.* recently reported the synthesis of different highly unstable five coordinated pyrrole based PNP iron pincer complexes $[\text{Fe}(\text{PNP}^{\text{CH}_2\text{-Cy}})(\text{pyr})\text{Cl}]$ by using FeCl₂ as metallizing agent. Treatment of the halogen species with a super hydride like

[NaBEt₃H] afforded a binuclear hydride complex. By doing the latter reaction and the former synthesis under CO gas atmosphere, the corresponding bicarbonyl hydride and chloride complexes were obtained. While the carbonyl ligands stabilised the pincer system, their reactivity towards migratory insertion and β -elimination decreased significantly (Scheme 1.11).^{58,59}

1.3 Nitrosyl a Non-Innocent Ligand

Discovery of the biological function of nitric oxide (NO) as a messenger molecule and regulator in the cardiovascular system has reinvigorated the interest in this simple molecule and numerous NO transition metal complexes have been reported over the last decades.^{60,61} It is considered to be a non innocent ligand that can change the formal oxidation state of the transition metal complex by two through interconversion between linear NO⁺ and bent NO⁻. The majority of reported nitrosyl complexes feature NO ligands that coordinate in a nearly linear fashion to the metal center assigning it a positive charge (NO⁺) which is isoelectronic to CO but the positive charge can increase the electrophilicity of the system. In contrast to CO, NO⁺ is an even better π acceptor due to the positive charge and the more electronegative N atom. Transition from linear to bent NO can enable a new coordination site without ligand dissociation while the reversed process can induce ligand dissociation (Figure 1.2).⁶² Such properties render NO to an interesting co-ligand in pincer complex chemistry and thus catalytic application.^{63,64}

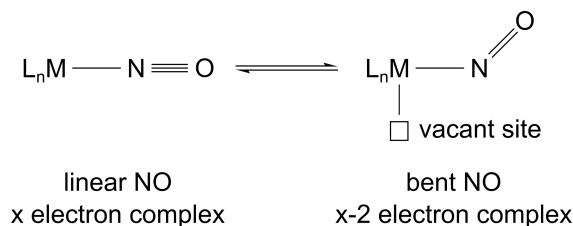


Figure 1.2: Simplified representation between the transition of linear and bent NO metal complexes.

Determination of the NO bonding mode as well as assignment of the oxidation number and electron count of a nitrosyl transition metal complex is in the most cases not a straight forward task. While the NO ligand exhibits intensive vibrational bands in the IR spectroscopy, prediction about the bonding angle have to be done with great care because the wave numbers between *lin*-NO and *bent*-NO complexes overlap over a broad spectrum (Figure 1.3). Even comparing similar systems can lead to a miss-judgement regarding the bonding angle. De la Cruz *et al.*⁶⁵ proposed corrections in the expected wave numbers for *lin*-NO transition metal complexes in dependence of the effective atomic number, charge and co-ligands. They collected and evaluated an enormous amount of data and used neutral mono carbonyl nitrosyl complexes as reference where the suggested corrections are illustrated as follows:

- positive/negative charge on the complex +100/-140 cm⁻¹
- PF₃, halides and bridging halides add 10, 15 and 30 cm⁻¹, respectively
- PPh₃, P(OPh)₃ and P(alkyl) subtract 15, 30 and 70 cm⁻¹, respectively

Despite the great work which was done by De la Cruz *et al.* there are too many variables to be considered to make a reliable prediction about the coordination mode of a nitrosyl

ligand only by IR spectroscopy. Therefore, crystallographic studies can provide better information regarding the configuration and bond metrics of NO. Free NO^{*} has a bonding order of 2.5 due to one unpaired electron located in the π^* orbital which reflects on the bond length of 1.15 Å (*cf.* double bond 1.18 Å, triple bond 1.06 Å).^{53,61,65}

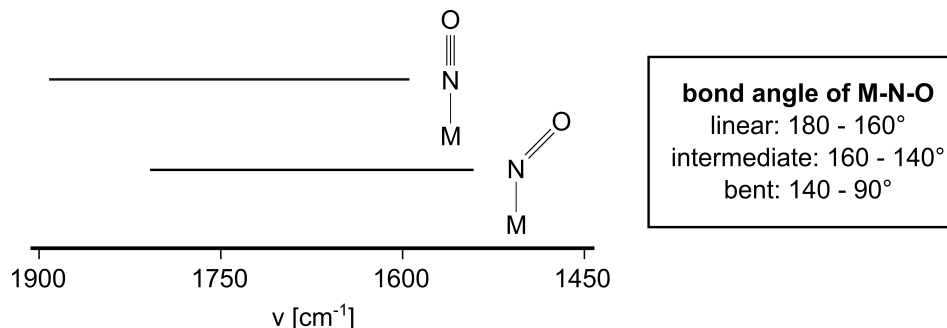


Figure 1.3: Simplified representation between the transition of linear and bent NO metal complexes.

If no assumptions are to be made concerning the oxidation state of such complexes, the Feltham-Enemark notation⁶⁶ $\{M(NO)_y\}^n$ (n = formal electron count) is a very useful tool because it ignores the bonding fashion of the NO ligand(s). Here the d electrons of the metal are counted while the nitrosyl ligand is considered to be neutral and then are summed up with the one unpaired electron in the π^* orbital of the NO. In this way the notation is consistent no matter which configuration NO adopts. For instance, the electron count for the pincer complex $[Fe(PCP^{NEt-iPr})(CO)(NO)]$ (**12**, presented in section 2.2) gives a d^7 configuration when removing the anionic pincer and neutral carbonyl ligands, leaving the $\{FeNO\}^+$ fragment behind. Adding the one π^* electron to the remaining seven d electrons equals eight valence electrons, resulting in the following notation: $\{FeNO\}^8$.^{53,66}

1.4 Phosphines in Pincer Chemistry

Phosphine ligands PR_3 play a very important role in pincer complex chemistry due to their unique properties.⁶⁷ They are strong σ donors through the lone pair on the phosphorous atom and mild π acceptors. In contrast to CO and NO, back bonding does not occur *via* donation of electrons from the metal into the π^* orbital but instead in the σ^* orbital of the P-R bond. With R getting more electronegative the π acidity increases as a consequence of lowering the atomic orbitals in energy.

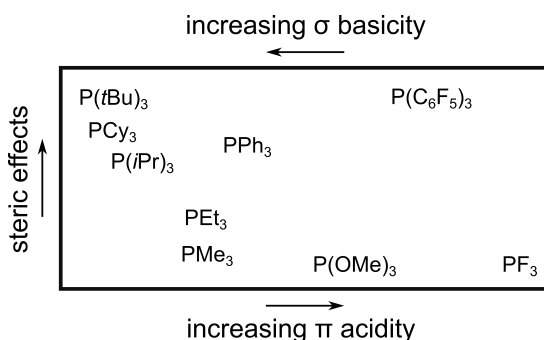


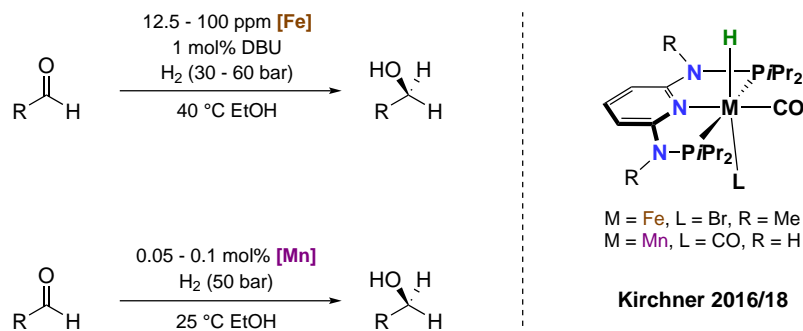
Figure 1.4: Simplified plot representing the correlation between electronic and steric affects of selected phosphine ligands according to Tolman.⁶⁸

Furthermore, the steric effects can be altered in a very predictable way by changing R as well (Figure 1.4). With such properties it is possible to stabilise a broad range of different transition metal complexes in various oxidation states and are often used to tune or promote catalytic reactions.^{53,67}

1.5 Metal Hydrides

Metal hydrides feature at least one M-H bond that is polarized due to the difference in the electronegativity and thus the hydrogen atom is assigned a negative charge. They play an important role in many chemical reaction like (transfer) hydrogenation, C-H functionalisation and olefin isomerisation as well as in energy converter processes and hydrogen storage application. The term *hydricity* is used to describe the reactivity of a metal hydride species and can be determined experimentally. A distinction is made between kinetic and thermodynamic hydricity with the former providing a value which is dependent on the relative rate of hydride transfer to a standard substance while the latter describes the cleavage of the M-H bond in terms of free enthalpy.⁶⁹

In respect to pincer chemistry with focus on iron and manganese a diverse number of (poly) hydride complexes have been reported with very specific and selective applications such as the hydrogenation of a broad spectrum of different substrates.^{9,48,49,70-72} Recently, the research group of Kirchner reported highly chemoselective hydrogenation of aldehydes with the related iron and manganese PNP pincer systems (Scheme 1.12).^{10,11}



Scheme 1.12: Chemoselective hydrogenation of aldehydes with iron and manganese PNP pincer complexes reported by Kirchner *et al.*^{10,11}

While these kinds of PNP pincer complexes are synthesised from the corresponding metal halogen carbonyl precursors, the PCP metal hydrides can be obtained directly by oxidative addition as shown in schemes 1.4 - 1.8. Therefore, the electron density of the metal precursor must be sufficient to cleave the C-H bond of the pincer ligand and create a thermodynamically stable hydride species. Figure 1.5 shows a simplified reaction path way for the synthesis of PCP hydride complexes. First the metal precursor interacts with the C-H bond of the ligand to form an agostic species (two electron three centre bond). Followed either by oxidative addition when using metallizing agents in low oxidation states that leads to the hydride complex^{3,27,29,36,37} or deprotonation of the agostic hydrogen with a base when using metal halogen salts. The former works to some extent for iron³ but not for lower first row transition metal complexes where in the case of chromium only the agostic species was formed.^{50,51} On the other hand it is possible to synthesise a variety of cobalt and nickel pincer complexes using metal halogen salts as metallizing agent and base.³

Regarding the characterisation, hydrides exhibit distinct signals in the range of 0 to -60 ppm (relative to SiMe_4) in the ^1H -NMR spectrum. Coupling with the phosphine donors produce different coupling constants depending on whether the hydride is in *cis* ($J = 15 - 30$ Hz) or *trans* ($J = 90 - 150$ Hz) position, which is useful in determining the configuration of the complex. Furthermore, it is possible to distinguish between classical (M-H, M-H-M) and non classical (M-H₂) hydride signals and inequitable hydrides can couple with each other ($J = 1-10$ Hz).

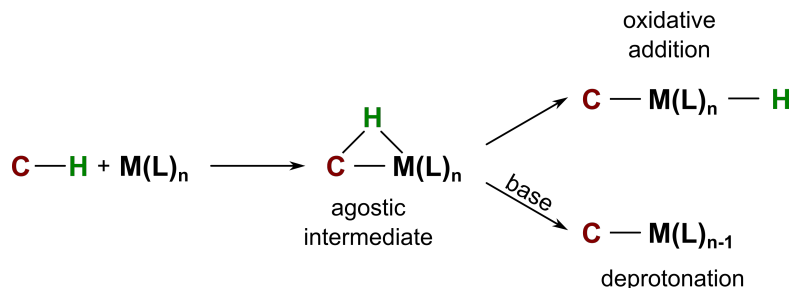


Figure 1.5: Simplified schematic process in the C-H activation of PCP ligands by a metal precursor where first an agostic intermediate is formed followed by either oxidative addition or deprotonation of the agostic hydrogen.

In the IR spectroscopy the stretching and deformational vibrations at 2200 - 1550 and 800 - 600 cm^{-1} , respectively, can be observed for terminal metal hydrides. The intensities of these signals are very weak and can overlap with vibrations from other ligands. In the solid state structure the bond distances between a terminal M-H is with 1.5 - 1.8 Å relative short and the detection of a hydride ligand in an X-ray measurement is often not straight forward due to the very low electron density of a hydrogen. Therefore, to improve the results most metal hydride crystals are measured at low temperatures and angles to decrease thermal motion and increase X-ray scattering, respectively.^{53,69}

1.6 Spectroscopic Methods for Paramagnetic Complexes

Over the last decades most reported organometallic complexes used in catalytic application were closed shell systems and thus diamagnetic. The reason behind this was the easy access to nuclear magnetic resonance (NMR) which is the most frequently used method in the characterisation of organometallic species and catalytic processes. In the last years, the interest in open shell (paramagnetic) complexes increased due to the motivation for using more earth abundant first row transition metals instead of precious ones. Paramagnetic species in organometallic chemistry feature at least one unpaired electron and NMR measurements are in most cases futile because of the usually very broad spectra. Electron paramagnetic resonances (EPR) measurement can be a very powerful tool in the characterisation of paramagnetic organometallic complexes and in describing the spin state properties of the unpaired electron(s).⁷³

Electron Paramagnetic Resonance

Most of the chemical properties and reactivities of organometallic complexes can be derived from their frontier orbitals. Hence, the characterisation of the singly occupied molecular orbitals (SOMO) of paramagnetic species play an important role in organometallic chemistry. Much information like the reactive site, type of radical and even mechanistic processes of catalytic reactions can be predicted by measuring the spin density distributions of the

unpaired electron. In this context, electron paramagnetic resonance spectroscopy can be a powerful method in measuring the spin density distribution and to describe the SOMO of the corresponding open shell complex.^{73,74}

Applying an external magnetic field to an open shell system results in the splitting of the electron spin state and the energy levels are no longer degenerate, where the energy difference between the two possible states increases with the strength of the applied magnetic field (Figure 1.6).⁷⁵

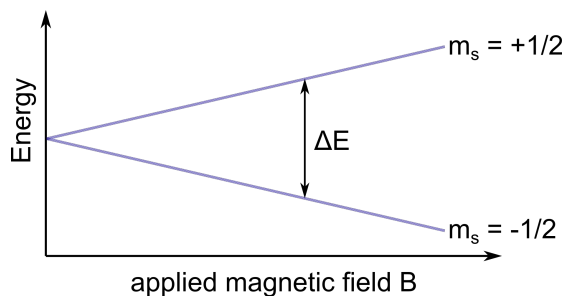


Figure 1.6: Splitting of the energy levels for an electron spin magnetic moment (m) when an external magnetic field is applied where ΔE increases with the strength of B .

$$\Delta E = h \cdot \nu = g \cdot m_B \cdot B \quad (1.1)$$

$$g = g_e + \Delta g \quad (1.2)$$

E ... energy [J]

h ... Planck's constant $6.626 \cdot 10^{-34} \text{ J s}$

ν ... frequency [Hz]

g ... proportionality factor (g -factor or Landé factor)

m_B ... Bohr magneton $9.274 \cdot 10^{-24} \text{ J/T}$

B ... magnetic field [T]

Similar to other spectroscopic methods, the absorption of electromagnetic radiation is measured and in most cases a phase-sensitive detector produces the first derivative of the absorption spectra. The proportionality factor (g -factor or Landé factor) can be seen as a molecular fingerprint of the paramagnetic molecule. This value represents the spin density distributions of the radical in a certain chemical environment and originates from the fundamental interaction between the unpaired electron and the applied magnetic field. It can be obtained using the EPR spectra and equation 1.1 describes the correlation of the g -factor with the frequency and the external magnetic field. From this relationship it is evident that infinite pairs of ν and B can be fitted into this equation. Therefore, in a typical experiment the frequency is held constant while the strength of the magnetic field is varied. At the center of the observed resonance(s), obtained from the spectra, the g -factor(s) can be determined (Figure 1.7).^{75,76}

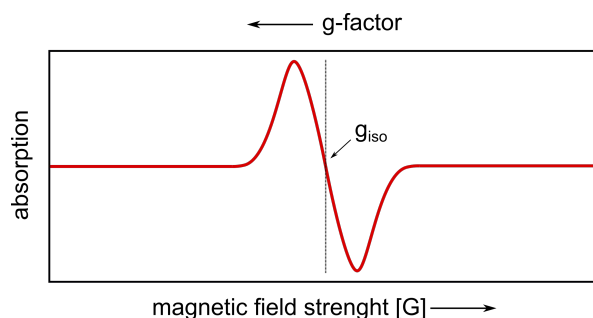


Figure 1.7: Possible example of an EPR spectrum with one signal of a dissolved sample with an isotropic g -value.

Depending on the chemical environment of the open shell molecule, the g -factor deviates from that of a free electron ($g_e = -2.0023$) due to spin-orbit interaction (equation 1.2). While organic radical substances have typically g values close to g_e , the shifts for transition metal complexes are more distinct. Compared to NMR, the g -factor represents the chemical environment of the radical and not the shift difference relative to a reference compound.

At this point it is important to mention that the g -factor has to be seen as a tensor that is dependent on the orientation of the molecule in the applied magnetic field and thus is not necessarily isotropic. Therefore, most EPR measurements are made from the solid state or frozen liquid of the sample because molecular tumbling in solution leads to an average value for the Landé factor and becomes $g_{iso} = g_x = g_y = g_z$. In organometallic chemistry the transition metal complexes are often measured dissolved in different solvents at very low temperatures (5 - 100 K). That is important since the anisotropy of the g -factor can reveal symmetric information about the electron distribution of the unpaired electron in the open shell system. In other words, the symmetry of the crystal field of a transition metal complex is expressed by the g -anisotropy. Hence, the g -factor can either be isotropic (g_{iso} , *e.g.* complexes that have cubic or perfect octahedral coordination geometry), axial ($g_{\perp} = g_x = g_y \neq g_z = g_{\parallel}$, *e.g.* transition metal ion with distorted octahedral coordination geometry) or rhombic ($g_x \neq g_y \neq g_z$) (Figure 1.8).^{75,76}

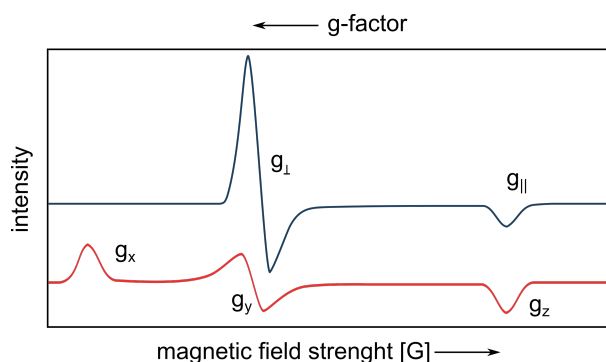


Figure 1.8: Simulated EPR spectra showing an axial signal (top) with $g_{\perp} > g_{\parallel}$ and a rhombic signal (bottom) with $g_x > g_y > g_z$ of an unpaired electron with no hyperfine coupling.

Another important parameter which can be derived from EPR spectra is the electron–nuclear hyperfine interaction (A) between the dipole moment of the radical and the surrounding nuclei. This interaction can provide information about the type and number of nuclei as well as their distance to the unpaired electron. When such an interaction occurs (usually with ^1H , ^{31}P , ^{13}C , ^{14}N , etc.), it comes to hyperfine splitting of the main signal similar to NMR spectroscopy as shown in equation 1.3, with n being the number of equivalent nuclei and I the spin quantum number of the corresponding nucleus. The hyperfine coupling consists of two processes. The first one is the Fermi contact interaction and is responsible for isotropic hyperfine coupling. This happens usually when the electron is located in an s-orbital which has, compared to the p, d and f orbitals, no node. The second one is dipole-dipole only interaction and induces anisotropic hyperfine coupling which can only be detected in the solid state or frozen solutions because A depends on the orientation of the molecule in the applied magnetic field.^{75,76}

$$\text{number of signals} = \prod_{i=1}^n (2 \cdot n_i \cdot I_i + 1) \quad (1.3)$$

To determine the g and A values of a measured EPR spectrum, a simulation is created using computational methods. Here the magnetic spin Hamiltonian parameters are calculated in combination with least-squares fitting algorithms.⁷⁷ Depending on the practical experiment, various factors can influence the obtained spectrum and which information is potentially extracted. For instance, the linewidth can broaden a signal and hyperfine

coupling information can get lost, and overlapping of axial or rhombic signals that are too close together can hide signal splitting (Figure 1.9).⁷⁸

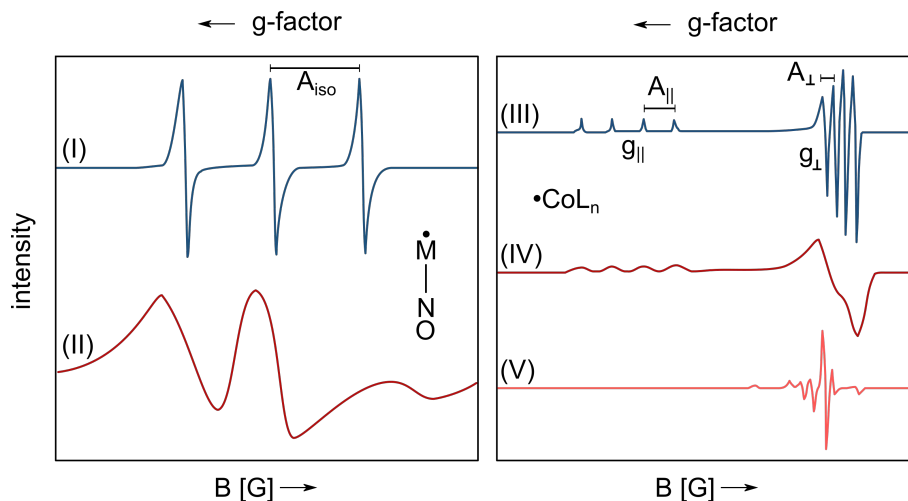


Figure 1.9: (left) Simulated EPR spectrum of a metal nitrosyl radical exhibiting a small linewidth (I) and very broad linewidth (II). (right) Simulated EPR spectrum of a cobalt transition metal exhibiting an axial signal with a small linewidth and no overlapping of g_{\perp} and g_{\parallel} (III), with a broad linewidth and no overlapping of g_{\perp} and g_{\parallel} (IV) and with a small linewidth and overlapping of g_{\perp} and g_{\parallel} (V).

EPR of Fe(I) pincer complexes

In recent years several Fe(I) pincer complexes ($S = 1/2$) have been reported and characterised by means of EPR studies. Table 1.1 provides a selected overview of different paramagnetic low-spin Fe(I) complexes with focus on d^7 systems featuring pincer ligands. In this context, it seems that most five coordinated iron complexes ($S = 1/2$) featuring a square pyramidal coordination geometry around the metal center, have g values between 2.02 and 2.05 when the electron density of the radical is located at the metal center (entry 1 - 7). Here, hyperfine coupling between the electron spin and the nuclear spin of the ^{31}P ($I = 1/2$) from the phosphine donors and ^{14}N ($I = 5/2$) of the nitrosyl ligand (if present) can be observed. When molecular tumbling is suppressed at low temperatures the hyperfine coupling has anisotropic properties (entry 1, 6), except for the complexes with a nitrosyl ligand where the hyperfine couplings are isotropic (entry 3, 7).^{79–83} In section 2.2 the spectra of entry 5 and 6 are shown (Figure 2.3 and 2.7) and discussed in more detail.¹² The pyrrole based Fe(I) pincer complex reported by Tonzetich *et al.* (entry 8) exhibits a nearly rhombic signal in the X-band EPR spectra with a \bar{g}_{iso} values of 2.126 which deviates clearly from the other iron pincer complexes ($S = 1/2$) with a square pyramidal coordination geometry. Furthermore, no hyperfine coupling with the phosphorous atoms is observed, indicating the possibility that the electron density of the unpaired electron is located at the bipyridine ligand.⁵⁹ On the other hand, four coordinated d^7 low spin iron complexes adopting a square planar coordination geometry, are exhibiting signals clearly in a lower field, compared to the five coordinated square pyramidal systems as described above which are very close to that of a free electron. A single isotropic signal ($g = 2.25$) at room temperature and a rhombic signal ($\bar{g}_{iso} = 2.256$) with isotropic hyperfine coupling to phosphorous atoms at 32 K can be observed for the Fe(I) PNP pincer complex with a pyrrole backbone (entry 9, 10).⁸⁴ Other four coordinated d^7 low spin iron complexes ($S = 1/2$) featuring N-heterocyclic carbenes as ligands have even higher g_{iso} values of 2.5.⁸⁵

Interestingly, the d^9 low-spin ($S = 1/2$) Fe(I) NCN pincer complex exhibit g values clearly at a higher field compared to its d^7 counterparts.⁸⁰ It is very uncommon for transition metal complexes to have g values very close to 2.0 which is in the literature mostly observed for pure organic radicals.⁷⁸ The SOMO of these complexes (entry 1 - 5) were investigated by means of DFT calculation giving it mostly d_{z^2} character.^{12,79-83}

Table 1.1: Selected EPR data from different iron complexes with focus on low spin systems and pincer ligands

structure	entry	g value(s)	A value(s) [G]	temp. [K] (solvent)	no. of signals	reference
	1 ^a	$g_x = 2.069$ $g_y = 2.038$ $g_z = 2.003$ $\bar{g}_{iso} = 2.037$	$A_{x,P} = 11.9$ $A_{y,P} = 13.9$ $A_{z,P} = 14.7$	5 (toluene)	9	79
	2 ^a	$g_x = 2.111$ $g_y = 2.043$ $g_z = 1.994$ $\bar{g}_{iso} = 2.049$	-	4.2 (1:1 toluene/ CH ₂ Cl ₂)	3	80
	3 ^a	-	$A_{iso,P} = 20.3$ $A_{iso,N} = 11.9$	100 (CH ₂ Cl ₂)	7	81
	4 ^a	-	$A_{iso,P} = 20.2$	293 (toluene)	3	82
	5 ^a	-	$A_{iso,P} = 19.5$	293 (toluene)	3	this work 12
	6 ^a	$g_x = 2.044$ $g_y = 2.034$ $g_z = 1.991$ $\bar{g}_{iso} = 2.023$	$A_{x,P} = 20.3$ $A_{y,P} = 20.5$ $A_{z,P} = 14.5$	100 (toluene)	7	this work
	7 ^a	-	$A_{iso,N} = 13$	220 (MeCN)	3	83
	8 ^a	$g_{\perp} = 2.170$ $g_{\parallel} = 2.038$ $\bar{g}_{iso} = 2.126$	-	20 (2-Methf)	2	59
	9 ^a	-	$g_{iso} = 2.25$	296 (toluene)	1	84
	10 ^a	$g_x = 2.591$ $g_y = 2.200$ $g_z = 1.976$ $\bar{g}_{iso} = 2.256$	$A_{iso,P} = 18$	32 (toluene)	2	79
	11 ^b	$g_{\perp} = 2.005$ $g_{\parallel} = 1.995$ $\bar{g}_{iso} = 1.995$	-	77 (toluene)	2	80

^a d^7 low spin $S = 1/2$ system. ^b d^9 low spin $S = 1/2$ system.

Evans Method

The Evans method⁸⁶ can be a simple and fast tool to determine the magnetic susceptibility of a substance which can provide information about the number of unpaired electrons and thus clues about the oxidation state and coordination geometry. The advantage of this method compared to SQUID (Superconducting Quantum Interference Device) measure-

ments or using a Gouy balance is that very small quantities of material are required and that nowadays NMR devices are usually part of the standard equipment of many research institutes. Here the shift differences between the solvent signal and the solution is measured in a simple ^1H -NMR experiment where a co-capillary NMR tube set-up is used (Figure 1.10). The differences in the chemical shift arises due to the interaction of the unpaired electron with the applied external magnetic field. Equation 1.4 describes how the magnetic susceptibility $\chi_{[M]}$ of a transition metal complex can be calculated by the chemical shift difference ($\Delta f[\text{Hz}]$), the spectrometer frequency ($F[\text{Hz}]$) and the concentration of the transition metal complex ($c_{[M]}[\text{mol/L}]$). The other two terms with χ_0 , d_0 and d_s being the susceptibility and density of the solvent as well as the density of the solution, respectively, describing the influence of the used solvent on the measured magnetic susceptibility are in the most cases negligibly small.⁸⁷

$$\chi_{[M]} = \frac{3\Delta f}{2\pi F c_{[M]}} + \chi_0 + \frac{\chi_0(d_0 - d_s)}{c_{[M]}} \quad (1.4)$$

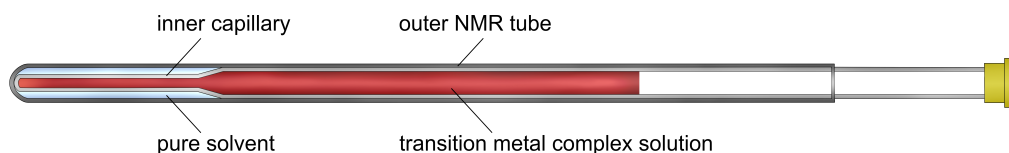


Figure 1.10: Example of a co-capillary NMR tube set-up.

From equation 1.4 it is evident that by increasing the concentration of the sample or using a spectrometer with a higher frequency, the chemical shift difference between both signals will increase. This allows the use of very small quantities, depending on the laboratory balance used for the preparation of the transition metal complex solution.



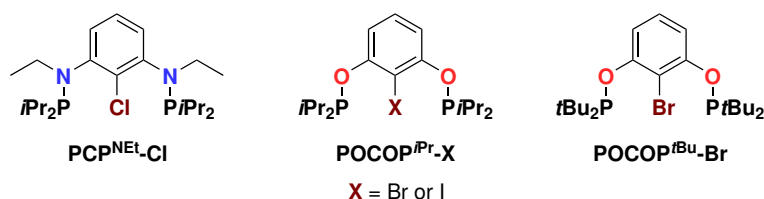
Die approbierte gedruckte Originalversion dieser Dissertation ist an der TU Wien Bibliothek verfügbar.
The approved original version of this doctoral thesis is available in print at TU Wien Bibliothek.

Chapter 2

Results and Discussion

As shown in section 1.1, it is not a straight forward task to form the carbon metal bond with PCP pincer ligands in respect to the first row transition elements iron, manganese and chromium. In regards to iron, metal precursors in low oxidation states bearing phosphine ligands that enhance the metal electron density by donating their lone pair to the metal center and prevent back bonding are needed to synthesise the corresponding pincer complexes.^{27,29-31,33-35} Using $\text{Fe}(\text{CO})_5$ as metallizing agent, UV radiation is necessary to cleave the carbonyl ligands in order to improve the capability of the metal to activate the C-H bond of the ligand and form the iron hydride PCP pincer complex by oxidative addition.^{36,37}

To enhance the formation of the carbon metal bond for the synthesis of first row transition metal PCP pincer complexes using carbonyl metal precursors as metallizing agents under solvothermal conditions, new types of PCP pincer ligands were synthesised in this work (Scheme 2.1).^{13,88,89} The first ligand feature a chloride at the *ipso*-carbon position and nitrogen linkers (spacers) with ethyl groups to preserve the innocent properties. The other ligands are composed of oxygen linkers, bearing different halogens and phosphine donors. The aim was to increase the probability of the oxidative addition reaction between these ligands and non-precious low valent metal precursors with focus on the first row transition elements. It has to be noted, that similar ligands composed of a halogen at the *ipso*-carbon position were already reported in the literature but feature none oxidative addition reaction,^{90,91} or only with precious metal precursors.¹⁸

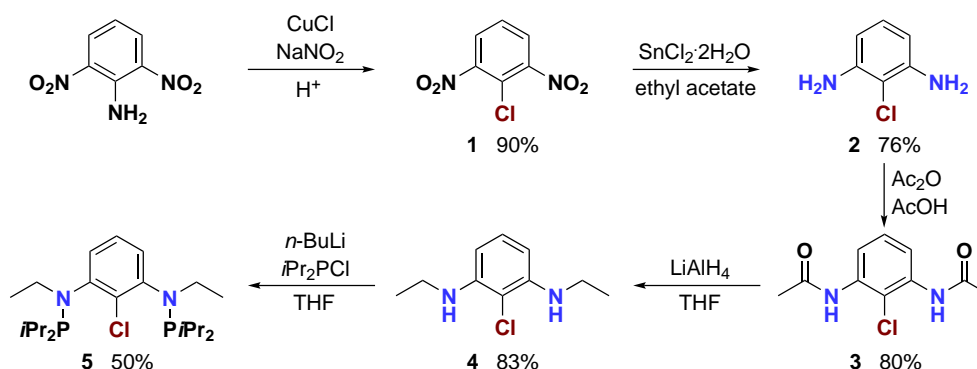


Scheme 2.1: New PCP ligands with a halogen on the *ipso*-carbon.^{13,88,89}

These ligand systems, shown in Scheme 2.1, were used to investigate the synthesis of PCP pincer complex using metal carbonyls as precursors like $\text{Fe}_2(\text{CO})_9$, $\text{Fe}(\text{CO})_5$, $\text{Mn}_2(\text{CO})_{10}$ and $\text{M}(\text{CO})_6$ ($\text{M} = \text{Cr}, \text{Mo}, \text{W}$) under solvothermal^{92,93} conditions. The synthesis of the ligands and corresponding PCP pincer complexes with the metal carbonyls as well as their characterisation and investigation of their reactivity and chemical properties are presented and discussed in the following sections.

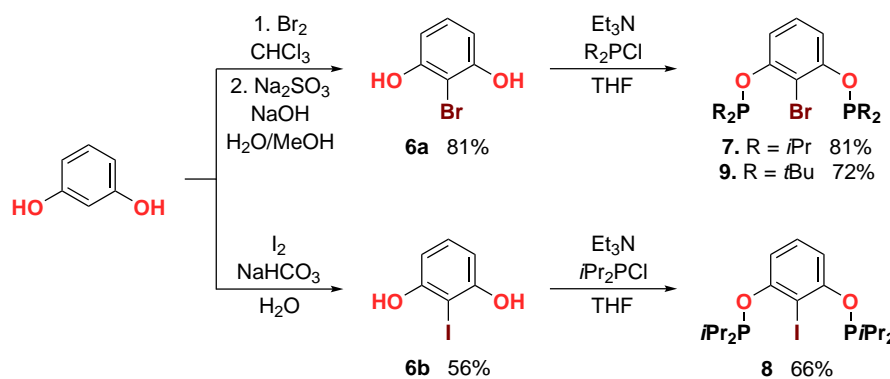
2.1 Synthesis of PCP and POCOP Ligands

For the nitrogen linker 2,6-dinitroaniline was used as starting material, introducing a chloride halogen to the *ipso* carbon (**1**) *via* a Sandmeyer reaction.⁹⁴ Then the nitro groups were reduced to amines (**2**) using $\text{SnCl}_2 \cdot 2\text{H}_2\text{O}$ in ethyl acetate followed by the acetylation of the amines by acetic anhydride in acetic acid. An advantage of this reaction under such conditions was that the acetylated product (**3**) precipitated directly from the reaction mixture and could be isolated where no further purification was necessary for the next reaction step. With LiAlH_4 the newly formed amides were reduced again, back to the amine bearing now an ethyl group (**4**). With *n*-BuLi as base and addition of $i\text{Pr}_2\text{PCl}$ it was possible to isolate the $\text{PCP}^{\text{NEt}}\text{-Cl}$ (**5**) ligand as white solid after recrystallisation from MeOH (scheme 2.2).¹³



Scheme 2.2: Synthesis of ligand **5** composed of nitrogen linkers and chloride as halogen.¹³

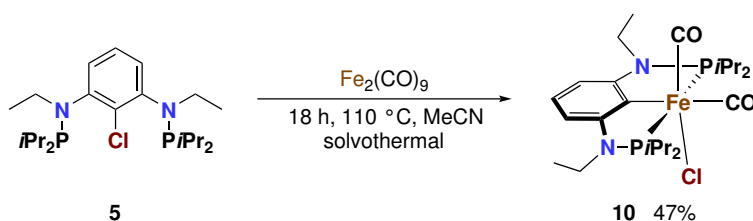
In Scheme 2.3 the synthesis of the respective POCOP ligands are described, where resorcinol was used as starting material. For the POCOP-Br ligands, resorcinol was first treated with bromine in chloroform and then with Na_2SO_3 and NaOH in a mixture of $\text{MeOH}/\text{H}_2\text{O}$, yielding **6a**.⁹⁵ With Et_3N as base and R_2PCl the corresponding POCOP^R-Br (**7**, $\text{R} = i\text{Pr}$; **9**, $\text{R} = t\text{Bu}$) ligands could be synthesised. For the POCOP-I ligand, resorcinol was treated with iodine and NaHCO_3 in water yielding **6b**. With Et_3N as base and $i\text{Pr}_2\text{PCl}$ the POCOP^{*i*Pr}-I ligand **8** could be isolated in a yield of 66%.^{88,89}



Scheme 2.3: Synthesis of the POCOP ligands **7**, **9** and **8**.^{88,89}

2.2 Iron PCP Pincer Complexes

When heating up a mixture of $\text{Fe}_2(\text{CO})_9$ and two equivalents of $\text{PCP}^{\text{NEt}}\text{-Cl}$ (**5**) in acetonitrile to $110\text{ }^\circ\text{C}$ in a sealed glass tube the complex $[\text{Fe}(\text{PCP}^{\text{NEt}}\text{-}i\text{Pr})(\text{CO})_2\text{Cl}]$ (**10**) could be isolated with a yield of 47% as yellow solid (Scheme 2.4). Crystallographic studies reveal a slightly distorted octahedral geometry with bond angles of P1-Fe1-P2 $162.99(5)^\circ$ and C23-Fe1-C1 $177.24(10)^\circ$ where the carbonyl ligands are in *cis* position to each other (Figure 2.1). The bond distance Fe1-C1 with $2.002(2)\text{ \AA}$ is in the expected metrics for such systems.^{29,30,36,37,96} The carbonyl ligands exhibit two resonances in the $^{13}\text{C}\{^1\text{H}\}$ -NMR at 215.6 ($J_{\text{CP}} = 27.4\text{ Hz}$) and 212.7 ppm ($J_{\text{CP}} = 11.6\text{ Hz}$), with the *ipso*-carbon of the ligand observed as a triplet at 137.5 ppm ($J_{\text{CP}} = 14.4\text{ Hz}$). Two strong absorption bands at 2002 and 1934 cm^{-1} detected in the IR (ATR) spectrum are in agreement with a *cis* CO arrangement.



Scheme 2.4: Synthesis of complex **10**.

It seems that only one Fe atom from the metal precursor Fe_2CO_9 reacts with a ligand molecule. Thus the yield is below 50% and not reacted starting material was detected in the reaction mixture using $^{31}\text{P}\{^1\text{H}\}$ -NMR. Using higher reaction temperatures and/or times had no effect on the overall yield. Decreasing the amount of ligand to one equivalent resulted in the formation of a variety of side products that were observed in the $^{31}\text{P}\{^1\text{H}\}$ -NMR, which could not be separated or characterised. Furthermore, instead of an orange reaction mixture a violet one was obtained. Interestingly, the synthesis of complex **10** works with toluene as well as with acetonitrile. With $\text{Fe}(\text{CO})_5$ as metal precursor no conversion to the complex **10** could be observed under the described conditions.

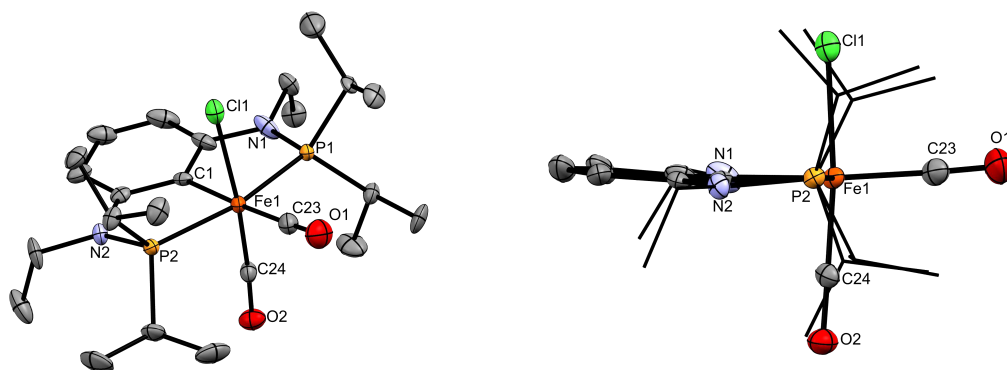
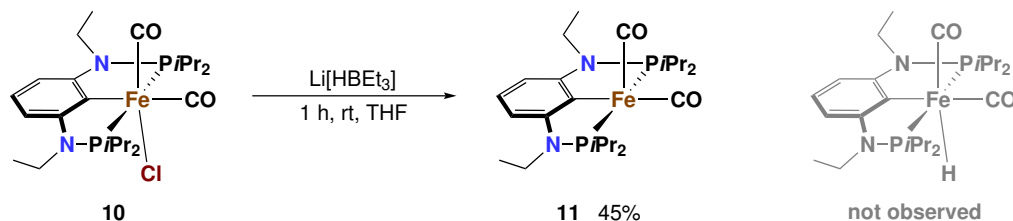


Figure 2.1: ORTEP view of $[\text{Fe}(\text{PCP}^{\text{NEt}}\text{-}i\text{Pr})(\text{CO})_2\text{Cl}]$ (**10**) showing 50% thermal ellipsoids (H atoms omitted for clarity). Selected bond lengths (\AA) and bond angles (deg): Fe1-C1 $2.002(2)$, Fe1-P1 $2.270(2)$, Fe1-P2 $2.2564(7)$, Fe1-Cl1 $2.334(2)$, Fe1-C23 $1.818(3)$, Fe1-C24 $1.713(8)$; P1-Fe1-P2 $162.99(5)$, C23-Fe1-C1 $177.24(10)$.

Treatment of ligand **5** with *n*-BuLi and FeCl_2 as metal precursor in THF under a carbon monoxide atmosphere at low temperatures was futile. At first, an intensive red coloured solution is formed that turns slowly black at room temperature. Only not converted ligand

and side products in the region of 0 - 10 ppm in the $^{31}\text{P}\{^1\text{H}\}$ -NMR could be detected. It seems that the main side-product is a substituted *n*-butyldi-*iso*-propylphosphine which was cleaved off from the ligand. Thus, the reaction was inefficient with different ligands than CO, like TMEDA, 2,2'-bipyridine or NO. Furthermore, some attempts have been made to verify and isolate a formed lithium species of the ligand after treating **5** with *n*-BuLi, similar to the work of Gerhard Müller *et al.*⁹⁷



Scheme 2.5: Formal one electron reduction of **10** with the super hydride $\text{Li}[\text{HBEt}_3]$ to complex **11**.

Due to the interest in hydride species and their versatile application in catalysed hydrogenation reactions,^{9,98} complex **10** was treated with one equivalent of the super hydride $\text{Li}[\text{HBEt}_3]$ in THF for a ligand exchange reaction between the chloride and the hydride. Contrary to expectations no ligand substitution took place and instead a formal one electron reduction of the Fe(II) complex **10** to the Fe(I) complex $[\text{Fe}(\text{PCP}^{\text{NEt-}i\text{Pr}})(\text{CO})_2]$ (**11**) could be observed (Scheme 2.5). This reduction was nicely represented by an instant color change from orange to violet after treating a solution of **10** with super hydride and complex **11** could be isolated with 45% yield as violet solid. Under this reaction condition no hydride species could be detected in the ^1H -NMR in the range between 0 to -50 ppm. A similar reaction was reported by Tonzetich *et al.* where the treatment of a pyrrole based Fe(II) dicarbonyl PNP^{Cy} pincer complex resulted in a likewise one electron reduction after treatment with super hydride.⁵⁸

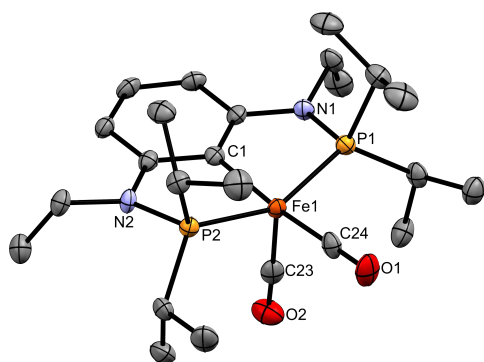


Figure 2.2: ORTEP view of $[\text{Fe}(\text{PCP}^{\text{NEt-}i\text{Pr}})(\text{CO})_2]$ (**11**) showing 50% thermal ellipsoids (H atoms omitted for clarity). Selected bond lengths (Å) and bond angles (deg): Fe1-C1 2.015(3), Fe1-P1 2.1791(8), Fe1-P2 2.1868(8), Fe1-C24 1.772(3), Fe1-C23 1.774(3); P1-Fe1-P2 153.25(3), C24-Fe1-C23 97.5(1), C24-Fe1-C1 172.4(3).

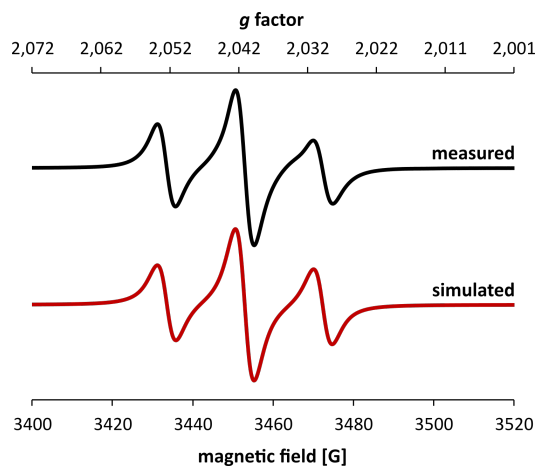
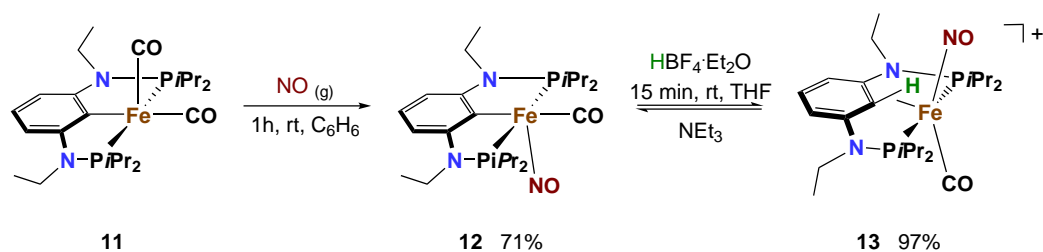


Figure 2.3: X-band EPR spectrum of $[\text{Fe}(\text{PCP}^{\text{NEt-}i\text{Pr}})(\text{CO})_2]$ (**11**) in toluene at 293 K at a microwave frequency of 9.86 GHz. The red line represents a simulation with parameters $g_{\text{iso}} = 2.038$ and $A_{\text{iso},P} = 19.5$ G.

Crystallographic studies of complex **11** reveal a square pyramidal coordination geometry around the metal center where the two carbonyl ligands are still in *cis* position to each

other (Figure 2.2). The bond distance between the *ipso*-carbon and the iron atom is with 2.015(3) Å similar to **10**, while the spacing between the iron and the other atoms are clearly shorter. Two strong absorption bands are exhibited by the carbonyl ligands of complex **11** in the IR at 1933 and 1864 cm⁻¹. Additionally, the SOMO with the unpaired electron was investigated by electron paramagnetic resonance (EPR), DFT calculations and solution magnetic susceptibility measurements. The latter indicates a solution effective magnetic moment of 1.8(1) μ_B (benzene, Evans method) which is in agreement with a low-spin *d*⁷ system having one unpaired electron. For the X-band CW EPR studies, complex **11** was dissolved in toluene and measured at 293 K exhibiting an isotropic triplet with hyperfine coupling (Figure 2.3) between the electron spin (*S* = 1/2) and the nuclear spin of the two phosphorous atoms (*I* = 1/2). The spectrum could be excellently simulated featuring a *g*_{iso} and *A*_{iso,P} value of 2.038 and 19.5 G, respectively, where the former deviates slightly from a free electron (2.002) and is similar to other reported five coordinated low-spin Fe(I) complexes.^{79–82} DFT calculations suggest that the unpaired electron is located at the metal center giving the SOMO *z*² symmetry pointing to the empty sixth coordination position.¹²



Scheme 2.6: Ligand exchange of **11** with NO gas to **12**, followed by reversible protonation with HBF₄·Et₂O to the agostic complex **13**.

After completion of the characterisation of complex [Fe(PCP^{NEt}-*i*Pr)(CO)₂] (**11**) the reactivity was investigated. Treating **11** with a strong acid like HBF₄·Et₂O resulted in the decomposition of the complex and free ligand as well as different side products were observed in the ³¹P{¹H}-NMR spectra. In an attempt to exchange the carbonyl ligands, **11** was dissolved in benzene and stirred under a nitric oxide atmosphere. Instantly a colour change from violet to red could be observed. After removal of the solvent complex [Fe(PCP^{NEt}-*i*Pr)(CO)(NO)] (**12**) could be isolated with a yield of 71% as red solid. When treating this compound with HBF₄·Et₂O in THF the agostic species [Fe(χ³P, CH, P-PCP^{NEt}-*i*Pr)(CO)(NO)]BF₄ (**13**) could be isolated with a yield of 97% (scheme 2.6). Both complexes were diamagnetic and characterised by NMR measurements where a hydride species ([Fe(PCP^{NEt}-*i*Pr)(CO)(NO)H]BF₄) could not be observed. In the ¹³C{¹H}-NMR, complex **12** and **13** exhibit both two triplet resonances at 228.3 (*J*_{CP} = 29.0 Hz), 216.6 (*J*_{CP} = 61.0 Hz) and 137.4 (*J*_{CP} = 24.1 Hz), 66.5 ppm (*J*_{CP} = 3.4 Hz) assignable to the carbonyl ligands and the *ipso*-carbons, respectively. Here, the *ipso*-carbon engaged in the agostic interaction of complex **13** is clearly shifted to the high field, out of the aromatic region with a low coupling constant of *J*_{CH} = 125.6 Hz (*cf.* benzene *J*_{CH} = 157.5 Hz⁹⁹). Another characteristic of such an interaction, is that the agostic hydrogen can easily be removed by a weak base like NEt₃. In the solid state structure the metal center adopts a trigonal bipyramidal coordination geometry with the phosphine ligands in an axial and the other three ligands in an equatorial position. Here, the agostic hydrogen is significantly bent out of the aromatic plane by ca. 29.2° (Figure 2.4). Compared to complex **10** and **11** the bond distance in **13** between the iron and the *ipso*-carbon is clearly longer with 2.158(1) Å. In related agostic PCP Ru, Rh and Co pincer complexes the hydrogen is shifted

out of the aromatic plane by approximately 14, 17 and 35°, respectively and a significantly longer bond distance between the *ipso*-carbon and the metal center is observed.^{100–103}

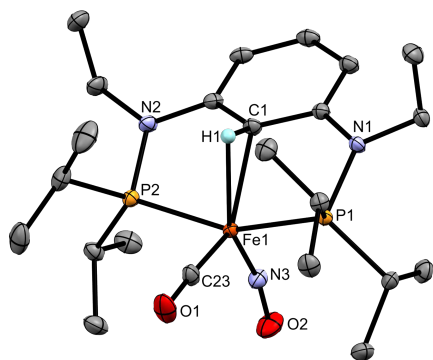


Figure 2.4: ORTEP view of $[\text{Fe}(\chi^3\text{P,CH,P-P}(\text{CH})\text{P}^{\text{iPr}})(\text{CO})(\text{NO})]\text{BF}_4$ (**13**) showing 50% thermal ellipsoids (H atoms omitted for clarity). Selected bond lengths (Å) and bond angles (deg): Fe1-C1 2.158(1), Fe1-N3 1.672(1), Fe1-C23 1.761(1), Fe1-P2 2.2596(4), Fe1-P1 2.22690(4), F1-H1 1.94(2), C1-H1 1.0(2); N3-Fe1-C23 113.17(5), C23-Fe1-C1 136.24(5), P2-Fe1-P1 154.72(2), Fe1-N3-O2 163.63(10).

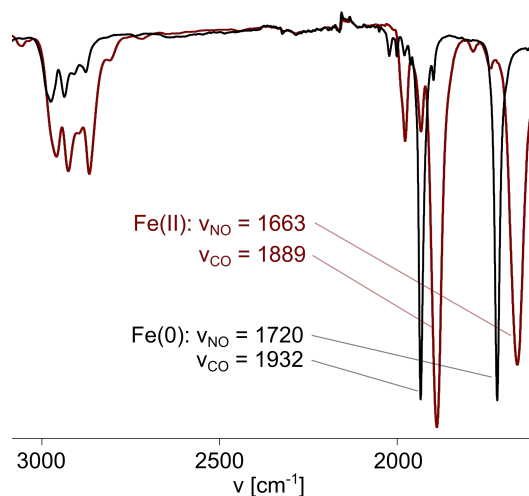


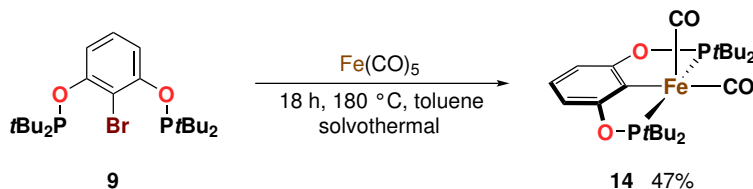
Figure 2.5: Overlay of a selected part from the IR spectra of $[\text{Fe}(\text{II})(\text{PCP}^{\text{iPr}})(\text{CO})(\text{NO})]$ (**12**, red line) and $[\text{Fe}(\text{0})(\chi^3\text{P,CH,P-P}(\text{CH})\text{P}^{\text{iPr}})(\text{CO})(\text{NO})]\text{BF}_4$ (**13**, black line).

The determination of the oxidation state of **12** and **13** was not straightforward since the nitric oxide radical can either be counted as NO^+ or NO^- . Even though the nitrosyl ligand in **13** is slightly bent with a bond angle of $\text{Fe1-N3-O2 } 163.63(10)^\circ$ (Figure 2.4) it most likely coordinates in a linear fashion¹⁰⁴ as NO^+ to the metal center. In the IR the stretching frequencies for CO and NO are observed at 1932 and 1720 cm^{-1} . With the support of DFT calculation and comparison to similar reported low-spin d^7 Fe(I) systems including $[\text{Fe}(\text{PNP}^{\text{Me-iPr}})(\text{NO})\text{Cl}]^+$ ⁸¹ with $\nu(\text{NO})$ 1751 cm^{-1} ($\text{Fe-N-O } 177.0(1)^\circ$) and $[\text{Fe}(\text{PNP}^{\text{O-iPr}})(\text{CO})(\text{NO})]^+$ ¹⁰⁵ with $\nu(\text{CO})$ 1948 and $\nu(\text{NO})$ 1732 cm^{-1} ($\text{Fe-N-O } 164.9(2)^\circ$), we suggest that the agostic **13** species adopts a metal oxidation state that has more Fe(0) character. Complex **12** on the other hand has stretching frequencies at lower wave numbers with CO and NO at 1889 and 1663 cm^{-1} , respectively, indicating a NO^- bonding mode (Figure 2.5). These suppositions are supported by DFT calculation which leads to a metal oxidation state closer to Fe(II) than to Fe(0) for complex **12**.¹²

Comparison of Fe POCOP Pincer Complexes

Treating a solution of $\text{POCOP}^{\text{R-Br}}$ ($\text{R} = \text{iPr}$ or Ph) ligand in toluene with $\text{Fe}_2(\text{CO})_9$ in a sealed glass tube at 130 - 180 °C an orange solution was formed with two different diamagnetic species, that gave rise to two resonances as singlets at 174.0 and 162.6 ppm with some smaller by-products in the $^{31}\text{P}\{^1\text{H}\}$ -NMR. The substance that gave rise to the signal at 162.6 ppm could be extracted with *n*-pentane in modest purity which yielded a yellow solid that exhibited two strong absorption bands at 1997 and 1942 cm^{-1} in the IR spectrum. In contrast to the nitrogen linker ligand (**5**) the POCOP ligands, bearing an oxygen linker, did react under these reaction conditions with $\text{Fe}(\text{CO})_5$. In this case three species could be detected in the $^{31}\text{P}\{^1\text{H}\}$ -NMR where two signals had the same chemical shift as previously described and the third one was observed at 167.0 ppm. If acetonitrile was used as a solvent, the same species were formed as described before with the formation of other various by-products. On a side note, no signal from the free ligand

could be detected in any of the finished reaction mixtures. None of these formed species detected in the $^{31}\text{P}\{^1\text{H}\}$ -NMR could be separated and characterised. Thus, it was not possible yet, to synthesise the oxygen linker analogous to **10** with the $\text{POCOP}^{\text{R}}\text{-Br}$ ($\text{R} = i\text{Pr}$ or Ph) ligands under solvothermal conditions. It is noteworthy that the treatment of an related $\text{PCP}^{\text{CH}_2}\text{-Br}$ ligand with carbon linkers and $i\text{Pr}_2\text{P}$ donors could be treated with $\text{Fe}_2(\text{CO})_9$ under solvothermal condition to yield $[\text{Fe}(\text{PCP}^{\text{CH}_2}\text{-}i\text{Pr})(\text{CO})_2\text{Br}]$.⁹⁶

Scheme 2.7: Synthesis of complex **14**

Interestingly, when heating up a solution of $\text{POCOP}^{t\text{Bu}}\text{-Br}$ (**9**) with $\text{Fe}(\text{CO})_5$ in toluene to $180\text{ }^\circ\text{C}$ in a sealed glass tube over night, a green solution was formed. After removal of all volatiles the paramagnetic complex $[\text{Fe}(\text{POCOP}\text{-}t\text{Bu})(\text{CO})_2]$ (**14**) could be extracted with *n*-pentane and isolated with a yield of 47% as green solid (scheme 2.7). Crystallographic studies reveal a distorted square pyramidal coordination geometry around the metal center with the bond distance of Fe1-C1 $1.990(4)\text{ \AA}$ being marginal shorter compared to complex **11** but in the expected bond metrics for such systems (Figure 2.6).^{29,30,36,37,96} The carbonyl ligands are in *cis* position to each other and exhibit two strong absorptions bands in the IR at 1933 and 1864 cm^{-1} . A solution effective magnetic moment of $1.8(1)\text{ }\mu_{\text{B}}$ (benzene, Evans method) is in agreement with a low-spin d^7 system. In order to investigate the frontier orbitals, an EPR measurement of a frozen toluene solution of complex **14** at 150 K was performed on an CW X-band spectrometer. The results are shown in Figure 2.7 and the spectrum could be simulated properly. At this temperature a rhombic splitting ($g_x = 2.044$, $g_y = 2.034$ and $g_z = 1.991$) and a well resolved hyperfine coupling between the unpaired electron ($S = 1/2$) and the nucleus of the two ^{31}P atoms ($I = 1/2$) is observed. Moreover, the observed g values can be well compared to other reported five coordinated $\text{Fe}(\text{I})$ low spins systems and all feature g values close to 2.0 .⁷⁹⁻⁸² The fate of the bromide and other remaining equivalents of the starting materials could not be established yet, while no free ligand could be detected in the finished reaction mixtures by $^{31}\text{P}\{^1\text{H}\}$ -NMR. Additionally, it is noteworthy that the reaction does work with $\text{Fe}(\text{CO})_5$ and can be performed nearly equally good with $\text{Fe}_2(\text{CO})_9$ too, while the nitrogen linker ligand **5** did only react with the latter.

Treatment of complex **14** with $\text{HBF}_4\cdot\text{Et}_2\text{O}$ resulted in decomposition and only free protonated ligand could be observed in the NMR. When adding *n*-BuLi to ligand **9** a similar decomposition could be observed as for the nitrogen linker **5** where mostly substituted *n*-butyl-di-*iso*-propylphosphine was formed which was cleaved off from the ligand when the reaction mixture reached a temperature of approximately $-40\text{ }^\circ\text{C}$. However, after treating a $\text{POCOP}^{\text{R}}\text{-X}$ ligand with BuLi at $-70\text{ }^\circ\text{C}$ and adding $\text{FeBr}_2\cdot x\text{THF}$ under a CO gas atmosphere or $\text{Fe}(\text{bipyridine})\text{Br}_2$ to the mixture, a red or violet solution was formed, respectively. The former always turned black when reaching room temperature and only free ligand and by-products in the region of 60 to 0 ppm could be observed while the latter showed, besides from similar by-products, a singlet with a chemical shift of 218.9 ppm . It was not possible yet to isolate and characterise the formed species mainly due to the poor reproducibility of these reactions.

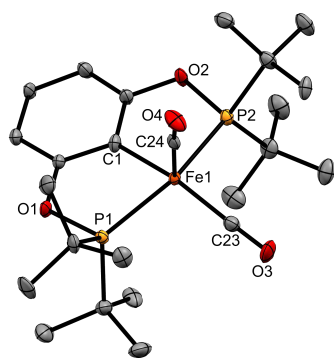


Figure 2.6: ORTEP view of $[\text{Fe}(\text{POCOP-}t\text{Bu})(\text{CO})_2]$ (**14**) showing 50% thermal ellipsoids (H atoms omitted for clarity). Selected bond lengths (Å) and bond angles (deg): Fe1-C24 1.781(4), Fe1-C23 1.795(5), Fe1-C1 1.990(4), Fe1-P2 2.2356(13), Fe1-P1 2.2384(13); C24-Fe1-C23 92.7(2), C24-Fe1-C1 107.00(17), P2-Fe1-P1 155.46(5).

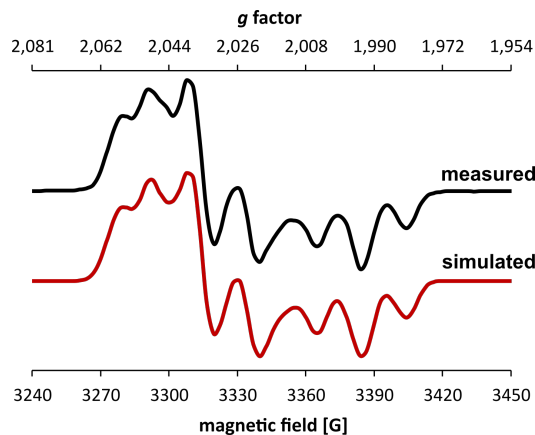
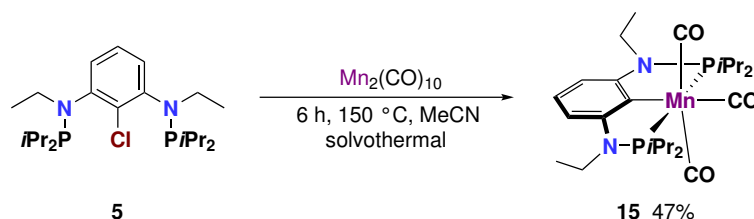


Figure 2.7: X-band EPR spectrum of $[\text{Fe}(\text{POCOP-}t\text{Bu})(\text{CO})_2]$ (**14**) in toluene at 100 K at a microwave frequency of 9.86 GHz. The red line represents a simulation with parameters $g_x = 2.044$, $g_y = 2.034$ and $g_z = 1.991$ and $A_x = 20.31$ G, $A_y = 22.47$ G and $A_z = 14.48$ G.

2.3 Manganese PCP Pincer Complexes

The complex $[\text{Mn}(\text{PCP}^{\text{NEt}}-i\text{Pr})(\text{CO})_3]$ (**15**) can be synthesised by stirring a suspension of the metal precursor $\text{Mn}_2(\text{CO})_{10}$ with the nitrogen linker ligand PCP^{NEt} (**5**) in a sealed glass tube at 150 °C for 6 h. After a work up procedure, complex **15** can be isolated in analytically pure form as white solid with a yield of 47% (Scheme 2.8). In this reaction the ligand works as oxidizing agent and breaks the Mn-Mn bond of the metal precursor. It was not possible yet to clarify the fate of the chloride atom and the remaining Mn fragment but it needs to be mentioned that in the finished reaction mixture free ligand was not detected by NMR measurements. While the isolated complex is colourless the reaction mixture was red which turned instantly brown when exposed to air. Interestingly, complex **15** is completely air stable and the purification process could be done by a silica gel chromatography under ambient conditions.



Scheme 2.8: Synthesis of **15**.

Investigation of the solid state structure reveals a distorted octahedral coordination geometry around the metal center where the angle between P1-Mn-P2 163.37(3)° and C25-Mn-C24 163.6(1)° deviates distinctly from 180° (Figure 2.8). The bond distance of Mn1-C1 2.049(2) Å and other bond metrics are in the expected range and are similar to a related manganese PCP pincer complex featuring carbon linkers.⁹⁶ Here, the tridentate ligand coordinates in an equatorial and the three carbonyl ligands in a meridional fashion to the metal center. The latter exhibits three strong absorption bands at 1912, 1900 and 1884 cm^{-1} and two broad unresolved resonances in a 2:1 ratio at 225.2 (br) and 222.6 ppm ($J_{\text{CP}} = 24.1$ Hz) in the IR and $^{13}\text{C}\{^1\text{H}\}$ -NMR spectrum, respectively. The *ipso*-carbon

can be detected as a triplet at 132.8 ppm ($J_{\text{CP}} = 10.7$ Hz). It is worth noting that the synthesis of related $[\text{Mn}(\text{POCOP-}i\text{Pr})(\text{CO})_3]$ and $[\text{Mn}(\text{PCP}^{\text{CH}_2-}i\text{Pr})(\text{CO})_3]$ ⁹⁶ PCP pincer complexes with the oxygen linker ligand (**7**) and the carbon linker ligand ($\text{PCP}^{\text{CH}_2-}i\text{Pr}$) works identically under solvothermal conditions as described above. In contrast, no conversion was achieved by treatment of analogous PCP ligands featuring $t\text{Bu}_2\text{P}$ donors and oxygen or carbon linkers with $\text{Mn}_2(\text{CO})_{10}$ under solvothermal conditions even when increasing the reaction temperatures up to nearly 200 °C.

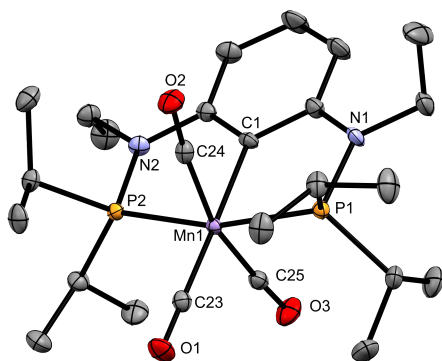


Figure 2.8: ORTEP view of $[\text{Mn}(\text{PCP}^{\text{NEt-}}i\text{Pr})(\text{CO})_3]$ (**15**) showing 50% thermal ellipsoids (H atoms omitted for clarity). Selected bond lengths (Å) and bond angles (deg): Mn1-C23 1.804(3), Mn1-C25 1.820(3), Mn1-C24 1.825(3), Mn1-C1 2.049(2), Mn1-P2 2.2551(7), Mn1-P1 2.2648(8); P2-Mn1-P1 163.37(3), C25-Mn1-C24 163.6(1), C23-Mn1-C1 179.0(1).

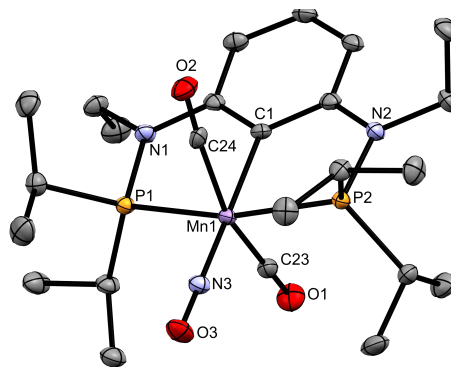
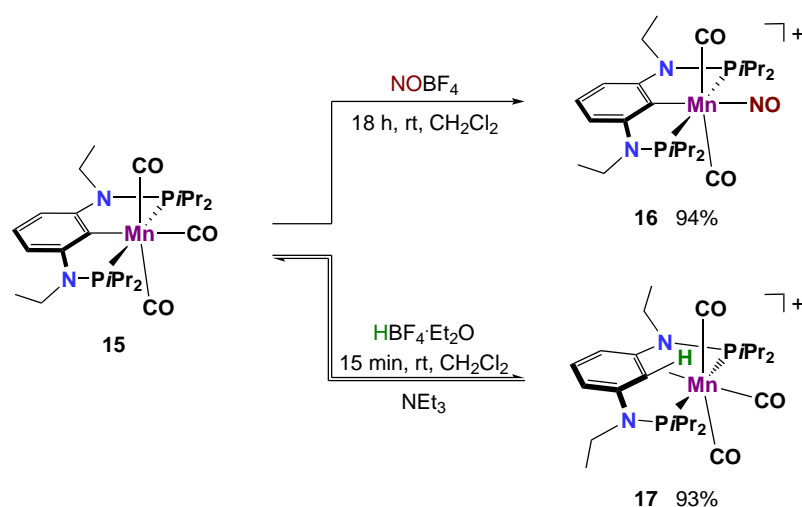


Figure 2.9: ORTEP view of $[\text{Mn}(\text{PCP}^{\text{NEt-}}i\text{Pr})(\text{CO})_2(\text{NO})]\text{BF}_4$ (**16**) showing 50% thermal ellipsoids (H atoms omitted for clarity). Selected bond lengths (Å) and bond angles (deg): Mn1-C23 1.804(3), Mn1-C1 2.064(2), Mn1-N3 1.864(2), Mn1-C24 1.866(2), Mn1-P1 2.3115(8), Mn1-P2 2.3123(7); P1-Mn1-P2 162.58(3), C23-Mn1-C24 159.4(1), Mn1-N3-O3 178.5(2).

After finishing the characterisation of complex **15** the reactivity was investigated similarly to the Fe complex **10**. In this context, no ligand exchange reaction could be observed when treating a solution of the tricarbonyl manganese pincer complex with NO gas or $\text{CN}t\text{Bu}$ which indicates very strongly coordinated carbonyl ligands to the metal center. This is partially reflected in the ESI-HMS (positive ion) where the complete molecule ion $[\text{M}]^+$ (m/z 534.1964) could be detected. However, adding NOBF_4 to a CH_2Cl_2 solution of **15**, one of the carbonyl ligands coordinated to the metal center was exchanged with NO^+ . After a small work up the cationic complex $\text{trans-}[\text{Mn}(\text{PCP}^{\text{NEt-}}i\text{Pr})(\text{CO})_2(\text{NO})]\text{BF}_4$ (**16**) could be isolated with a yield of 94% as red solid (Scheme 2.9). Evidence of the *cis*-isomer has not been found. Interestingly, both ligand types coordinate in a strongly bound fashion to the metal center. In the ESI-MS, the fully intact cationic molecule $[\text{M}]^+$ (m/z 536.2) could be detected in addition to the cationic fragment $[\text{M-2CO}]^+$ (m/z 480.2) due to the loss of two carbonyl ligands. This indicates that the NO is more strongly bound to the metal center than both CO ligands. In the solid state structure the angle of Mn1-N3-O3 178.5(2)° is nearly linear which indicates that the nitric oxide is coordinated as NO^+ to the metal center making it clearly Mn(I) which is supported by DFT calculations.¹³ With bond angles of 162.58(3) and 159.4(1)° for P1-Mn1-P2 and C23-Mn1-C24, respectively, the metal center adopts a clearly distorted octahedral coordination geometry (Figure 2.9). The bond distance Mn1-C1 is with 2.064(2) Å nearly identical as its precursor. In the $^{13}\text{C}\{^1\text{H}\}$ -NMR the carbonyl and *ipso*-carbon resonances could not be detected. Such occurrences can happen due to the quadrupole moments of ^{55}Mn ($I = 5/2$) with a relative abundance of 100%.¹⁰⁵ However, in the IR spectra three strong absorption bands of the two carbonyl and NO ligands can be detected at 2017, 1913 and 1767 cm^{-1} , respectively.

Treating a CH_2Cl_2 solution of $[\text{Mn}(\text{PCP}^{\text{NEt}_3-i\text{Pr}})(\text{CO})_3]$ (**15**) with $\text{HBF}_4 \cdot \text{Et}_2\text{O}$ for 15 min at room temperature the agostic cationic complex $[\text{Mn}(\chi^3\text{P}, \text{CH}, \text{P-P}(\text{CH})\text{P}^{\text{NEt}_3-i\text{Pr}})(\text{CO})_3]\text{BF}_4$ (**17**) could be isolated with a yield of 93% as yellow solid (Scheme 2.9). Evidence of a formed hydride species has not been found. In the solid state structure a distorted trigonal bipyramidal coordination geometry around the metal center is adopted. Thus, the $\eta^2\text{-C}_{\text{aryl}}\text{-H}$ and the carbonyl ligands are located in an equatorial plane with the phosphine moieties in an axial position (Figure 2.10). The bond distance of Mn1-C1 2.249(2) Å is clearly elevated in relation to complex **15** and the agostic H is removed from the aromatic plane by ca. 31.2° (C4-C1-H1). All the other bond metrics are in the expected range and other similar system with agostic interaction feature bond distances between the *ipso*-carbon and the metal center of 2.323(2), 2.433(1), 2.2917(6) and 2.395(4) Å with the agostic hydrogen elevated from the aromatic plane by approximately 32, 28, 35 and 30° for Cr, Mo^{50} , Co^{103} and Ru^{106} PCP pincer complexes.



Scheme 2.9: Ligand exchange reaction of **15** with NO and reversible protonation.

Despite the bond distance being between C1-H1 of 0.97(3) Å of complex **17**, which is in the area of non-activated hydrocarbons (*cf.* 1.08 Å for benzene⁹⁹), the agostic hydrogen can be easily removed using a weak base like Et_3N . Furthermore, the agostic C-H interaction can be well monitored with NMR measurements where the hydrogen exhibits a poorly resolved triplet in the ^1H -NMR, that is shifted significantly into the high-field region to 1.36 ppm ($J_{\text{HP}} = 4.6$ Hz). The *ipso*-carbon resonance is detected at 48.8 ppm in the $^{13}\text{C}\{^1\text{H}\}$ -NMR and is therefore clearly shifted out of the aromatic region. In an HSQC experiment the cross-peak between the H1 and C1 atoms can be observed (Figure 2.11 top). Another characteristic is the low coupling constant $J_{\text{CH}} = 127.9$ Hz of the *ipso*-carbon with the agostic hydrogen compared to the other two $\text{C}_{\text{aryl}}\text{H}$ resonances featuring coupling constants of $J_{\text{CH}} = 161.0$ and $J_{\text{CH}} = 165.1$ Hz (*cf.* benzene $J_{\text{CH}} = 157.5$ Hz⁹⁹; Figure 2.11 bottom). These lower coupling constants observed for $\eta^2\text{-C}_{\text{aryl}}\text{-H}$ interactions are distinctively for strong C-H metal interaction.^{50,101,103,106–108} In addition, the carbonyl ligands exhibit three modest resolved triplets at 221.7 (br), 216.7 ($J_{\text{CP}} = 17.9$ Hz) and 215.0 ($J_{\text{CP}} = 19.1$ Hz) ppm and three strong absorption bands at 1942, 1899 and 1880 cm^{-1} in the $^{13}\text{C}\{^1\text{H}\}$ -NMR and IR spectrum, respectively. Similar to the metal precursor **15** and the cationic nitrosyl PCP pincer species **16**, the carbonyl ligands of complex **17** are strongly coordinated to the metal center. In the ESI-HMS (positive ion) the fully intact cationic molecule $[\text{M}]^+$ (m/z 535.2042) could be detected.

On the other hand oxidative addition of $[\text{Mn}(\text{PCP}^{\text{NEt-}i\text{Pr}})(\text{CO})_3]$ (**15**) with bromine or different fluorinating agents like F-TEDA or 1-Fluoro-2,4,6-trimethylpyridinium triflate were futile and resulted in the decomposition of the starting material. It is noteworthy that in previous works the successful oxidative addition of related molybdenum pincer complexes were reported.^{109,110}

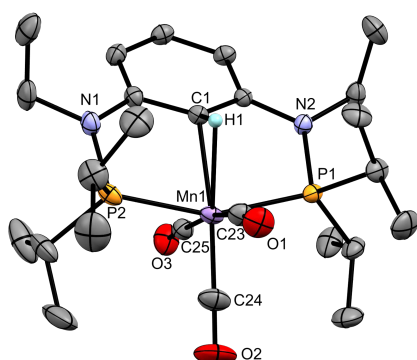


Figure 2.10: ORTEP view of $[\text{Mn}(\chi^3\text{P},\text{CH},\text{P}-\text{P}(\text{CH})\text{P}^{\text{NEt-}i\text{Pr}})(\text{CO})_3]\text{BF}_4$ (**17**) showing 50% thermal ellipsoids (H atoms omitted for clarity). Selected bond lengths (Å) and bond angles (deg): Mn1-C24 1.789(2), Mn1-C23 1.839(2), Mn1-C25 1.845(2), Mn1-C1 2.249(2), Mn1-P2 2.3142(8), Mn1-P1 2.3147(7), Mn1-H11.99(3), C1-H1 0.97(3); P2-Mn1-P1 157.74(2), C23-Mn1-C25 171.01(9), C24-Mn1-C1 164.67(9).

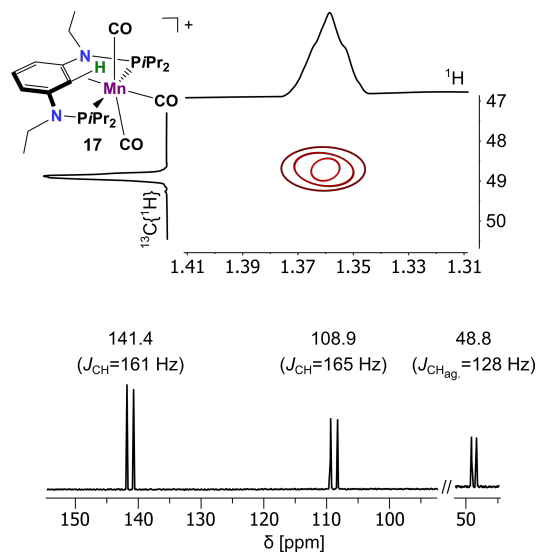
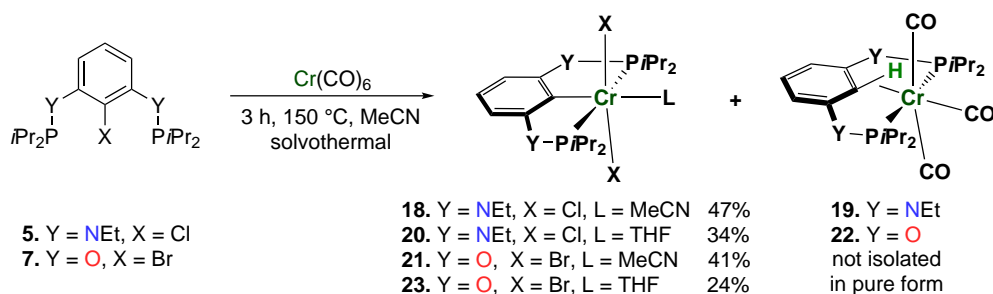


Figure 2.11: Selected parts of a HSQC (top) and ^{13}C with no decoupling of $[\text{Mn}(\chi^3\text{P},\text{CH},\text{P}-\text{P}(\text{CH})\text{P}^{\text{NEt-}i\text{Pr}})(\text{CO})_3]\text{BF}_4$ (**17**).

2.4 Chromium PCP Pincer Complexes

When heating up a mixture of $\text{PCP}^{\text{NEt-}i\text{Pr}}\text{-Cl}$ (**5**) and $\text{Cr}(\text{CO})_6$ in MeCN in a sealed glass tube at 150 °C for 3 h a mixture of the two complexes *trans*- $[\text{Cr}(\text{III})(\text{PCP}^{\text{NEt-}i\text{Pr}})\text{Cl}_2(\text{CH}_3\text{CN})]$ (**18**) and $[\text{Cr}(0)(\chi^3\text{P},\text{CH},\text{P}-\text{P}(\text{CH})\text{P}^{\text{NEt-}i\text{Pr}})(\text{CO})_3]$ (**19**) was formed (Figure 2.10).⁸⁸

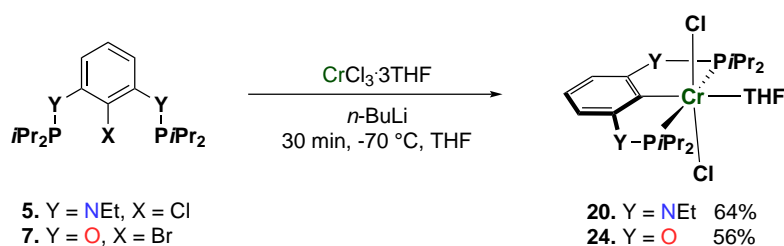


Scheme 2.10: Synthesis of chromium PCP^iPr pincer complexes with N and O linkers.

Both species could be separated from each other, whereby **18** was isolated in pure form with a yield of 47% as red solid by precipitation from a CH_2Cl_2 solution by adding *n*-pentane. The agostic complex **19** remained in solution and could be characterised but the isolated product was contaminated with approximately 10% of unknown impurities. However, the ^1H and $^{31}\text{P}\{^1\text{H}\}$ -NMR measurements of **19** were in agreement with a reported analogous agostic chromium PCP pincer complex (with NMe linkers).⁵⁰ This reaction was performed

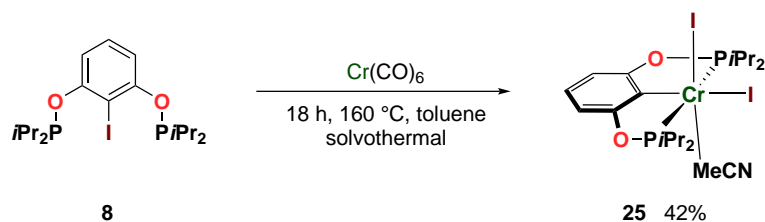
in toluene too where complex **20** could be isolated in pure form after recrystallisation from THF and complex **19** remained in solution.

When treating $\text{POCOP}^{i\text{Pr}}\text{-Br}$ (**7**) with $\text{Cr}(\text{CO})_6$ in MeCN in a sealed glass tube at 150 °C for 3 h a mixture of the analogous oxygen linker complexes *trans*-[Cr(III)(POCOP-*i*Pr)Br₂(CH₃CN)] (**21**) and [Cr(0)($\chi^3\text{P}$, *CH*, *P*-PO(CH)OP-*i*Pr)(CO)₃] (**22**) were formed and isolated with the same procedure as described above (Figure 2.10).⁸⁹ This reaction also was performed in toluene where complex **23** could be isolated in pure form after recrystallisation from THF and complex **22** remained in solution. In this context, treating the carbon linker analogous ligand $\text{PCP}^{\text{CH}_2}\text{-Br}$ with $\text{Cr}(\text{CO})_6$ under similar solvothermal condition, resulted in the formation of a mixture of the corresponding complexes *trans*-[Cr(III)(PCP^{CH₂}-*i*Pr)Br₂(CH₃CN)] and [Cr(0)($\chi^3\text{P}$, *CH*, *P*-P(CH)P^{CH₂}-*i*Pr)(CO)₃].¹¹¹ The source of the agostic hydrogen in complexes **19** and **22** could not be determined, but it is most likely that the agostic proton derived from traces of water or solvent.



Scheme 2.11: Another procedure for synthesising Cr(III) pincer complexes **20** and **24**.

Furthermore, it was possible to synthesise the two complexes **20** and *trans*-[Cr(III)(POCOP-*i*Pr)Cl₂(THF)] (**24**) with another procedure by treating ligand **5** or **7** with *n*-BuLi in THF at -70 °C and then adding $\text{CrCl}_3 \cdot 3\text{THF}$ as metal precursor. Both complexes could be obtained in slightly better yield of 64% and 56%, respectively, compared to the solvothermal method (Scheme 2.11). Here, an important parameter during the addition of *n*-BuLi is the temperature which should not exceed -60 °C. Otherwise it is possible that *i*Pr₂P will be cleaved from the ligand and *n*-butyldi-*iso*-propylphosphine is formed.



Scheme 2.12: Synthesis of the *cis* Cr pincer complex **25**.

Contrary to our expectation, when treating $\text{POCOP}^{i\text{Pr}}\text{-I}$ (**8**) with $\text{Cr}(\text{CO})_6$ in a sealed glass tube at 180 °C for 18 h a mixture of *cis*-[Cr(III)(POCOP-*i*Pr)I₂(CH₃CN)] (**25**) and **22** were formed and isolated with the same procedure as described above (Scheme 2.12). Complex **25** was isolated as red solid with a yield of 42%. In addition, changing the amount of ligand during the reaction described in schemes 2.10 - 2.11 to two equivalent had no effect on the outcome and in addition to the formed complexes, unreacted ligand was detected in the ³¹P{¹H}-NMR.

Solution magnetic susceptibility measurements of the paramagnetic Cr(III) complexes (**18**, **20**, **21** and **23** - **25**) with effective magnetic moments of 3.8 - 4.0(1) μ_B (CH₂Cl₂, Evans method) are in agreement with *d*³ high-spin species (three unpaired electrons).

Most reported chromium(III) pincer complexes feature three unpaired electrons with a d^3 configuration.^{111–115} Crystals for X-ray analysis in sufficient quality could be obtained for complex **18** (Figure 2.12), **20** (Figure 2.13), **23** (Figure 2.14) and **25** (Figure 2.15) with selected bond lengths and angles given in the caption. All structures adopt a slightly distorted octahedral coordination geometry around the metal center. The bond lengths between the *ipso*-carbon and the chromium are very similar with approximately 2.05 – 2.07 Å and the remaining bond metrics are in the expected range compared to related chromium pincer complexes.^{113–115} In these structures, the chloride and bromide are in *trans*-position while the iodide atoms are in *cis*-position to each other.

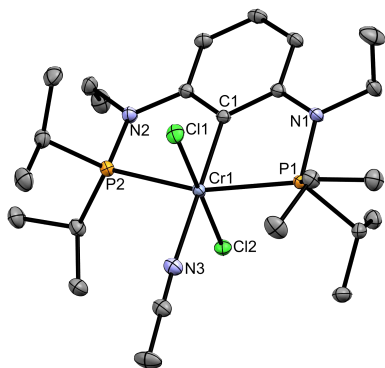


Figure 2.12: ORTEP view of *trans*-[Cr(PCP^{NEt}-*i*Pr)Cl₂(CH₃CN)] (**18**) showing 50% thermal ellipsoids (H atoms omitted for clarity). Selected bond lengths (Å) and bond angles (deg): Cr1-C1 2.0515(12), Cr1-N3 2.1310(12), Cr1-Cl1 2.3211(4), Cr1-Cl2 2.3211(4), Cr1-P1 2.4506(4), Cr1-P2 2.4582(4); C1-Cr1-N3 179.58(5), Cl1-Cr1-Cl2 179.399(16), P1-Cr1-P2 160.731(14).

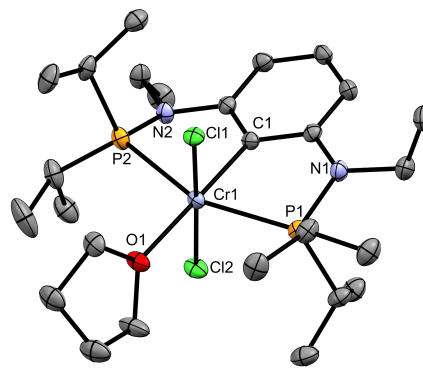


Figure 2.13: ORTEP view of *trans*-[Cr(PCP^{NEt}-*i*Pr)Cl₂(THF)] (**20**) showing 50% thermal ellipsoids (H atoms omitted for clarity). Selected bond lengths (Å) and bond angles (deg): Cr1-C1 2.063(2), Cr1-O1 2.1658(16), Cr1-Cl1 2.3238(6), Cr1-Cl2 2.3024(6), Cr1-P1 2.4789(7), Cr1-P2 2.4791(7); C1-Cr1-O1 179.20(8), Cl1-Cr1-Cl2 175.59(2), P1-Cr1-P2 156.95(3).

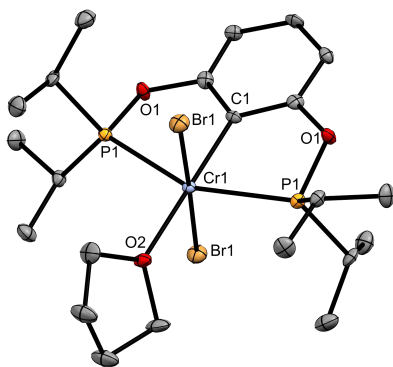


Figure 2.14: ORTEP view of *trans*-[Cr(POCOP-*i*Pr)Br₂(THF)] (**23**) showing 50% thermal ellipsoids (H atoms omitted for clarity). Selected bond lengths (Å) and bond angles (deg): Cr1-C1 2.067(5), Cr1-O2 2.153(4), Cr1-Br1 2.46630(6), Cr1-P1 2.4812(7); C1-Cr1-O2 180.0, Br1-Cr1-Br1 177.85(5), P1-Cr1-P1 153.27(6).

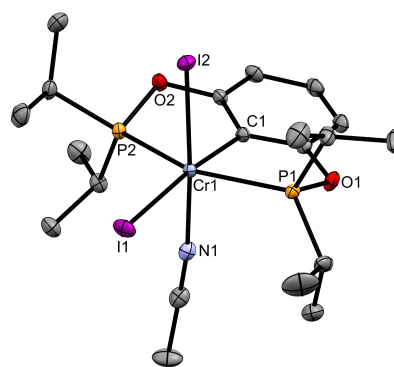
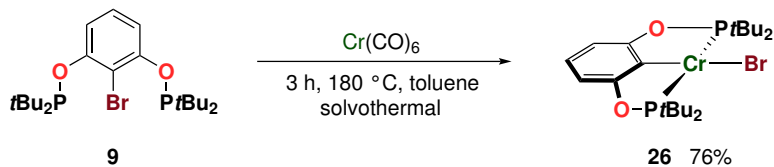


Figure 2.15: ORTEP view of *cis*-[Cr(POCOP-*i*Pr)I₂(MeCN)] (**25**) showing 50% thermal ellipsoids (H atoms omitted for clarity). Selected bond lengths (Å) and bond angles (deg): Cr1-I1 2.7445(5), Cr1-I2 2.6700(5), Cr1-P1 2.4751(6), Cr1-P2 2.4493(6), Cr1-C1 2.0708(17), Cr1-N1 2.0596(18); I1-Cr1-C1 174.25(5), P1-Cr1-P2 151.977(19), N1-Cr1-I2 175.86(5).

Investigation of the chemical properties of these Cr(III) pincer complexes focused on the reduction with different reducing agents like KC₈, sodium naphthalenide or cobaltocene under a N₂ atmosphere. The goal was to achieve the activation of nitrogen which was

reported for a similar molybdenum pincer system by Schrock *et al.*⁹⁰ However, it was not possible to isolate any reduced chromium species regardless of which solvents or reaction conditions were used. Exposure to NO gas had no effect either and an absorption band was never observed in the IR.



Scheme 2.13: Synthesis of the four coordinated Cr(II) complex **26**.

Interestingly, when heating up a mixture of POCOP^{*t*Bu}-Br (**9**) with Cr(CO)₆ in a sealed glass tube at 180 °C for 3 h the four coordinated 12 electron complex [Cr(POCOP-*t*Bu)Br] (**26**) could be isolated in analytical pure form directly from the reaction mixture as red crystalline solid with a yield of 76% (Scheme 2.13). Single crystals suitable for X-ray diffraction measurement could be collected directly from the precipitated solid of the reaction solution. The structure shows a distorted square planar coordination geometry around the metal center with bond angles Br1-Cr1-C1 and P1-Cr1-P2 being 178.78(7) and 154.03(3)°, respectively (Figure 2.16). The bond length of C1-Cr1 with 2.084(3) Å and the remaining bond metrics are similar to the previous described molecular structures of the Cr(III) pincer complexes along with a related Cr(II) aryl complex.¹¹⁶ The solution effective magnetic moment of 4.8(4) μ_B (CH₂Cl₂, Evans method) is in agreement with a *d*⁴ high spin configuration (four unpaired electrons). Organometallic complexes with an electron count of 12 are very rare especially for first row transition elements and only a few were reported in the literature.^{117,118} With four unpaired electrons this complex is surprisingly thermally stable but as expected very sensitive to air. When a solution of **26** was exposed to ambient atmosphere the colour changed within seconds from red to brown and in the ³¹P{¹H}-NMR free and oxidized ligand was detected. As solid it decomposed within one hour completely and the colour changed from red to green.

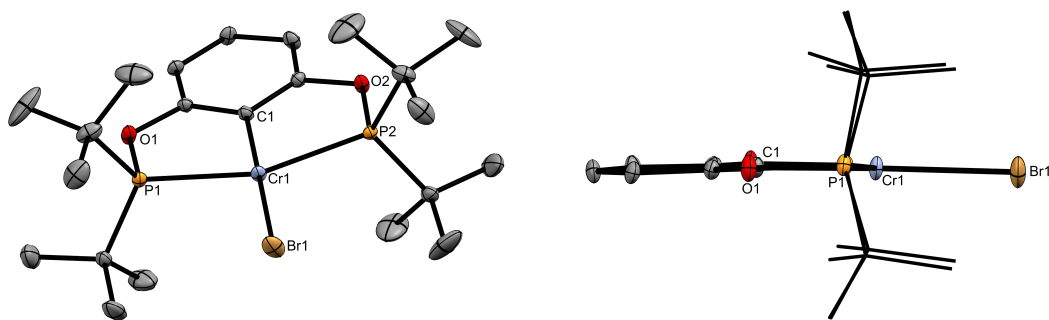
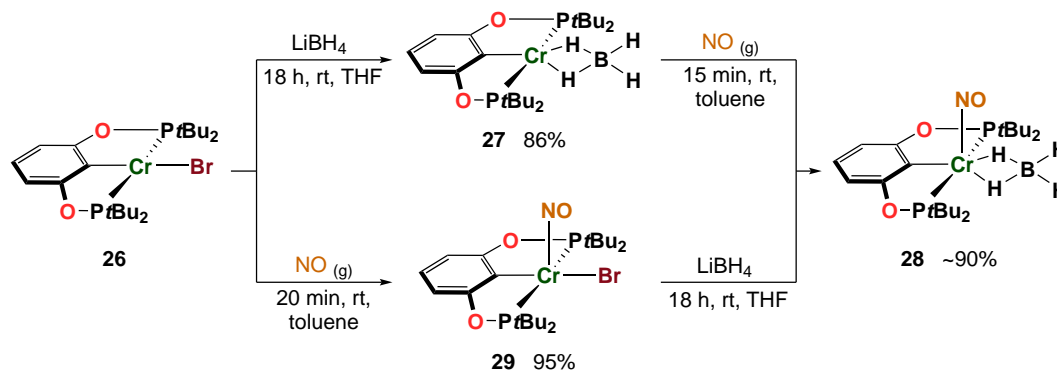


Figure 2.16: ORTEP view of [Cr(POCOP-*t*Bu)Br] (**26**) showing 50% thermal ellipsoids (H atoms omitted for clarity). Selected bond lengths (Å) and bond angles (deg): Br1-Cr1 2.4527(7), Cr1-P1 2.4566(10), Cr1-P2 2.4566(10), Cr1-C1 2.084(3); Br1-Cr1-C1 178.68(6), P1-Cr1-P2 154.08(3).

After concluding the characterisation of complex **26**, the catalytic activity and chemical reactivity was investigated. Hydrosilylation of 4'-fluoroacetophenone with Et₃SiH and hydrogenation of 4'-fluoroacetophenone and phenylacetylene with hydrogen gas showed absolutely no conversion of the substrate regardless of the reaction time, temperature and used solvent (THF, CH₂Cl₂, toluene and dme). Reduction of **26** with KC₈ and treatment with N₂ gas or azobenzene showed no sign of reactivity. Neither could the formation of

a reduced chromium complex, the activation of nitrogen or the cleavage of azobenzene be verified. Moreover, complex **26** does not react with CO gas at ambient pressure and only the starting material was recovered when treated with methyl magnesium chloride or methyl lithium.



Scheme 2.14: Synthesis of chromium PCP pincer complexes **27**, **29** and **28**.

Treatment of a solution of complex $[\text{Cr}(\text{POCOP-}t\text{Bu})\text{Br}]$ (**26**) in THF with LiBH_4 at room temperature over night, yielded the borohydride complex $[\text{Cr}(\text{POCOP-}t\text{Bu})\text{BH}_4]$ (**27**) as red solid with a yield of 86% (Scheme 2.13). To obtain this substance in analytically pure form complex **27** has to be recrystallised from *n*-pentane diffusion into a saturated THF solution or filtered quickly through a small pad of silica gel or basic activated Al_2O_3 , where the two latter methods reduced the yield significantly. It was insufficient to remove all traces of the formed lithium salts by filtration of the crude product, dissolved in CH_2Cl_2 , through a pad of celite[®]. Two relative weak IR absorption bands can be observed at 2407 and 2068 cm^{-1} which are assigned to the terminal and bridging hydrogen, respectively, from the BH_4 moiety (Figure 2.17 (a)). Complex **27** was investigated by crystallographic studies and solution magnetic susceptibility measurements. The latter indicates a solution effective magnetic moment of 4.9(1) μ_{B} (CH_2Cl_2 , Evans method) which is in agreement with a high-spin d^4 system (four unpaired electrons).

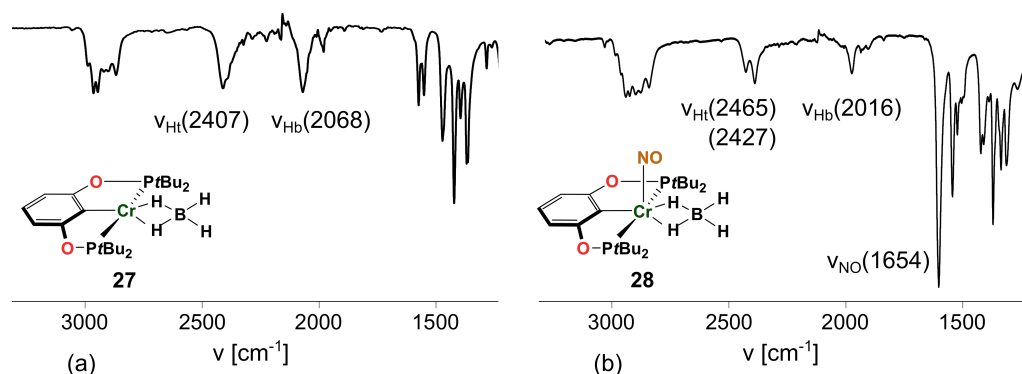


Figure 2.17: (a) Selected part of the IR spectra from $[\text{Cr}(\text{POCOP-}t\text{Bu})(\text{BH}_4)]$ (**27**) and (b) $[\text{Cr}(\text{POCOP-}t\text{Bu})(\text{NO})(\text{BH}_4)]$ (**28**).

The molecular structure of **27** exhibits essentially a distorted square pyramidal coordination geometry around the metal center (Figure 2.18). Here, the two bonding hydrogen and the *ipso*-carbon atom from the pincer ligand form the equatorial plane and the two phosphorous atoms are located in the axial positions. The BH_4 moiety is coordinated in a symmetric χ^2 fashion to the metal center with the bond length of both bonding

hydrogen Cr1-H1 and Cr1-H2 being 1.91(2) and 1.93(2) Å, respectively. Such bonding metrics are similar to other chromium borohydride complexes like $[\text{Cr}(\text{TMEDA})(\chi^2\text{-BH}_4)]$ ¹¹⁹, $[\text{Cr}(\chi^2\text{-BH}_4)(\text{H})(\text{dmppe})_2]$ ¹²⁰ and related Co(II) pincer complexes.¹²¹

Exposing a solution of complex $[\text{Cr}(\text{POCOP-}t\text{Bu})\text{BH}_4]$ (**27**) in toluene to NO gas at ambient pressure the five coordinated nitrosyl borohydride Cr(I) complex $[\text{Cr}(\text{POCOP-}t\text{Bu})(\text{NO})(\text{BH}_4)]$ (**28**) could be isolated as red solid with a yield of 88% (Scheme 2.13). In the IR three weak and one strong absorption bands are observed at 2465, 2427, 2016 and 1654 cm^{-1} assignable to the BH_4 moiety and the NO ligand, respectively (Figure 2.17). Single crystals suitable for crystallographic studies could be obtained by slow evaporation of a saturated *n*-pentane solution of **28** at -20 °C. The coordination sphere around the metal center is best described as a strongly distorted octahedron with the bond angles P1-Cr1-P2 being 150.11(4)° (Figure 2.19). The nitrosyl ligand coordinates in a nearly linear fashion (Cr1-N1-O3 173.4(3)°) to the metal center thus assigning it a distinct linear coordination mode as NO^+ which is supported by means of DFT calculations.⁸⁹ The solution effective magnetic moment of 2.0(1) μ_{B} (CH_2Cl_2 , Evans method) is in agreement with a d^5 low-spin configuration (one unpaired electron). X-band CW-EPR studies of complex **28** dissolved in CH_2Cl_2 exhibit an isotropic signal with hyperfine coupling of the electron spin ($S = 1/2$) with the nuclei spin of the two ^{31}P ($I = 1/2$), two ^1H ($I = 1/2$) and one ^{14}N ($I = 5/2$) atoms. The signal could be perfectly simulated with $g_{\text{iso}} = 1.983$, which is close to the value of a free electron (Figure 2.20).

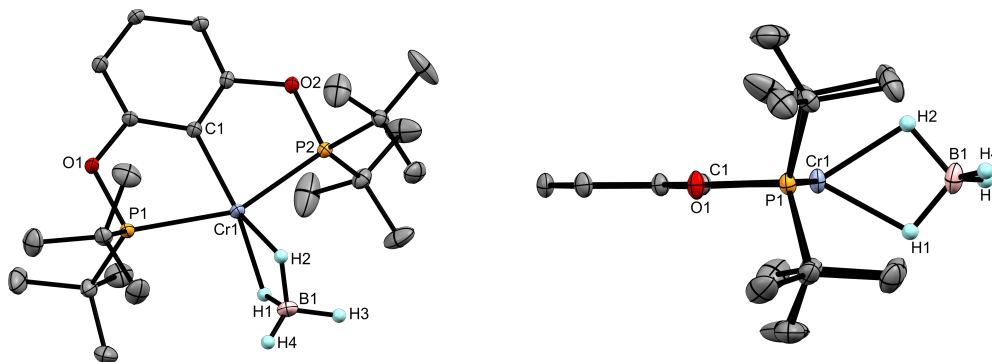


Figure 2.18: ORTEP view of $[\text{Cr}(\text{POCOP-}t\text{Bu})\text{BH}_4]$ (**27**) showing 50% thermal ellipsoids (H atoms omitted for clarity). Selected bond lengths (Å) and bond angles (deg): Cr1-P1 2.4464(6), Cr1-P2 2.4515(7), Cr1-C1 2.0762(14), Cr-H1 1.91(2), Cr-H2 1.93(2), B1-H1 1.25(2), B1-H2 1.31(3), B1-H3 1.12(3), B1-H4 0.96(1), Cr1...B1 2.47(2); P1-Cr1-P2 154.368(17).

It was not possible to isolate or even verify the formation of a chromium hydride pincer complex by treating both borohydride complexes **27** and **28** with Et_3N which worked for a related borohydride PCP nickel complex.¹²¹ Even after treatment of a solution of complex **26** with the super hydride $\text{Na}[\text{HBEt}_3]$, only starting material could be isolated.

In addition, the five coordinated nitrosyl Cr(I) complex $[\text{Cr}(\text{POCOP-}t\text{Bu})(\text{NO})\text{Br}]$ (**29**) was obtained as red solid with a yield of 95% by exposing a solution of complex **26** in toluene to NO gas at ambient pressure. This complex could be treated with LiBH_4 in THF to synthesise complex **28** too with a yield of 91% (Scheme 2.13). The molecular structure of complex **29** features a square pyramidal coordination geometry around the metal center with the tridentate pincer and bromide ligand in the basal and the nitric oxide in the apical position. The latter coordinates in a nearly linear fashion to the metal center and has a bond angle Cr1-N1-O3 of 177.3(3)° and is thus being counted as NO^+ . Therefore, this reaction can be considered as a formal one electron reduction from Cr(II) to Cr(I) which is supported by the means of DFT calculations.⁸⁹ All the other bond metrics from the

molecular structure of **29** are in the expected range and identical to the other described chromium pincer complexes discussed above.

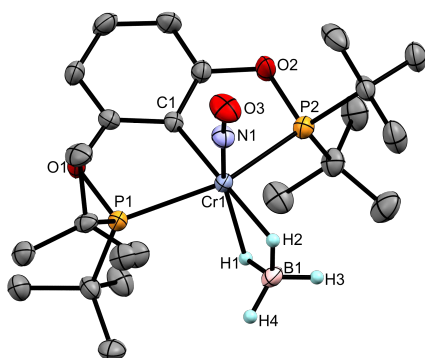


Figure 2.19: ORTEP view of $[\text{Cr}(\text{POCOP-}t\text{Bu})(\text{NO})(\text{BH}_4)]$ (**28**) showing 50% thermal ellipsoids (H atoms omitted for clarity). Selected bond lengths (\AA) and bond angles (deg): P1-Cr1 2.4470(10), P2-Cr1 2.4614(10), Cr1-N1 1.658(3), C1-Cr1 2.068(3), Cr1 \cdots B1 2.292(4), Cr1-H1 1.90(3), Cr1-H2 1.84(4); O3-N1-Cr1 173.4(3), P1-Cr1-P2 150.11(4).

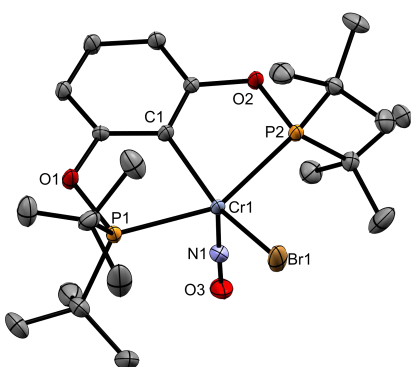


Figure 2.21: ORTEP view of $[\text{Cr}(\text{POCOP-}t\text{Bu})(\text{NO})\text{Br}]$ (**29**) showing 50% thermal ellipsoids (H atoms omitted for clarity). Selected bond lengths (\AA) and bond angles (deg): Cr1-N1 1.662(7), Cr1-C1 2.044(3), Cr1-Br1 2.4151(19), Cr1-P1 2.4189(15), Cr1-P2 2.4380(14); N1-Cr1-C1 102.0(3), C1-Cr1-Br1 151.56(17), P1-Cr1-P2 150.98(7), Cr1-N1-O1 175.8(6).

EPR studies of **29** dissolved in CH_2Cl_2 at 293 K on a X-band spectrometer shows an isotropic signal with a well resolved hyperfine coupling between the electron spin ($S = 1/2$) and the nuclei spin of the two ^{31}P ($I = 1/2$) and one ^{14}N ($I = 5/2$) atoms. The simulation of the resonance could be performed well with a g_{iso} value of 1.996 which is close to that of a free electron and other parameters are provided in the caption (Figure 2.22). These observations are in agreement with a low-spin d^5 species which is supported by magnetic susceptibility measurements with an effective magnetic moment of 1.8(1) μ_{B} (CH_2Cl_2 , Evans method, one unpaired electron). In the IR spectra a strong absorption band at 1654 cm^{-1} assigned to the NO ligand can be detected which is shifted to lower wave numbers compared to a related nitrosyl Cr(I) NNN pincer complex (*cf.* 1720 cm^{-1})¹²²

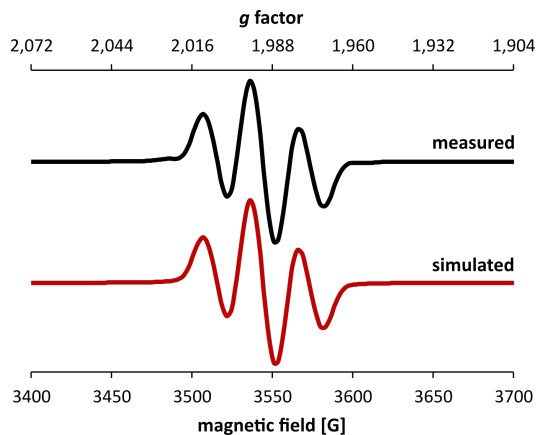


Figure 2.20: X-band CW EPR spectrum of $[\text{Cr}(\text{POCOP-}t\text{Bu})(\text{NO})(\text{BH}_4)]$ (**28**) in CH_2Cl_2 at 293 K at a microwave frequency of 9.86 GHz. The red line represents a simulation with parameters $g_{\text{iso}} = 1.983$ and $A_{\text{iso,P}} = 29.0\text{ G}$, $A_{\text{iso,N}} = 5.3\text{ G}$ and $A_{\text{iso,H}} = 5.5\text{ G}$.

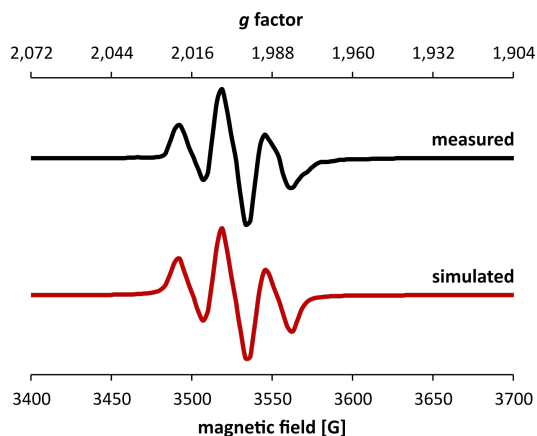
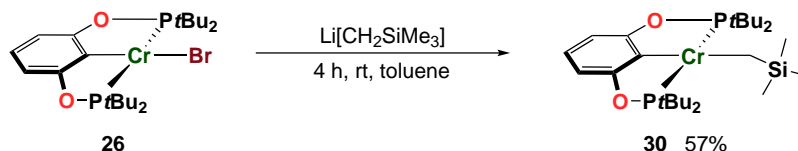


Figure 2.22: X-band EPR spectrum of $[\text{Cr}(\text{POCOP-}t\text{Bu})(\text{NO})\text{Br}]$ (**29**) in CH_2Cl_2 at 293 K at a microwave frequency of 9.86 GHz. The red line represents a simulation with parameters $g_{\text{iso}} = 1.996$ and $A_{\text{iso,P}} = 26.87\text{ G}$ and $A_{\text{iso,N}} = 5.53\text{ G}$.

and other nitrosyl chromium complexes with NO coordinating in a linear fashion to the metal center.⁶⁵

After completing the characterisation of the complexes **27** - **29** their catalytic properties were investigated. No conversion of the substrates 4'-fluoroacetophenone and styrene were achieved by hydrogenation, hydrosilylation and hydroboration transformations utilizing hydrogen gas at 50 bar, Et₃SiH and HBpin, respectively. While complex **29** showed absolutely no catalytic activity the borohydride complexes **27** and **28** converted 4'-fluoroacetophenone to the alcohol with hydrogen gas at 50 bar only in the amount corresponding to the stoichiometric quantity of the used catalyst.



Scheme 2.15: Synthesis of **30**.

The alkyl Cr(II) complex [Cr(POCOP-*t*Bu)(CH₂SiMe₃)] (**30**) can be afforded in analytically pure form as red solid and a yield of 57% after recrystallisation from *n*-pentane by treating a toluene solution of **26** with Li[CH₂SiMe₃] (Figure 2.15). The molecular structure of **30** shows a distorted square planar arrangement around the metal center with the bonding angles C1-Cr1-C7 and P2-Cr1-P1 being 168.91(8) and 152.15(2)°, respectively (Figure 2.23). In this context, the bond length between the Cr and the *ipso*-carbon is distinctly longer being 2.1229(19) Å compared to the molecular structures **26** - **29** and of a related Cr(II) NCN pincer complex (1.985(4) Å).¹¹⁷ However, the increased bond length is attributed to the *trans*-effect of the alkyl ligand and the remaining bond metrics are still in the expected range for chromium pincer complexes.^{112,115,123,124} Solution magnetic susceptibility studies produce an effective magnetic moment of 4.8(1) μ_B (benzene, Evans method) and are in agreement with a paramagnetic *d*⁴ high spin complex (four unpaired electrons).

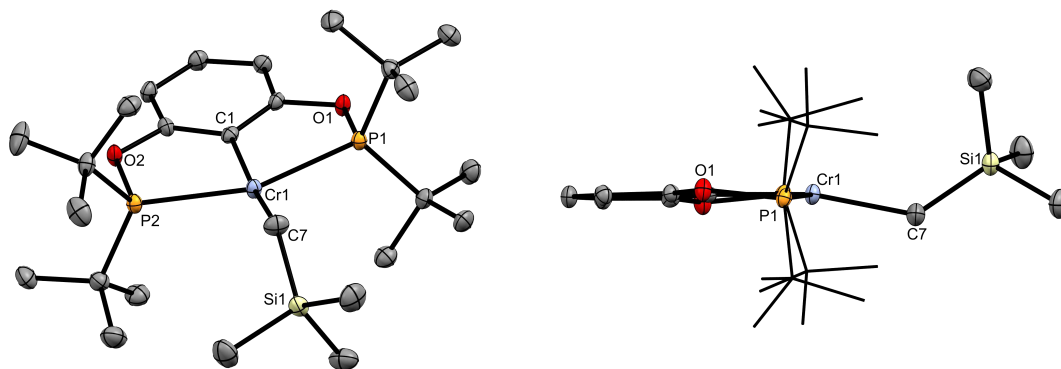


Figure 2.23: ORTEP view of [Cr(POCOP-*t*Bu)(CH₂SiMe₃)] (**30**) showing 50% thermal ellipsoids (H atoms omitted for clarity). Selected bond lengths (Å) and bond angles (deg): Cr1-C1 2.1229(19), Cr1-C7 2.145(2), Cr1-P2 2.4719(7), Cr1-P1 2.4722(7); C1-Cr1-C7 168.91(8), P2-Cr1-P1 152.15(2).

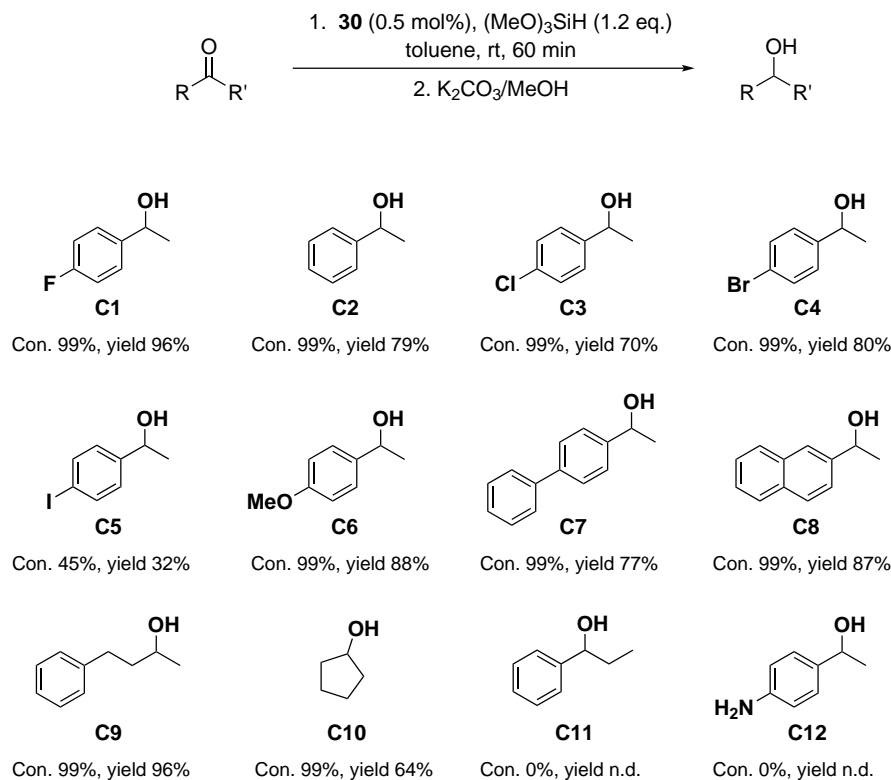
Recently, a related Cr(II) NNN pincer complex was reported that showed catalytic activity for the transformation of ketones to alcohols using hydrosilanes as hydrogen source.¹²⁴ Consequently, the catalytic activity of the alkyl chromium complex **30** for hydrosilylation reactions was investigated (table 2.1). Within 15 min complete conversion

of 4'-fluoroacetophenone to the corresponding alcohol could be achieved with 0.5 mol% of complex **30** and 1.2 equivalent (MeO)₃SiH in toluene and room temperature. Different substrates were tested for this transformation reaction and the results are summarized in Scheme 2.16. Most of the substrates featuring aromatic aryl-ketones with different halogens, phenyl or methoxy in the *p* position were tolerated, except for iodide (**C5**) where a mixture of starting material and product in a ratio of 1:1 were obtained. Cyclopentanone was completely converted to **C10** and no conversion was achieved under the above described conditions with propiophenone and 4'-aminoacetophenone.

Table 2.1: Optimisation of the hydrosilylation reaction using [Cr(POCOP-*t*Bu)(CH₂SiMe₃)] (**30**) as catalyst.

No	silane	cat. [mol%]	time	temp. [°C]	solvent	conversion ^a [%]	yield ^b [%]
1	(MeO) ₃ SiH (2 eq.)	5	18 h	rt	C ₆ D ₆	>99	n.d.
2	Et ₃ SiH (2 eq.)	3	24 h	rt	C ₆ D ₆	0	n.d.
3	(MeO) ₃ SiH (2 eq.)	1	15 min	rt	C ₆ D ₆	>99	77%
4	(MeO) ₃ SiH (2 eq.)	0.1	15 min	rt	Et ₂ O	0	n.d.
5	(MeO) ₃ SiH (1.2 eq.)	0.5	15 min	rt	toluene	>99	n.d.
6	(MeO) ₃ SiH (1.2 eq.)	0.5	60 min	rt	toluene	>99	96%

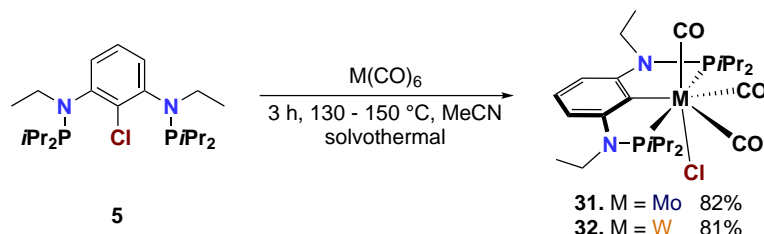
^a Determined by ¹H-NMR and TLC. ^b Isolated yields.



Scheme 2.16: Hydrosilylation of ketones with (MeO)₃SiH utilizing [Cr(POCOP-*t*Bu)(CH₂SiMe₃)] (**30**) as catalyst. Conversions were determined by ¹H-NMR and yield values refer to isolated product.

2.5 Molybdenum and Tungsten PCP pincer complexes

Treating the ligand PCP^{NEt}-Cl (**5**) with M(CO)₆ (M = Mo or W) in a sealed glass tube in MeCN for 3 h at 130 and 150 °C the Mo(II) and W(II) pincer complexes [Mo(PCP^{NEt}-*i*Pr)(CO)₃Cl] (**31**) and [W(PCP^{NEt}-*i*Pr)(CO)₃Cl] (**32**) could be isolated as orange and yellow solid with yields of 82 and 81%, respectively (Scheme 2.17). Both products can be collected in analytically pure form directly from the reaction mixture.



Scheme 2.17: Synthesis of complex **31** and **32**.

In the case of Mo, the reaction mixture turned completely green during the reaction and stayed green at 130 °C. After the sealed glass tube was allowed to reach room temperature the colour changed to orange and the Mo(II) complex **31** precipitated as orange crystals from the reaction mixture. Interestingly, the colour of the reaction mixture turned back to green when exposed to ambient pressure after opening the sealed glass vial. But only the reaction mixture turned back to green while the already precipitated molybdenum complex stayed orange. When dissolving complex **31** in THF, *n*-pentane, CH₂Cl₂ or MeCN the solution turned instantly green. On the other hand, the W(II) complex **32** didn't change colour during temperature changes or when dissolving it. After this observation, both complexes were characterised by ¹H, ¹³C{¹H} and ³¹P{¹H}-NMR measurements, ESI-MS and IR.⁸⁸

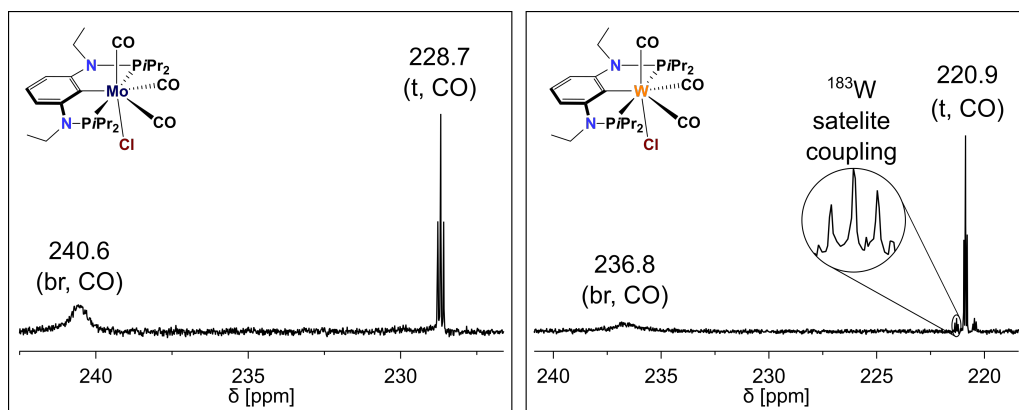


Figure 2.24: Selected part of the ¹³C{¹H}-NMR at 20 °C from [Mo(PCP^{NEt}-*i*Pr)(CO)₃Cl] (**31**, left) and [W(PCP^{NEt}-*i*Pr)(CO)₃Cl] (**32**, right) showing the carbonyl resonances.

In the ¹³C{¹H}-NMR, the carbonyl ligands of complex **31** and **32** give rise to one broad and one sharp triplet resonance in a 2:1 ratio at 240.6 and 228.7 ppm ($J_{CP} = 14.5$ Hz) for Mo(II) and 236.8 and 220.9 ppm ($J_{CP} = 11.6$ Hz) for W(II), respectively (Figure 2.24). Here, the satellite coupling ($J_{CW} = 126$ Hz) between ¹³C and ¹⁸³W ($I = 1/2$, 14% natural abundance) can be observed. The broadening of the resonance is induced by a fast interchange process between two of the three carbonyl ligands. Such fluxional behaviour is not uncommon.^{50,125–127} In this context, it was not possible to resolve the broad signals

during an $^{13}\text{C}\{^1\text{H}\}$ -NMR experiment at low temperatures (down to $-50\text{ }^\circ\text{C}$). The *ipso*-carbon resonances could be detected at 135.4 ($J_{\text{CP}} = 8.1\text{ Hz}$) and 136.6 ppm ($J_{\text{CP}} = 8.4\text{ Hz}$) for Mo(II) (**31**) and W(II) (**32**), respectively. In addition, both complexes exhibit one singlet resonance in the $^{31}\text{P}\{^1\text{H}\}$ -NMR at 143.3 ppm for Mo and 124.0 ppm for W where for the latter the satellite coupling ($J_{\text{CW}} = 104\text{ Hz}$) can be observed too but these are superimposed over the dominant singlet.

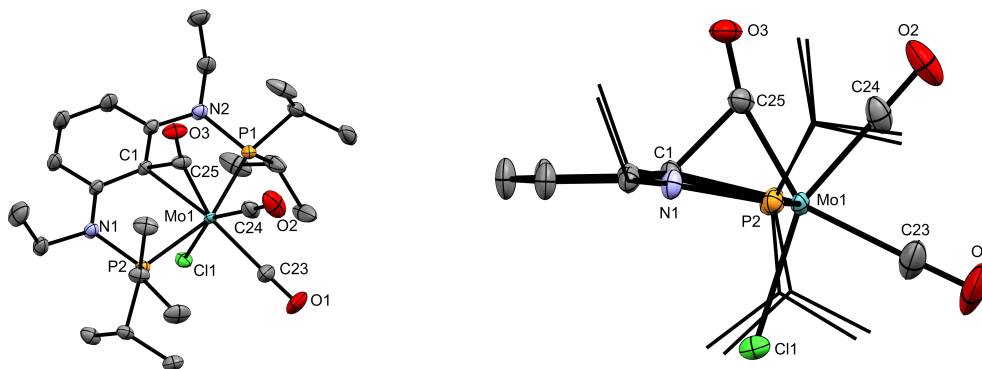


Figure 2.25: ORTEP view of $[\text{Mo}(\text{PCP}^{\text{NEt-}i\text{Pr}})(\text{CO})_3\text{Cl}]$ (**31**) showing 50% thermal ellipsoids (H atoms omitted for clarity). Selected bond lengths (\AA) and bond angles (deg): Mo1-C1 2.227(2), Mo1-C23 2.095(2), Mo1-C24 1.986(3), Mo1-C25 1.985(2), Mo1-Cl1 2.5170(17), Mo1-P1 2.419(3), Mo1-P2 2.492(3); Mo1-C25-O3 162.49(15), C25-C1-Mo1 59.15(8), P1-Mo1-P2 158.12(8).

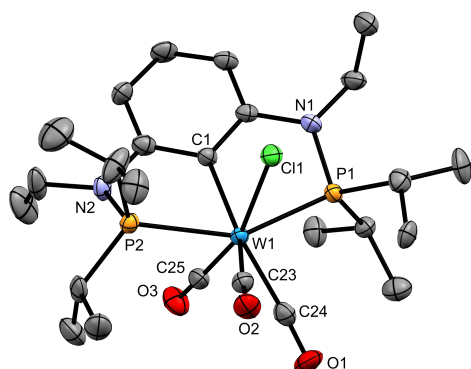


Figure 2.26: ORTEP view of $[\text{W}(\text{PCP}^{\text{NEt-}i\text{Pr}})(\text{CO})_3\text{Cl}]$ (**32**) showing 50% thermal ellipsoids (H atoms omitted for clarity). Selected bond lengths (\AA) and bond angles (deg): W1-C24 1.982(6), W1-C25 1.982(5), W1-C23 2.018(5), W1-C1 2.219(4), W1-P2 2.5048(12), W1-P1 2.5063(12), W1-Cl1 2.5471(12); P2-W1-P1 148.49(4), C1-W1-Cl1 84.10(11), C24-W1-C1 139.75(18), C25-W1-C1 79.52(18).

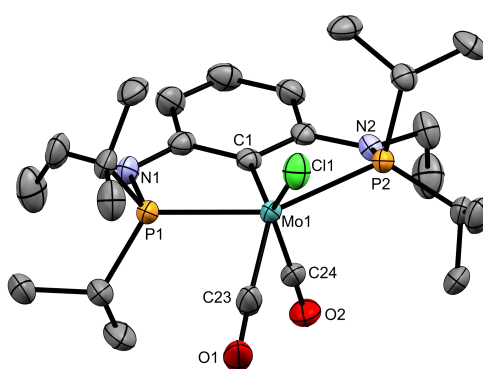


Figure 2.27: ORTEP view of $[\text{Mo}(\text{PCP}^{\text{NEt-}i\text{Pr}})(\text{CO})_2\text{Cl}]$ (**31-CO**) showing 50% thermal ellipsoids (H atoms omitted for clarity). Selected bond lengths (\AA) and bond angles (deg): Mo1-C1 2.180(4), Mo1-C23 1.963(5), Mo1-C24 1.935(5), Mo1-Cl1 2.4380(12), Mo1-P1 2.4306(11), Mo1-P2 2.5028(11); P1-Mo1-P2 150.70(4), C1-Mo1-Cl1 132.64(11), C24-Mo1-C1 73.51(17), C23-Mo1-C1 135.96(19).

The solid state structure of $[\text{Mo}(\text{PCP}^{\text{NEt-}i\text{Pr}})(\text{CO})_3\text{Cl}]$ (**31**) revealed an unexpected coordination mode where one of the CO ligands is bridged between the Mo center and the *ipso*-carbon of the benzene moiety (Figure 2.25). Such a formation is rare and only a few similar systems were reported in the literature.^{128–130} Here the PCP ligand coordinates in a typical meridional fashion to the metal center forming the first plane. Both terminal carbonyl ligands with the bridging carbonyl and chloride ligand form the second plane and coordinate in a meridional fashion to the metal center. The Mo1-C1 bond length, being 2.227(2) \AA , is significantly longer compared to a related $[\text{Mo}(\text{POCOP-}t\text{Bu})(\text{N})(\text{I})]^-$

complex⁹⁰ but similar to the analogous $[\text{Mo}(\text{PCP}^{\text{CH}_2-i\text{Pr}})(\text{CO})_3\text{Br}]$ complex.¹¹¹ The C1-C25 bond length being 1.674 Å is unusually long for a carbonyl metal bond and the bond angle Mo1-C25-O3 being 162.49(15)° deviates clearly from 180°. In contrast, the molecular structure of $[\text{W}(\text{PCP}^{\text{NEt}_t-i\text{Pr}})(\text{CO})_3\text{Cl}]$ (**32**) does not feature a bridged carbonyl ligand (Figure 2.26). As expected the ligand coordinates in a meridional and the carbonyl ligands in a terminal fashion to the metal center with the chloride in an axial position. All bond metrics are in an expected range and similar to the related $[\text{W}(\text{PCP}^{\text{CH}_2-i\text{Pr}})(\text{CO})_3\text{Br}]$ complex.¹¹¹ In the IR complex **31** and **32** exhibits three strong absorption bands assignable to the carbonyl ligands at 2007, 1921 and 1899 cm^{-1} and 2002, 1915 and 1878 cm^{-1} , respectively. An IR of the bulk matter containing a mixture of **31** and **31-CO** indicated that the two carbonyl ligands of **31-CO** exhibit two absorption bands at 1873 and 1851 cm^{-1} .

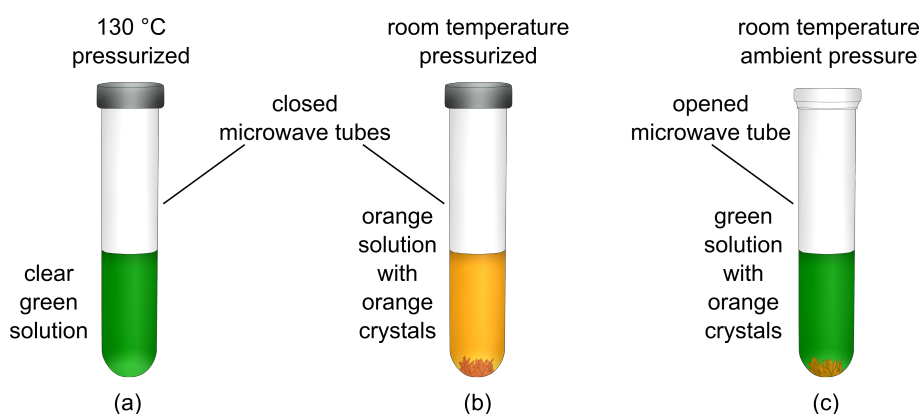


Figure 2.28: Illustration of (a) complex $[\text{Mo}(\text{PCP}^{\text{NEt}_t-i\text{Pr}})(\text{CO})_3\text{Cl}]$ (**31**) in solution after the reaction at 130 °C, (b) at room temperature where **31** precipitated as crystalline solid and (c) when the pressurized tube is opened the solution turned back to green while the solid kept its orange colour.

As mentioned above, the solution of the Mo(II) complex **31** can either adopt a green or orange colour, depending on the environmental conditions as illustrated in Figure 2.28 and dissolving the orange solid of complex **31** forms a green solution. If then (after stirring at ambient pressure) the solvent evaporates slowly a mixture of **31** and the sixfold coordinated $[\text{Mo}(\text{PCP}^{\text{NEt}_t-i\text{Pr}})(\text{CO})_2\text{Cl}]$ (**31-CO**) complex starts to crystallise as orange and green solid, respectively, with **31** being clearly the dominating species. Even at longer reaction times and temperatures, the conversion of **31** to **31-CO** by loss of one CO remained very low and it was not possible to characterise **31-CO** by NMR and IR measurements. Though, it was feasible to isolate a single crystal for X-ray measurement (Figure 2.27). The geometry around the molybdenum center is best described as a distorted trigonal prismatic arrangement. The bond metrics are similar to the previous described seven coordinated molybdenum complex **31** with the bond lengths Mo1-C1 2.180(4) Å being marginally and Mo1-Cl1 2.4380(12) Å distinctly shorter. It has to be mentioned that the measured single crystal of **31-CO** co-crystallised with **31** and was contaminated by approximately 15%.

The process of the pseudo rotation of the carbonyl ligands as well as the bridging carbonyl ligand of complexes **31** and **32** were investigated by the means of DFT calculation (Figure 2.29). The interchange between the CO² and CO³ have an energy barrier of 13.8 and 14.2 kcal/mol for Mo and W, respectively, and it is the process which induced the broadening resonance in the $^{13}\text{C}\{^1\text{H}\}$ -NMR spectra. An exchange of CO¹ with one of the other carbonyl ligands is strongly inhibited under these conditions because of a high energy barrier of 26.2 for Mo and 27.5 kcal/mol for W. The fastest process is the formation of the bridged carbonyl ligand between the metal center and the *ipso* carbon where merely

2.7 and 4.8 kcal/mol are needed for this reversible reaction. In the case of Mo the bridged state is slightly more stable than the terminal coordinated carbonyl species while for W both states exhibit similar free energies. In accordance to this data, it seems likely that those species exist in a fast equilibrium in solution but the bridged CO complex $[\text{Mo}(\text{PCP}^{\text{NEt}}-i\text{Pr})(\text{CO})_2(\mu\text{-CO})\text{Cl}]$ (**31**) can be isolated in the solid state.⁸⁸

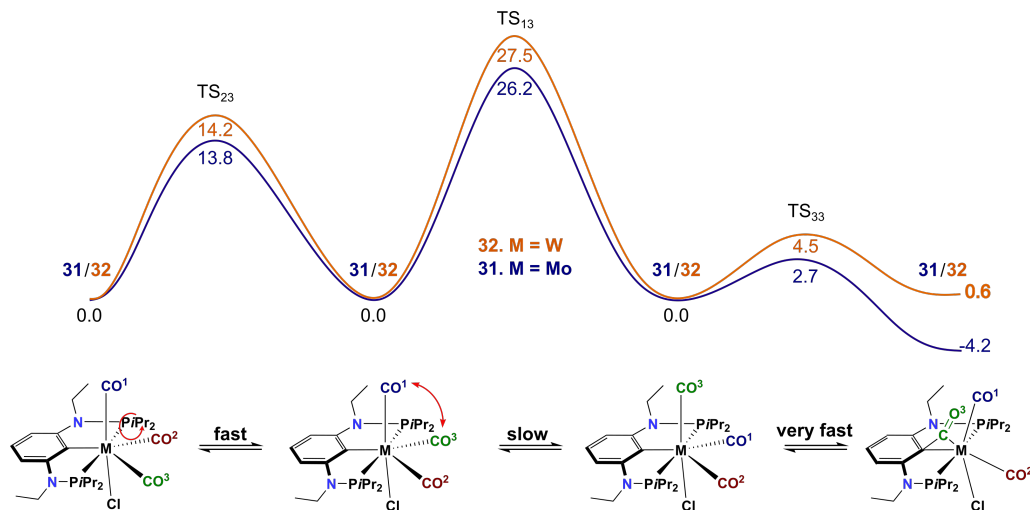
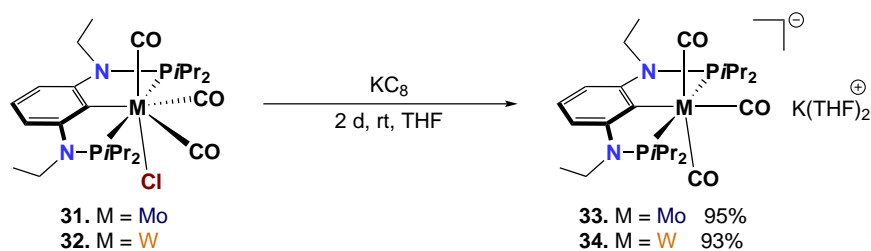


Figure 2.29: Free energy profile (kcal/mol) for the pseudorotations of the carbonyl ligands and the reversible process of the bridged CO ligand in **31** (PBE0/6-31G**).

Treatment of $\text{M}(\text{CO})_6$ ($\text{M} = \text{Mo}$ or W) with the analogous oxygen linker ligand POCOP $i\text{Pr}\text{-Br}$ (**7**) in toluene or MeCN at 110 - 150 °C for 3 - 18 h in a sealed glass tube proved to be unsuccessful in isolating the corresponding Mo and W pincer complexes. During the reaction the ligand was completely converted and a vast amount of signals were exhibited in the $^{31}\text{P}\{^1\text{H}\}$ -NMR spectra, indicated the formation of a countless number of different species. Besides, it should be mentioned that the synthesis of the related molybdenum and tungsten pincer complexes $[\text{M}(\text{PCP}^{\text{CH}_2}-i\text{Pr})(\text{CO})^3\text{Br}]$ ($\text{M} = \text{Mo}, \text{W}$) worked well under solvothermal conditions utilising the $\text{PCP}^{\text{CH}_2}\text{-Br}$ ligand and the $\text{M}(\text{CO})_6$ ($\text{M} = \text{Mo}$ or W) metal precursors.¹¹¹



Scheme 2.18: Reduction of **31** and **32**.

After concluding the characterisation and DFT investigation of the chloro tricarbonyl Mo(II) and W(II) complexes, their chemical properties were studied. Reduction of **31** and **32** with KC_8 in THF at room temperature for 2 d led to the Mo(0) and W(0) complexes, $[\text{K}(\text{THF})_2][\text{Mo}(\text{PCP}^{\text{NEt}}-i\text{Pr})(\text{CO})_3]$ (**33**) and $[\text{K}(\text{THF})_2][\text{W}(\text{PCP}^{\text{NEt}}-i\text{Pr})(\text{CO})_3]$ (**34**), with a yield of 95% and 93% as red and yellow solid, respectively (Scheme 2.18). Due to the very high air sensitivity, characterisation was only possible by NMR and IR measurements and crystallographic studies.

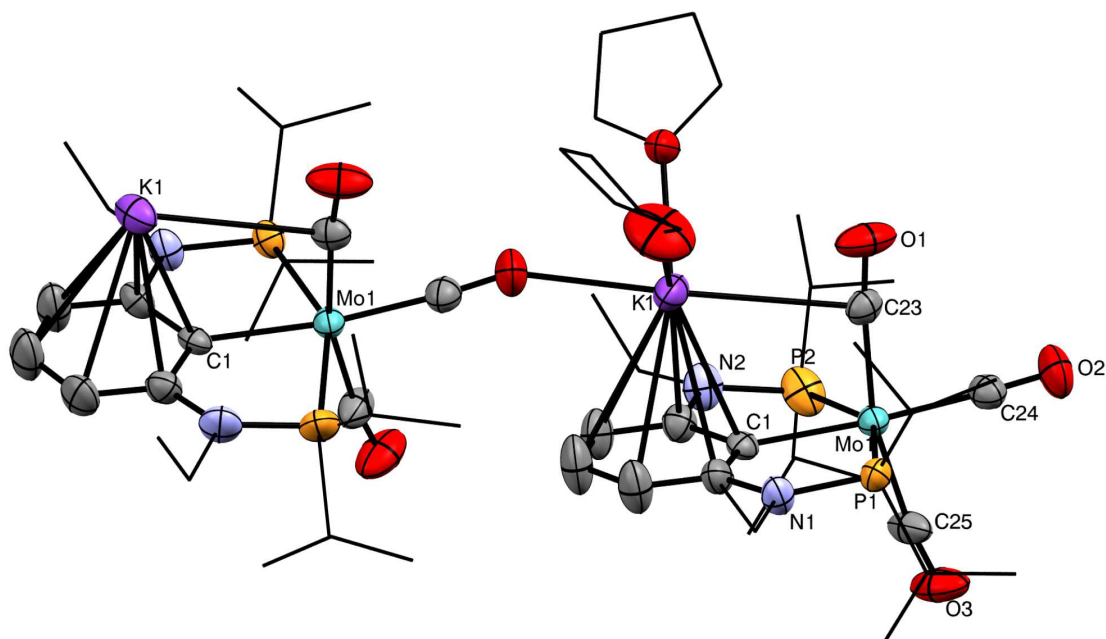


Figure 2.30: ORTEP view of $[\text{K}(\text{THF})_2][\text{Mo}(\text{PCP}^{\text{NEt-}i\text{Pr}})(\text{CO})_3]$ (**33**) showing 50% thermal ellipsoids (H atoms omitted for clarity). Selected bond lengths (Å) and bond angles (deg): Mo1-C1 2.242(3), Mo1-C24 1.956(4), Mo1-C23 1.989(4), Mo1-C25 2.008(4), Mo1-P1 2.3990(10), Mo1-P2 2.4178(11); C23-Mo1-C25 166.09(16), C24-Mo1-C1 173.76(13), P1-Mo1-P2 151.42(4).

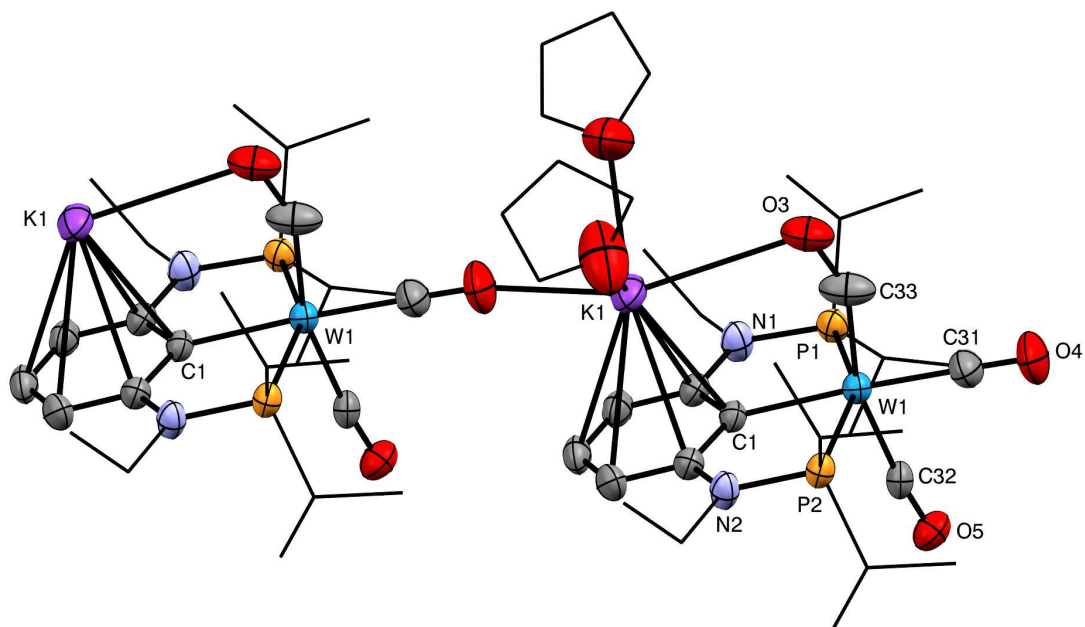
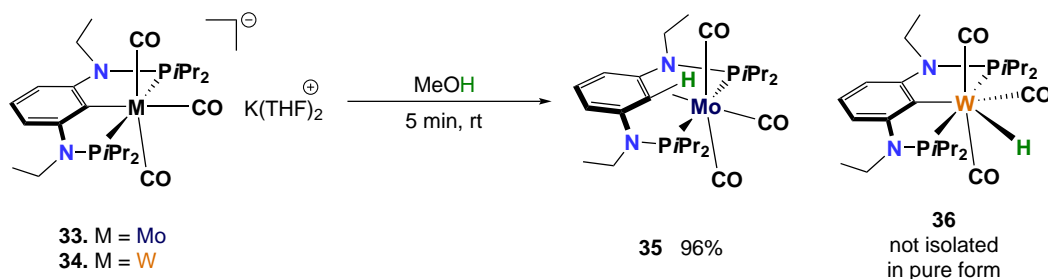
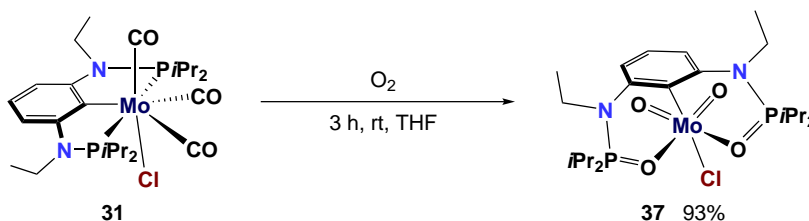


Figure 2.31: ORTEP view of $[\text{K}(\text{THF})_2][\text{W}(\text{PCP}^{\text{NEt-}i\text{Pr}})(\text{CO})_3]$ (**34**) showing 50% thermal ellipsoids (H atoms omitted for clarity). Selected bond lengths (Å) and bond angles (deg): W1-C1 2.242(5), W1-C31 1.949(6), W1-C32 2.001(5), W1-C33 1.996(6), W1-P1 2.4075(13), W1-P2 2.4297(13); C33-W1-C32 163.1(3), C31-W1-C1 177.1(2), P1-W1-P2 152.80(4).

The solid state structure of **33** shows a one dimensional polymer where the potassium atom is coordinated in an η^6 fashion to the benzene moiety while the remaining coordination sites were occupied by CO and two THF molecules (Figure 2.30). Such an arrangement in the solid state structure is not uncommon with potassium as cation^{131,132} and Tonzetich *et al.* reported a similar observation with an related pyrrole based Fe pincer system.⁵⁹ The coordination geometry around the metal center could be best described as a distorted octahedral arrangement with the bond angle P1-Mo1-P2 being 151.42(4)°. The bond length between the *ipso*-carbon and the Mo being 2.242(3) Å was in the expected range and comparable to its precursor **31** (C_{ipso} -Mo(II) 2.227(2) Å). The molecular structure of [K(THF)₂][W(PCP^{NEt}-*i*Pr)(CO)₃] (**34**) shows the same coordination arrangements and formation of a one dimensional polymer with the bond metrics being in the expected range and are provided in the caption (Figure 2.31). In the ¹³C{¹H}-NMR the carbonyl ligands of complex **33** and **34** gave rise to two resonances in a 2:1 ratio at 239.6, 227.1 and 233.4, 219.1 ppm, respectively. The *ipso*-carbon from the benzene moiety of Mo(0) and W(0) exhibits a triplet at 150.0 ($J_{CP} = 10.6$ Hz) and 143.7 ppm ($J_{CP} = 8.7$ Hz), respectively.

Scheme 2.19: Synthesis of complex **35** and **36**.

The complexes Mo(0) (**33**) and W(0) (**34**) can both be readily protonated by MeOH forming the complexes [Mo(χ^3 P,CH,P-P(CH)₂P^{NEt}-*i*Pr)(CO)₃] (**35**) and [W(PCP^{NEt}-*i*Pr)(CO)₃H] (**36**) (Scheme 2.19). While the agostic molybdenum complex could be isolated with a yield of 96% as orange solid the tungsten complex could not be obtained in pure form. However, the latter gives rise to a triplet resonance at -5.6 ppm ($J_{HP} = 40.0$ Hz) assigned to the hydride ligand in the ¹H-NMR. In the ³¹P{¹H}-NMR two doublets are exhibited at 138.9 and 122.8 ppm with a geminal coupling constant of 91.1 Hz. The agostic Mo complex **35** on the other hand give rise to a high-field shifted triplet of a triplet at 1.61 ($J_{HP} = 4.2$ Hz and $J_{HP} = 1.9$ Hz) and 75.5 ppm ($J_{CP} = 4.7$ Hz) assigned to the agostic proton and the *ipso*-carbon in the ¹H and ¹³C{¹H}-NMR, respectively.⁸⁸ These measurements were in agreement to the recently reported analogous Mo and W pincer complexes (with NMe linkers).⁵⁰

Scheme 2.20: Oxidation of **31**.

When measuring ESI high resolution mass spectrometry (positive ion) of complex [Mo(PCP^{NEt}-*i*Pr)(CO)₃Cl] (**31**) the mass peak $m/z = 557.1595$ corresponding to [M-

$3(\text{CO})\text{-Cl}+4\text{O}]^+$, which referred to a highly oxidized molybdenum species, could be monitored. Therefore, **31** was dissolved in THF and exposed to dried air. After stirring at room temperature for 3 h a colour change from green to orange was observed and the unusual Mo(VI) complex $[\text{Mo}(\text{OCO}^{\text{NEt}}\text{-OP}i\text{Pr})(\text{O})_2\text{Cl}]$ (**37**) could be obtained with a yield of 93% as orange solid (Scheme 2.20). A selected part of the high resolution MS spectrum of this Mo(VI) fragment is shown in Figure 2.32. A molybdenum mono-oxo species could not be observed which was reported for a related cationic $[\text{Mo}(\text{PNP}^{\text{Me}}\text{-}i\text{Pr})(\text{O})\text{I}]\text{SbF}_6$ complex.¹³³

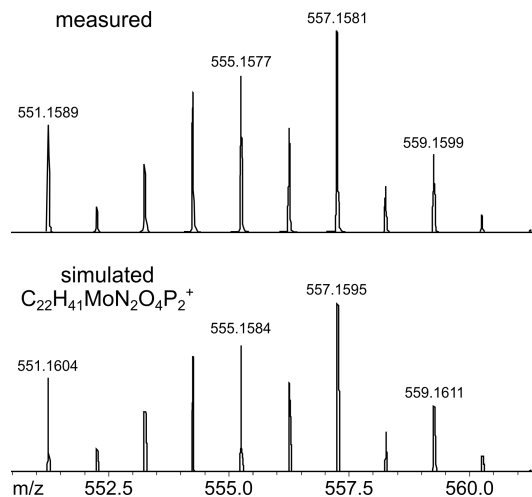


Figure 2.32: Selected part of HMS spectra (positive ion ESI) of $[\text{Mo}(\text{OCO}^{\text{NEt}}\text{-OP}i\text{Pr})(\text{O})_2\text{Cl}]$ (**37**, top) and simulated spectra (bottom) showing $[\text{M}-\text{Cl}]^+$.

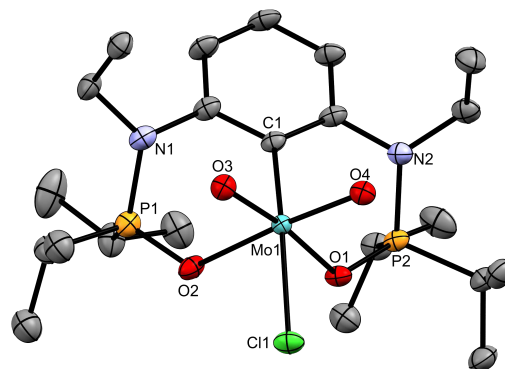
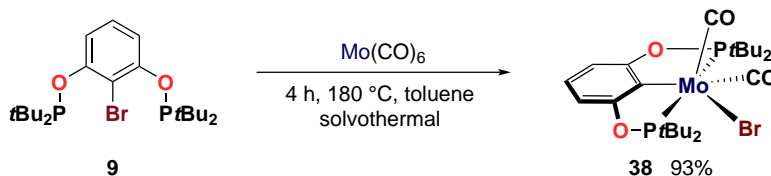


Figure 2.33: ORTEP view of $[\text{Mo}(\text{OCO}^{\text{NEt}}\text{-OP}i\text{Pr})(\text{O})_2\text{Cl}]$ (**37**) showing 50% thermal ellipsoids (H atoms omitted for clarity). Selected bond lengths (Å) and bond angles (deg): Mo1-C1 2.187(4), Mo1-O1 2.244(3), Mo1-O2 2.212(4), Mo1-O3 1.687(4), Mo1-O4 1.733(4), Mo1-Cl1 2.4069(12); O4-Mo1-O2 166.92(17), O3-Mo1-O1 167.6(2), C1-Mo1-Cl1 158.50(9).

The solid state structure of **37** shows a distorted octahedral arrangement around the metal center (Figure 2.33). Interestingly, the bond length between the *ipso*-carbon and the metal center is with 2.187(4) Å marginally different compared to the above described molybdenum pincer complexes (*cf.* **31** being 2.227(2), **31-CO** being 2.180(4) and **33** being 2.242(3) Å). The Mo1-O3 and Mo1-O4 bond distances of 1.687(4) and 1.733(4) Å, respectively, are similar to the related $[\text{Mo}(\text{PNP}^{\text{Me}}\text{-}i\text{Pr})(\text{O})\text{I}]\text{SbF}_6$ and $[\text{Mo}(\chi^2\text{O},\text{O-ONO}^{\text{Me}}\text{-}i\text{Pr})(\text{O})\text{Cl}_3]\text{SbF}_6 \cdot 1/2\text{CH}_2\text{Cl}_2$ complexes¹³³ and other molybdenum mono/di-oxo species.¹³⁴⁻¹³⁷ In the $^{31}\text{P}\{^1\text{H}\}$ -NMR one singlet at 65.8 ppm is observed while in the $^{13}\text{C}\{^1\text{H}\}$ -NMR the *ipso*-carbon exhibits a singlet at 145.3 ppm.



Scheme 2.21: Synthesis of **38**.

Interestingly, treatment of ligand $\text{POCOP}^t\text{Bu-Br}$ (**9**) with $\text{Mo}(\text{CO})_6$ in toluene at 180 °C for 4 h in a sealed glass tube resulted in the formation of the six coordinated dicarbonyl Mo(II) complex $[\text{Mo}(\text{POCOP-}t\text{Bu})(\text{CO})_2\text{Br}]$ (**38**). After recrystallisation from *n*-pentane, complex **38** could be isolated with a yield of 93% as blue solid. Treatment of ligand **9** with $\text{W}(\text{CO})_6$ resulted in the formation of three different species as judged by $^{31}\text{P}\{^1\text{H}\}$ -NMR which could not be separated and characterised (yet).

The carbonyl ligands exhibit two strong absorption bands in the IR at 1954 and 1873 cm^{-1} . In the $^{13}\text{C}\{^1\text{H}\}$ -NMR, three sharp triplet resonances at 245.0 (J_{CP} is 9.1 Hz) and 244.7 ($J_{\text{CP}} = 12.1$ Hz) and 148.4 ppm ($J_{\text{CP}} = 10.6$ Hz) assigned to the two carbonyl ligands and the *ipso*-carbon can be observed. Single crystals with sufficient quality for X-ray diffraction measurement could be isolated (Figure 2.34). While the bond metrics are in the expected range the complex adopts an interesting coordination geometry around the metal center which could be best described as a highly distorted trigonal prismatic arrangement. Here the tridentate ligand is slightly bent and does not align in a perfect meridional fashion and the carbonyl ligands were in *cis* position to each other.

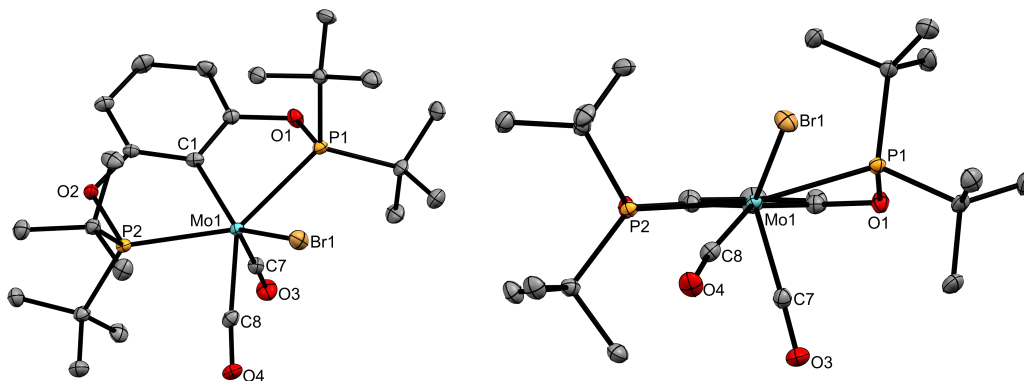


Figure 2.34: ORTEP view of $[\text{Mo}(\text{POCOP-}t\text{Bu})(\text{CO})_2\text{Br}]$ (**38**) showing 50% thermal ellipsoids (H atoms omitted for clarity). Selected bond lengths (\AA) and bond angles (deg): Mo1-C1 2.209(4), Mo1-C7 1.919(4), Mo1-C8 1.985(4), Mo1-P1 2.5735(12), Mo1-P2 2.4772(12), Mo1-Br1 2.6080(7); P2-Mo1-P1 142.68(4).



Die approbierte gedruckte Originalversion dieser Dissertation ist an der TU Wien Bibliothek verfügbar.
The approved original version of this doctoral thesis is available in print at TU Wien Bibliothek.

Chapter 3

Conclusion

Most non-precious metals of the first-row transition elements fail to activate the C-H bond of a PCP pincer ligand. In this work, it was demonstrated by exchanging the hydrogen of the *ipso*-carbon position with a halogen of PCP pincer ligands featuring an aromatic backbone and nitrogen or oxygen linkers (**5**, **7-9**) that different low valent carbonyl metal precursors ($\text{Fe}_2(\text{CO})_9$, $\text{Mn}_2(\text{CO})_{10}$ and $\text{M}(\text{CO})_6$ ($\text{M} = \text{Cr}, \text{Mo}, \text{W}$) could be utilized as metallizing agents for the synthesis of new non-precious PCP pincer complexes. Thus, this change in the electronic properties of the pincer ligands enhanced the oxidative addition pathway. In this context, the iron PCP pincer complex $[\text{Fe}(\text{PCP}^{\text{NEt}}-i\text{Pr})(\text{CO})_2\text{Cl}]$ (**10**) and $[\text{Fe}(\text{POCOP}-t\text{Bu})(\text{CO})_2]$ (**14**) could be synthesised under solvothermal conditions using $\text{Fe}_2(\text{CO})_9$ and $\text{Fe}(\text{CO})_5$ as metal precursors, respectively, without the presence of UV radiation. Furthermore, it was possible to synthesise the first manganese and chromium PCP pincer complexes $[\text{Mn}(\text{PCP}^{\text{NEt}}-i\text{Pr})(\text{CO})_3]$ (**15**) and *trans*- $[\text{Cr}(\text{III})(\text{POCOP}-i\text{Pr})\text{Br}_2(\text{CH}_3\text{CN})]$ (**21**) by treatment of ligand **5** with $\text{Mn}_2(\text{CO})_{10}$ and $\text{Cr}(\text{CO})_6$, respectively, under solvothermal conditions. In addition, the Mo and W complexes $[\text{Mo}(\text{PCP}^{\text{NEt}}-i\text{Pr})(\text{CO})_3\text{Cl}]$ (**31**), $[\text{Mo}(\text{POCOP}-t\text{Bu})(\text{CO})_2\text{Br}]$ (**38**) and $[\text{W}(\text{PCP}^{\text{NEt}}-i\text{Pr})(\text{CO})_3\text{Cl}]$ (**32**) could be synthesised upon treatment of **5** and **9** with $\text{M}(\text{CO})_6$ ($\text{M} = \text{Mo}$ or W) under solvothermal conditions.

Investigation of the chemical properties led to some unexpected results. For example the treatment of $[\text{Fe}(\text{PCP}^{\text{NEt}}-i\text{Pr})(\text{CO})_2\text{Cl}]$ (**10**) with super hydride resulted in a formal one electron reduction instead of a ligand exchange reaction. Thus, the complex $\text{Fe}(\text{PCP}^{\text{NEt}}-i\text{Pr})(\text{CO})_2$ (**11**) could be isolated. Furthermore, treatment of $\text{Cr}(\text{CO})_6$ with the different $\text{POCOP}^{\text{R}}-\text{Br}$ ligands (**7** $\text{R} = i\text{Pr}$, **9** $\text{R} = t\text{Bu}$) resulted in the synthesis of either a mixture of *trans*- $[\text{Cr}(\text{III})(\text{POCOP}-i\text{Pr})\text{Br}_2(\text{CH}_3\text{CN})]$ (**21**) and $[\text{Cr}(0)(\chi^3\text{P},\text{CH},\text{P}-\text{PO}(\text{CH})\text{OP}-i\text{Pr})(\text{CO})_3]$ (**22**) or the four coordinated 12 electron complex $[\text{Cr}(\text{POCOP}-t\text{Bu})\text{Br}]$ (**26**) featuring four unpaired electrons. This demonstrated that just by (slightly) varying the stereo electronic properties of the pincer ligands, by changing the alkyl rests of the phosphine donors changed in this case the outcome of the reaction.

With complex $[\text{Cr}(\text{POCOP}-t\text{Bu})\text{Br}]$ (**26**) it was possible to synthesise the borohydride and nitrosyl chromium pincer complexes $[\text{Cr}(\text{POCOP}-t\text{Bu})\text{BH}_4]$ (**27**), $[\text{Cr}(\text{POCOP}-t\text{Bu})(\text{NO})\text{Br}]$ (**29**) and $[\text{Cr}(\text{POCOP}-t\text{Bu})(\text{NO})(\text{BH}_4)]$ (**28**). This was an interesting development since chromium borohydride and nitrosyl complexes are in general scarce in the literature. While the borohydride chromium pincer complexes **27** and **28** were promising candidates as catalysts for hydrogenation reactions, they showed no catalytic activity. In the end the alkyl chromium complex $[\text{Cr}(\text{POCOP}-t\text{Bu})(\text{CH}_2\text{SiMe}_3)]$ (**30**), which could be obtained by treatment of **26** with $\text{Li}[\text{CH}_2\text{SiMe}_3]$, was active for hydrosilylation transformations of ketones to alcohols.

Another unexpected observation was the fact that treatment of the ligands **5** and **7**

(both featuring $i\text{Pr}_2\text{P}$ as donor atoms) with these first-row transition metal precursors resulted in the formation of (at least) two different species. Only in the case of chromium it was possible to characterise both formed complexes (Cr(III) **21** and Cr(0) **22**). It has yet to be proven that first a Cr(II) species is formed during the reaction which then disproportionates to the dihalogen Cr(III) **21** and tricarbonyl Cr(0) **22** complexes or both products are directly formed from the starting materials. If the former reaction happens, it can be carefully assumed that during the synthesis of the tricarbonyl Mn(I) complex **15** also a highly reactive dichloride Mn(III) complex was formed and maybe a dibromide Fe(III) complex during the synthesis of the dicarbonyl Fe(I) complex **14**.

Exposure of the fourfold coordinated square planar chromium complexes $[\text{Cr}(\text{POCOP-}t\text{Bu})\text{Br}]$ (**26**) and $[\text{Cr}(\text{POCOP-}t\text{Bu})\text{BH}_4]$ (**27**) to NO gas resulted in the formal one electron reduction of Cr(II) to Cr(I) by addition of NO^+ to the metal center and the five coordinated square pyramidal chromium complexes $[\text{Cr}(\text{POCOP-}t\text{Bu})(\text{NO})\text{Br}]$ (**29**) and $[\text{Cr}(\text{POCOP-}t\text{Bu})(\text{NO})(\text{BH}_4)]$ (**28**) could be obtained, respectively. On the other hand complex $[\text{Fe}(\text{PCP}^{\text{NEt-}i\text{Pr}})(\text{CO})_2]$ (**11**) underwent a formal one electron oxidation upon treatment with NO gas by a ligand exchange reaction between one CO and NO^- to obtain complex $[\text{Fe}(\text{PCP}^{\text{NEt-}i\text{Pr}})(\text{CO})(\text{NO})]$ (**12**). While $[\text{Mn}(\text{PCP}^{\text{NEt-}i\text{Pr}})(\text{CO})_3]$ (**15**) did not react with NO gas it could be treated with NOBF_4 to synthesise complex *trans*- $[\text{Mn}(\text{PCP}^{\text{NEt-}i\text{Pr}})(\text{CO})_2(\text{NO})]\text{BF}_4$ (**16**). Protonation of the complexes **12** and **15** to form the corresponding hydride complexes failed as predicted by the means of DFT calculations and the agostic complexes $[\text{Fe}(\chi^3\text{P},\text{CH},\text{P}-\text{P}(\text{CH})\text{P}^{\text{NEt-}i\text{Pr}})(\text{CO})(\text{NO})]\text{BF}_4$ (**13**) and $[\text{Mn}(\chi^3\text{P},\text{CH},\text{P}-\text{P}(\text{CH})\text{P}^{\text{NEt-}i\text{Pr}})(\text{CO})_3]\text{BF}_4$ (**17**) could be isolated.

The bridged carbonyl ligand observed in the molecular structure of $[\text{Mo}(\text{PCP}^{\text{NEt-}i\text{Pr}})(\text{CO})_3\text{Cl}]$ (**31**) was an interesting observation and could help in the understanding of the carbon metal bond interaction and how it potentially influences the remaining ligands. To better understand the implications of the results from this work, future studies could address the investigation of the treatment of $\text{Co}_2(\text{CO})_8$ with such ligands under solvothermal conditions. This could further provide insight into these processes and how the different linkers and phosphine donors of the ligands influence the outcome of the reactions.

Chapter 4

Experimental

General Information. All reactions were performed under an inert atmosphere of argon by using Schlenk techniques or in a MBraun inert-gas glovebox, unless otherwise noted. The solvents were purified according to standard procedures.¹³⁸ The deuterated solvents were purchased from Aldrich and dried over 3 Å molecular sieves. All starting materials are known compounds and were used as obtained from commercial suppliers. The nitric oxide (NO) gas was purchased from Messer (Austria) with a 10 vol% concentration and the rest being N₂. ¹H and ¹³C{¹H} and ³¹P{¹H} NMR spectra were recorded on Bruker AVANCE-250, AVANCE-400, and AVANCE-600 spectrometers. ¹H and ¹³C{¹H} NMR spectra were referenced internally to residual protio-solvent and solvent resonances, respectively, and are reported relative to tetramethylsilane ($\delta = 0$ ppm). ³¹P{¹H} NMR spectra were referenced externally to H₃PO₄ (85%) ($\delta = 0$ ppm). High resolution-accurate mass spectra were recorded on a hybrid Maxis Qq-aoTOF mass spectrometer (Bruker Daltonics, Bremen, Germany) fitted with an ESI-source. Measured accurate mass data of the [M]⁺ ions for confirming calculated elemental compositions were typically within 5 ppm accuracy. The mass calibration was done with a commercial mixture of perfluorinated trialkyl-triazines (ES Tuning Mix, Agilent Technologies, Santa Clara, CA, USA). All IR measurements were performed on a Bruker Tensor 27 with an ATR unit. CW-EPR spectroscopic measurements were performed on a X-band Bruker Elexsys-II E500 EPR spectrometer (Bruker Biospin GmbH, Rheinstetten, Germany) in solution at 293 K or as frozen solution at 100 K. A high sensitivity cavity (SHQE1119) was used for measurements setting the microwave frequency to 9.86 GHz, the modulation frequency to 100 kHz, the center field to 6000 G, the sweep width to 12000 G, the sweep time to 30.0 s, the modulation amplitude to 6 G, the microwave power to 15.9 mW, the conversion time to 7.33 ms, and the resolution to 4096 points. The spectra were analysed using the Bruker Xepr software. Single crystals suitable for the X-ray studies were selected under a polarizing microscope and measured on a Bruker SMART-CCD area diffractometer system with a Mo-K α -radiation and a graphite monochromator. The data were processed with the SADABS¹³⁹ algorithm and the crystal structures were solved and refined with the SHELXTL¹⁴⁰ software suite.

4.1 Synthesis of PCP Ligands

2-Chloro-1,3-dinitrobenzene (1)

H₂SO₄ (100 mL, 98%) was placed in a 500 mL three-necked round-bottom flask and NaNO₂ (6.2 g, 90 mmol) was added slowly in small portions. After complete addition the temperature raised to 65 °C and the solution was heated up to 80 °C for 10 min. Then

the reaction mixture was cooled with an ice bath and 2,6-dinitroaniline (15 g, 82 mmol) dissolved in hot acetic acid (200 mL, 99%) was added slowly so that the temperature remained between 25-35 °C. After complete addition the mixture was stirred at rt for 2 h. Meanwhile CuCl (17.8 g 180 mmol) dissolved in HCl (200 ml, 36%) was placed in a 1000 mL Erlenmeyer-flask. The diazonium salt was added in portions to the cooled and stirred CuCl solution. After complete addition of the diazonium salt the reaction mixture was heated to 80 °C and stirred for another hour. Afterwards the mixture was cooled again with an ice bath and H₂O (500 mL) was added. A yellow solid precipitated which was filtered and washed three times with water and dried under high vacuum. The yield of **1** as yellow precipitate was 15 g (90%). ¹H-NMR (400 MHz, DMSO, 20 °C): δ 8.39 (d, *J* = 8.2, 2H, CH), 7.87 (t, *J* = 8.2, 1H, CH). ¹³C{¹H}-NMR (101 MHz, DMSO, 20 °C): δ 148.9 (s, C-N), 129.9 (s, CH), 128.8 (s, CH), 118.2 (s, C-Cl) ppm.

2-Chloro-1,3-diaminobenzene (**2**)

A mixture of **1** (2.1 g, 10.4 mmol) and SnCl₂·2H₂O (20 g, 89 mmol) were placed in a 250 mL round-bottom flask and suspended in EtOAc (100 mL) at 0 °C. The reaction mixture was stirred 24 h at reflux. After cooling down to rt the reaction mixture was alkalisied with a NaOH solution while chilled to 0 °C with an ice bath. Then the product was extracted with EtOAc and the combined organic layers were dried over Na₂SO₄ and the solvent was removed under reduced pressure. The crude product was purified by silica gel chromatography (25 g, *n*-heptane/EtOAc 1:1) to yield 1.1 g (74%) as white solid. ¹H-NMR (400 MHz, DMSO, 20 °C): δ 6.67 (t, *J* = 7.9, 1H, CH), 6.02 (d, *J* = 7.9, 2H, CH), 4.99 (s, 4H, NH₂). ¹³C{¹H}-NMR (101 MHz, DMSO, 20 °C): δ 144.9 (s, C-N), 127.0 (s, CH), 103.2 (s, CH), 103.1 (s, C-Cl). HR-MS (ESI⁺, CH₃CN/MeOH + 1%H₂O): *m/z* calcd for C₆H₈ClN₂ [M+H]⁺ 143.0371, found 143.0366.

N,N'-(2-Chloro-1,3-phenylene)diacetamide (**3**)

2 (11.3 g, 79.5 mmol) was dissolved in acetic acid (200 mL) with H₂SO₄ (4 drops) and at 0 °C acetic anhydride (17.2 g, 168.5 mmol) was added slowly. The reaction mixture was stirred for 3 h at rt. A white precipitate was formed, which was filtered and washed three times with water and dried yielding 14.4 g (80%) as white solid. ¹H-NMR (600 MHz, DMSO, 20 °C): δ 9.54 (s, 2H, NH), 7.47 (d, *J* = 7.8 Hz, 2H, CH), 7.26 (t, *J* = 8.1 Hz, 1H, CH), 2.09 (s, 6H, CH₃). ¹³C{¹H}-NMR (151 MHz, DMSO, 20 °C): δ 168.6 (s, C=O), 135.7 (s, C-N), 126.5 (s, CH), 122.6 (s, CH), 121.0 (s, C-Cl) 23.4 (s, CH₃). HR-MS (ESI⁺, CH₃CN/MeOH + 1%H₂O): *m/z* calcd for C₁₀H₁₂ClN₂O₂ [M+H]⁺ 227.0582, found 227.0577.

2-Chloro-N¹,N³-diethylbenzene-1,3-diamine (**4**)

LiAlH₄ (11.2 g, 295 mmol) was suspended in THF (200 mL) and **3** (8.9 g, 39.3 mmol) was added slowly in small portions at 0 °C. The reaction mixture was stirred over night at reflux and then carefully quenched with a saturated aqueous Na₂CO₃ solution. The formed precipitate was removed by filtration and the filter cake was washed with ethyl acetate. The filtrate was dried over Na₂SO₄ and the solvent was removed under reduced pressure. The crude product was purified by silica gel chromatography (120 g, *n*-pentane/EtOAc 9:1) yielding 6.3 g (81%) as white solid. ¹H-NMR (400 MHz, DMSO, 20 °C): δ 6.92 (t, *J* = 8.1 Hz, 1H, CH), 6.02 (d, *J* = 8.1 Hz, 2H, CH), 4.85 (t, *J* = 4.9 Hz, 2H, NH), 3.11 (qd, *J* = 7.1, *J* = 5.8, 4H, CH₂), 1.15 (t, *J* = 7.1 Hz, 6H, CH₃). ¹³C{¹H}-NMR (101 MHz, DMSO, 20 °C): δ 144.4 (s, C-N), 127.7 (s, C-Cl), 102.7 (s, CH), 99.7 (s, CH), 37.4 (s, CH₂), 14.6

(s, CH₃). **HR-MS** (ESI⁺, CH₃CN/MeOH + 1%H₂O): m/z calcd for C₁₀H₁₆ClN₂ [M+H]⁺ 199.0997, found 199.0993.

PCP^{NEt}-Cl (5)

4 (8.3 g, 41.8 mmol) was placed in a 250 mL three-necked round-bottom flask with dropping funnel and thermometer to monitor the reaction temperature and dissolved in THF (75 mL). At -75 °C *n*-BuLi (16.8 mL, 2.5 M in THF, 42 mmol) was added in a drop-wise fashion, so that the temperature remained below -70 °C. After complete addition the dropping funnel was washed with THF and (*i*Pr₂)PCl (6.4 g, 41.9 mmol) was added in a drop-wise fashion at -75 °C. The reaction mixture was stirred for 2 h, allowing it to slowly warm up to -30 °C. Then the second equivalent *n*-BuLi (16.8 mL, 2.5 M in THF, 42 mmol) and (*i*Pr₂)PCl (6.4 g, 41.9 mmol) were added in the same fashion as described before. The yellow reaction mixture was allowed to reach slowly rt and was stirred overnight. The solvent was removed under vacuum and toluene (40 mL) was added. The mixture was stirred for another 20 min at 60 °C and then filtered through a pad of silica gel and washed three times with *n*-pentane. The solvent was removed and the oily like product was dried in high vacuum. The product was purified by recrystallisation from MeOH (15 mL) yielding 9.0 g (50%) as white solid. **¹H-NMR** (400 MHz, CD₂Cl₂, 20 °C): δ 7.03 (m, 3H, CH), 3.53 (qd, *J* = 7.1 Hz, *J* = 1.9 Hz, 4H, CH₂), 2.09 (heptd, *J* = 7.1 Hz, *J* = 1.7 Hz, 4H, P-CH), 1.25 (dd, *J* = 12.1 Hz, *J* = 7.1 Hz, 12H, CHCH₃), 1.09 (dd, *J* = 14.9 Hz, *J* = 7.1 Hz, 12H, CHCH₃), 0.88 (t, *J* = 7.1 Hz, 6H, CH₂CH₃). **¹³C{¹H}-NMR** (101 MHz, CD₂Cl₂, 20 °C): δ 148.0 (d, *J* = 16.2 Hz, C-N), 131.5 (t, *J* = 4.1 Hz, C-Cl), 126.1 (dd, *J* = 8.0 Hz, *J* = 1.8 Hz, CH), 126.1 (s, CH), 44.6 (s, CH₂), 27.0 (d, *J* = 18.9 Hz, P-CH), 20.5 (d, *J* = 12.8 Hz, CHCH₃), 19.6 (d, *J* = 21.4 Hz, CHCH₃), 14.9 (s, CH₂CH₃). **³¹P{¹H}-NMR** (162 MHz, CD₂Cl₂, 20 °C): δ 84.2 (s, P). **HR-MS** (ESI⁺, CH₃CN/MeOH + 1%H₂O): m/z calcd for C₂₂H₄₂ClN₂P₂ [M+H]⁺ 431.2506, found 431.2504.

2-Bromobenzene-1,3-diol (6a)

Resorcinol (10.0 g, 90.8 mmol) was placed in a 250 mL round-bottom flask and CHCl₃ (170 mL) was added. The solution was treated with Br₂ (48 g, 300 mmol) at 0 °C within 5 min. Then the reaction mixture was stirred at reflux for 2 h. After cooling down to room temperature all volatiles were removed under reduced pressure and the remaining solid was dissolved in MeOH (50 mL) and water (200 mL). Then treated with a solution of Na₂SO₃ (23 g, 182 mmol) and NaOH (7.3 g, 183 mmol) in water (300 mL). The reaction mixture was stirred at rt over night. The next day the mixture was acidified with HCl (5%) at 0 °C and the product could be extracted with ether. The combined organic layers were dried over Na₂SO₄ and the solvent was removed under reduced pressure. The crude product was purified by silica gel chromatography (125 g, *n*-heptane/EtOAc 5:1) forming a nearly colourless oil which was put in the freezer over night. The next day white crystals were formed which were collected and recrystallised from CHCl₃/*n*-hexane yielding 13.9 g (81%) of **6a** as white crystalline solid. **¹H-NMR** (400 MHz, CD₂Cl₂, 20 °C): δ 7.11 (t, *J* = 8.2 Hz, 1H, CH), 6.59 (d, *J* = 8.2 Hz, 2H, CH), 5.50 (s, 2H, OH). **¹³C{¹H}-NMR** (101 MHz, CD₂Cl₂, 20 °C): δ 153.6 (S, C-N), 129.4 (s, CH), 108.4 (s, CH), 99.5 (s, C-Br).

2-Iodobenzene-1,3-diol (6b)

Iodine (28.5 g, 0.112 mol) and resorcinol (11.2 g, 0.102 mmol) were placed in a 500 mL round-bottom flask and dissolved in H₂O (150 mL). Then NaHCO₃ (8.8 g, 0.105 mol) was

added in portions to the reaction mixture at 0 °C and after complete addition the solution was stirred for 1 h at room temperature. Then the reaction was quenched with a Na₂SO₃ and with diethyl ether the product was extracted (3 x 150 mL). The combined organic layers were dried over Na₂SO₄ and the solvent was removed under reduced pressure yielding 15.0 g of the crude product as nearly colourless solid. After purification with silica gel chromatography 13.4 g (56%) of **6b** could be isolated as white solid. ¹H-NMR (250 MHz, DMSO, 20 °C): δ 10.03 (s, 2H, OH), 6.93 (t, *J* = 8.0 Hz, 1H, CH), 6.33 (d, *J* = 8.0 Hz, 2H, CH).

POCOP^{*i*Pr}-Br (7)

To a solution of **6a** (0.48 g, 2.54 mmol) in toluene/THF (10 mL, 1:1) Et₃N (0.55 g, 5.4 mmol) was added. The solution was treated with *i*Pr₂PdCl (0.85 g, 5.57 mmol) at 0 °C in a drop-wise fashion. Instantly white precipitate was formed and the reaction mixture was stirred at rt for 10 min. Then filtered over a glass frit and the solid was washed three times with *n*-pentane and all volatiles were removed under reduced pressure. The crude product was redissolved in *n*-pentane and filtered through a pad of silica gel. Again all volatiles were removed under reduced pressure yielding 0.87 g (81%) of **7** as colourless oil. ¹H-NMR (400 MHz, CD₂Cl₂, 20 °C): δ 7.11 (m, 1H, CH), 6.96 (m, 2H, CH), 1.99 (heptd, *J* = 7.1 Hz, *J* = 3.2 Hz, 4H, CH), 1.21 (dd, *J* = 10.8 Hz, *J* = 7.0 Hz, 12H, CHCH₃), 1.11 (dd, *J* = 15.9 Hz, *J* = 7.3 Hz, 12H, CHCH₃). ¹³C{¹H}-NMR (101 MHz, CD₂Cl₂, 20 °C): δ 157.4 (d, *J* = 9.6 Hz, C-N), 127.7 (s, CH), 111.5 (d, *J* = 21.5 Hz, CH), 106.1 (s, C-Br), 28.8 (d, *J* = 18.2 Hz, P-CH), 17.8 (d, *J* = 18.8 Hz, CHCH₃), 17.3 (d, *J* = 8.6 Hz, CHCH₃). ³¹P{¹H}-NMR (162 MHz, CD₂Cl₂, 20 °C): δ 153.7 (s, P).

POCOP^{*i*Pr}-I (8)

This ligand was prepared analogously to **7** with **6b** (0.50 g, 2.12 mmol), Et₃N (0.47 g, 4.67 mmol) and (*i*Pr₂)PdCl (0.66 g, 4.34 mmol) yielding 0.66 g (66%) as colorless oil. ¹H-NMR (250 MHz, CD₂Cl₂, 20 °C): δ 7.01 (m, 1H, CH), 6.79 (m, 2H, CH), 1.87 (m, 4H, CH), 1.04 (m, 24H, CHCH₃). ¹³C{¹H}-NMR (63 MHz, CD₂Cl₂, 20 °C): δ 159.8 (d, *J* = 9.5 Hz, C-N), 129.2 (s, CH), 110.4 (d, *J* = 22.9 Hz, CH), 83.7 (s, C-I), 28.7 (d, *J* = 17.9 Hz, CH), 17.8 (d, *J* = 19.5 Hz, CHCH₃), 17.4 (d, *J* = 8.6 Hz, CHCH₃). ³¹P{¹H}-NMR (101 MHz, CD₂Cl₂, 20 °C): δ 152.1 (s, P).

POCOP^{*t*Bu}-Br (9)

To a solution of **6a** (0.48 g, 2.54 mmol) in THF (20 mL) Et₃N (0.55 g, 5.44 mmol) was added. The solution was treated with *t*Bu₂PdCl (0.94 g, 5.20 mmol) and stirred at 80 °C for 6 d. Then 3/4 of the solvent were removed under reduced pressure and *n*-pentane (15 mL) was added. The reaction mixture was filtered over a glass frit and the solid was washed three times with *n*-pentane and all volatiles were removed from the filtrate and a white solid was formed. The crude product was redissolved in toluene and filtered through a pad of silica gel. Again all volatiles were removed under reduced pressure forming a white solid which was dried with a heat gun yielding 0.87 g (72%). ¹H-NMR (400 MHz, CD₂Cl₂, 20 °C): δ 7.04 (m, 3H, CH), 1.19 (d, *J* = 11.9, 36H, CH₃). ¹³C{¹H}-NMR (101 MHz, CD₂Cl₂, 20 °C): δ 157.8 (d, *J* = 10.1 Hz, C-N), 127.6 (s, CH), 110.5 (d, *J* = 22.2 Hz, CH), 105.2 (s, C-Br), 36.2 (d, *J* = 26.1 Hz, P-C), 27.5 (d, *J* = 15.6 Hz, CH₃). ³¹P{¹H}-NMR (162 MHz, CD₂Cl₂, 20 °C): δ 156.3 (s, P). HR-MS (ESI⁺, CH₃CN/MeOH + 1% H₂O): *m/z* calcd for C₂₂H₄₀BrO₂P₂ [M+H]⁺ 477.1681, found 477.1672.

4.2 Synthesis of Fe PCP Pincer Complexes

[Fe(PCP^{NEt}-*i*Pr)Cl(CO)₂] (10)

5 (200 mg, 0.46 mmol) and Fe₂(CO)₉ (84 mg, 0.23 mmol) were placed in a 20 mL microwave vial and suspended in MeCN (2 mL). The reaction mixture was stirred over night at 110 °C and then filtered through a syringe filter (PTFE, 0.2 μm) in a Schlenk flask and all volatiles were removed under reduced pressure. The residue was washed three times with *n*-pentane yielding 117 mg (47%) of **10** as yellow powder. Crystals suitable for X-ray diffraction measurement could be obtained by cooling a saturated *n*-pentane solution of **10** to -30 °C. Anal. Calcd for C₂₄H₄₁ClFeN₂O₂P₂ (542.85): C, 53.10; H, 7.61; N, 5.16. Found: C, 53.35; H, 7.59; N, 5.20. ¹H-NMR (600 MHz, C₆D₆, 20 °C): δ 7.20 (t, *J* = 8.0 Hz, 1H, CH), 6.27 (d, *J* = 8.0 Hz, 2H, CH), 3.10 (m, 4H, N-CH₂), 2.92 (m, 2H, P-CH), 2.34 (m, 2H, P-CH), 1.46 (dd, *J* = 22.5 Hz, *J* = 7.9 Hz, 6H, CHCH₃), 1.25 (dd, *J* = 20.6 Hz, *J* = 7.0 Hz, 6H, CHCH₃), 1.20 (dd, *J* = 22.4 Hz, *J* = 8.1 Hz, 6H, CHCH₃), 1.11 (dd, *J* = 20.6 Hz, *J* = 6.8 Hz, 6H, CHCH₃), 1.05 (t, 6H, *J* = 6.8 Hz, CH₂CH₃). ¹³C{¹H}-NMR (151 MHz, C₆D₆, 20 °C): δ 215.6 (t, *J* = 27.4 Hz, CO), 212.7 (t, *J* = 11.6 Hz, CO), 156.8 (t, *J* = 13.7 Hz, C-N), 137.5 (t, *J* = 14.4 Hz, C-Fe), 126.6 (s, CH), 103.0 (t, *J* = 5.4 Hz, CH), 41.1 (s, CH₂), 30.7 (t, *J* = 11.6 Hz, P-CH), 29.0 (t, *J* = 11.0 Hz, P-CH), 22.1 (s, CHCH₃), 19.5 (s, CHCH₃), 19.5 (s, CHCH₃), 18.9 (t, *J* = 3.4 Hz, CHCH₃), 14.2 (s, CH₂CH₃). ³¹P{¹H}-NMR (243 MHz, C₆D₆, 20 °C): δ 151.5 (s, P). HR-MS (ESI⁺, CH₃CN/MeOH + 1%¹⁸O): *m/z* calcd for C₂₄H₄₁FeN₂O₂P₂ [M-Cl]⁺ 507.1987, found 507.1990, calcd for C₂₃H₄₁FeN₂O₂P₂ [M-Cl-CO]⁺ 479.2038, found 479.2041. IR (ATR, cm⁻¹): 2002 (ν_{CO}), 1934 (ν_{CO}).

[Fe(PCP^{NEt}-*i*Pr)(CO)₂] (11)

10 (50 mg, 0.092 mmol) was dissolved in THF (3 mL) and Li[HBEt₃] (0.06 mL, 1.7 M in THF, 0.10 mmol) was added. The reaction mixture was stirred at rt for 1 h and the color instantly changed from orange to violet. Then all volatiles were removed under reduced pressure and an oily residue was formed. The product was redissolved in *n*-pentane and filtered through a syringe filter (PTFE, 0.2 μm). Crystals suitable for X-ray diffraction measurement could be obtained by cooling the *n*-pentane solution to -30 °C over night. All volatiles were removed under reduced pressure yielding 21 mg (45%) of **11** as violet solid. Anal. Calcd for C₂₄H₄₁FeN₂O₂P₂ (507.40): C, 56.81; H, 8.15; N, 5.52. Found: C, 56.95; H, 8.39; N, 5.45. HR-MS (ESI⁺, CH₃CN/MeOH + 1%¹⁸O): *m/z* calcd for C₂₄H₄₁FeN₂O₂P₂ [M]⁺ 507.1987, found 507.1988, *m/z* calcd for C₂₃H₄₁FeN₂O₂P₂ [M-CO]⁺ 479.2038, found 479.2038. μ_{eff} = 1.8(1) μ_B (benzene, Evans method). IR (ATR, cm⁻¹): 1933 (ν_{CO}), 1864 (ν_{CO}).

[Fe(PCP^{NEt}-*i*Pr)(CO)(NO)] (12)

11 (80 mg, 0.16 mmol) was placed in a Schlenk flask and dissolved in benzene (2 mL). The solution was stirred at rt for 1 h under a NO gas (1 bar) atmosphere turning from violet to red. All volatiles were removed under reduced pressure and the product was dissolved in *n*-pentane and filtered through a syringe filter (PTFE, 0.2 μm). Then all volatiles were removed under reduced pressure yielding 57 mg (71%) of **12** as red solid. Anal. Calcd for C₂₃H₄₁FeN₃O₂P₂ (509.39): C, 54.23; H, 8.11; N, 8.25. Found: C, 54.37; H, 8.09; N, 8.10. ¹H-NMR (600 MHz, C₆D₆, 20 °C): δ 7.19 (t, *J* = 7.9 Hz, 1H, CH), 6.21 (d, *J* = 7.9 Hz, 2H, CH), 3.16 (m, 2H, N-CH₂), 3.03 (m, 2H, N-CH₂), 2.39 (hept, *J* = 6.8 Hz, 2H, P-CH), 2.30 (hept, *J* = 7.1 Hz, 2H, P-CH), 1.33 (dd, *J* = 24.6 Hz, *J* = 10.6 Hz, 6H, CHCH₃), 1.08

(m, 12H, CHCH₃, CH₂CH₃), 0.99 (dd, $J = 22.9$ Hz, $J = 8.5$ Hz, 6H, CHCH₃), 0.90 (dd, $J = 19.9$ Hz, $J = 5.9$ Hz, 6H, CHCH₃). **¹³C{¹H}-NMR** (151 MHz, C₆D₆, 20 °C): δ 228.3 (t, $J = 29.0$ Hz, CO), 157.9 (t, $J = 15.4$ Hz, C-N), 137.4 (t, $J = 24.1$ Hz, C-Fe), 126.9 (s, CH), 101.5 (t, $J = 6.2$ Hz, CH), 40.3 (s, CH₂), 31.8 (t, $J = 11.0$ Hz, P-CH), 28.1 (t, $J = 13.6$ Hz, P-CH), 18.2 (s, CHCH₃), 17.9 (s, CHCH₃), 17.2 (s, CHCH₃), 17.1 (t, $J = 4.1$ Hz, CHCH₃), 14.2 (s, CH₂CH₃). **³¹P{¹H}-NMR** (243 MHz, C₆D₆, 20 °C): δ 171.6 (s, P). **HR-MS** (ESI⁺, CH₃CN/MeOH + 1% H₂O): m/z calcd for C₂₃H₄₁FeN₃NaO₂P₂ [M+Na]⁺ 532.1916, found 532.1923, calcd for C₂₂H₄₁FeN₃OP₂ [M-CO]⁺ 481.2069, found 481.2075. **IR** (ATR, cm⁻¹): 1889 (ν_{CO}), 1663 (ν_{NO}).

[Fe(κ^3 P,CH,P-P(CH)P^{NEt}-*i*Pr)(CO)(NO)]BF₄ (**13**)

12 (57 mg, 0.11 mmol) was placed in a Schlenk flask and dissolved in THF (2 mL) forming an intensive red solution. HBF₄·Et₂O (24 mg, 0.15 mmol) was added and the reaction mixture was stirred 15 min at rt. All volatiles were removed under reduced pressure and the residue was washed with Et₂O (2 x 5 mL) yielding 65 mg (97%) of **13** as red solid. Crystals suitable for X-ray diffraction measurement were obtained by Et₂O diffusion into a THF solution of **13**. Anal. Calcd for C₂₃H₄₂BF₄FeN₃O₂P₂ (597.20): C, 46.26; H, 7.09; N, 7.04. Found: C, 46.39; H, 7.12; N, 7.13. **¹H-NMR** (600 MHz, CD₃CN, 20 °C): δ 7.51 (tt, $J = 8.2$ Hz, $J = 1.5$ Hz, 1H, CH), 6.42 (d, $J = 8.3$ Hz, 2H, CH), 3.61 (m, 2H, N-CH₂), 3.42 (m, 2H, N-CH₂), 2.84 (m, 2H, P-CH), 2.76 (t, $J = 6.1$ Hz, 1H, CH-Fe) 2.69 (m, 2H, P-CH), 1.24 (dd, $J = 18.0$ Hz, $J = 7.1$ Hz, 6H, CHCH₃), 1.19 (dd, $J = 16.1$ Hz, $J = 7.1$ Hz, 6H, CHCH₃), 1.06 (t, $J = 7.1$ Hz, 6H, CH₂CH₃), 1.01 (dd, $J = 20.9$ Hz, $J = 6.9$ Hz, 6H, CHCH₃), 0.88 (dd, $J = 17.0$ Hz, $J = 7.0$ Hz, 6H, CHCH₃). **¹³C{¹H}-NMR** (151 MHz, CD₃CN, 20 °C): δ 216.6 (t, $J = 61.0$ Hz, CO), 167.5 (t, $J = 10.2$ Hz, C-N), 142.7 (s, CH), 107.4 (t, $J = 4.2$ Hz, CH), 66.5 (t, $J = 3.4$ Hz, C(H)-Fe), 41.7 (s, CH₂), 30.9 (t, $J = 14.0$ Hz, P-CH), 30.0 (t, $J = 11.5$ Hz, P-CH), 18.2 (s, CHCH₃), 17.7 (s, CHCH₃), 16.9 (s, CHCH₃), 15.2 (t, $J = 4.0$ Hz, CHCH₃), 13.2 (s, CH₂CH₃). **³¹P{¹H}-NMR** (243 MHz, CD₃CN, 20 °C): δ 142.2 (s, P). **HR-MS** (ESI⁺, CH₃CN/MeOH + 1% H₂O): m/z calcd for C₂₂H₄₁FeN₃OP₂ [M-H-CO]⁺ 481.2069, found 481.2068. **IR** (ATR, cm⁻¹): 1932 (ν_{CO}), 1720 (ν_{NO}).

[Fe(POCOP-*t*Bu)(CO)₂] (**14**)

A solution of **9** (56 mg, 0.12 mmol) and Fe(CO)₅ (22 mg, 0.11 mmol) in toluene (3 mL) was placed in a 8 mL microwave vial and stirred at 180 °C over night. The reaction mixture was cooled to room temperature without stirring and transferred in a Schlenk flask. All volatiles were removed under reduced pressure and the product could be extracted with *n*-pentane and was filtered through a syringe filter (PTFE, 0.2 μm). After drying the product could be obtained with a yield of 28 mg (47%) as green solid. Crystals suitable for X-ray diffraction measurement were obtained by cooling a saturated *n*-pentane solution of **14** to -20 °C. **HR-MS** (ESI⁺, CH₃CN/MeOH + 1% H₂O): m/z calcd for C₂₃H₃₉FeO₃P₂ [M-CO]⁺ 481.1718, found 481.1713. μ_{eff} = 1.8(1) μ_B (benzene, Evans method). **IR** (ATR, cm⁻¹): 1947 (ν_{CO}), 1876 (ν_{CO}).

4.3 Synthesis of Mn PCP Pincer Complexes

[Mn(PCP^{NEt}-*i*Pr)(CO)₃] (15)

A suspension of Mn₂(CO)₁₀ (90 mg, 0.23 mmol) and **5** (100 mg, 0.23 mmol) in CH₃CN (1 mL) were placed in a 20 mL microwave vial and stirred for 6 h at 150 °C. The reaction mixture was allowed to cool to rt. The microwave vial was opened at ambient conditions and all volatiles were removed under reduced pressure. The crude product was purified by silica gel chromatography (*n*-hexane/ethyl acetate 4:1) and recrystallized from *n*-hexane ethyl acetate yielding 49 mg (40%) as white solid from which a single crystal suitable for x-ray diffraction measurement could be obtained. Anal. Calcd for C₂₅H₄₁MnN₂O₃P₂ (534.50): C, 56.18; H, 7.73; N, 5.24. Found: C, 56.26; H, 7.69; N, 5.33. ¹H-NMR (600 MHz, CD₂Cl₂, 20 °C): δ 6.88 (t, *J* = 7.8 Hz, 1H, CH), 6.10 (d, *J* = 7.9 Hz, 2H, CH), 3.48 (m, 4H, N-CH₂), 2.68 (m, 4H, P-CH), 1.38 (dd, 12H, *J* = 14.9 Hz, *J* = 6.8 Hz, CHCH₃), 1.25 (m, 18H, CHCH₃, CH₂CH₃). ¹³C{¹H}-NMR (151 MHz, CD₂Cl₂, 20 °C): δ 225.2 (br, CO), 222.6 (t, *J* = 24.1 Hz, CO), 157.3 (t, *J* = 14.2 Hz, C-N), 132.8 (t, *J* = 10.7 Hz, C-Mn), 125.2 (s, CH), 101.7 (t, *J* = 5.2 Hz, CH), 41.3 (s, CH₂), 32.3 (m, P-CH), 20.3 (s, CHCH₃), 19.3 (s, CHCH₃), 14.4 (s, CH₂CH₃). ³¹P{¹H}-NMR (243 MHz, CD₂Cl₂, 20 °C): δ 162.5 (s, P). HR-MS (ESI⁺, CH₃CN/MeOH + 1% H₂O): *m/z* calcd for C₂₅H₄₁MnN₂O₃P₂ [M]⁺ 534.1967, found 534.1964. IR (ATR, cm⁻¹): 1912 (ν_{CO}), 1900 (ν_{CO}), 1884 (ν_{CO}).

[Mn(PCP^{NEt}-*i*Pr)(CO)₂(NO)]BF₄ (16)

To a solution of **15** (118 mg, 0.22 mmol) in CH₂Cl₂ (5 mL) NOBF₄ (30 mg, 0.26 mmol) was added. The reaction mixture was stirred for 18 h at rt and the colour changed from pale yellow to dark red. Then the mixture was filtered through a pad of celite[®] and all volatiles were removed under reduced pressure. The remaining solid was washed three times with *n*-pentane and dried under vacuum yielding 129 mg (94%) as red solid. Crystals suitable for X-ray diffraction measurement were obtained by *n*-pentane diffusion into an acetone solution of **16**. Anal. Calcd for C₂₄H₄₁BF₄MnN₃O₃P₂ (623.30): C, 46.25; H, 6.63; N, 6.74. Found: C, 46.35; H, 6.51; N, 6.82. ¹H-NMR (400 MHz, CD₂Cl₂, 20 °C): δ 7.17 (t, *J* = 8.1 Hz, 1H, CH), 6.31 (d, *J* = 8.1 Hz, 2H, CH), 3.59 (m, 4H, N-CH₂), 3.04 (m, 4H, P-CH), 1.44 (ddd, *J* = 27.4 Hz, *J* = 17.0 Hz, *J* = 7.3 Hz, 24H, CHCH₃), 1.33 (t, *J* = 7.0 Hz, 6H, CH₂CH₃). ¹³C{¹H}-NMR (101 MHz, CD₂Cl₂, 20 °C): δ 157.3 (t, *J* = 12.2 Hz, C-N), 131.5 (s, CH), 106.0 (t, *J* = 5.0 Hz, CH), 42.3 (s, CH₂), 32.7 (t, *J* = 11.1 Hz, P-CH), 19.8 (s, CHCH₃), 18.8 (s, CHCH₃), 14.0 (s, CH₂CH₃). The resonances of the *ipso*-carbon and the CO ligands could not be detected. ³¹P{¹H}-NMR (162 MHz, CD₂Cl₂, 20 °C): δ 148.4 (br, P). MS (ESI⁺, CH₃CN) *m/z* calcd for C₂₄H₄₁MnN₃O₃P₂ [M]⁺ 536.2, found 536.2. IR (ATR, cm⁻¹): 2017 (ν_{CO}), 1913 (ν_{CO}), 1767 (ν_{NO}).

[Mn(κ³P,CH,P-P(CH)P^{NEt}-*i*Pr)(CO)₃]BF₄ (17)

A solution of **15** (34 mg, 0.064 mmol) in CH₂Cl₂ (4 mL) was treated with HBF₄·Et₂O (12 mg, 0.074 mmol). The reaction mixture was stirred for 15 min at rt and the colour changed from colourless to yellow. All volatiles were removed under reduced pressure and the residue was washed three times with Et₂O yielding 37 mg (93%) as yellow solid. Crystals suitable for X-ray diffraction measurement were obtained by *n*-pentane diffusion into a THF solution of **17**. Anal. Calcd for C₂₅H₄₂BF₄MnN₂O₃P₂ (622.31): C, 48.25; H, 6.80; N, 4.50. Found: C, 47.96; H, 6.91; N, 4.58. ¹H-NMR (600 MHz, CD₂Cl₂, 20 °C): δ 7.63 (t, *J* = 8.2 Hz, 1H, CH), 6.52 (d, *J* = 8.2 Hz, 2H, CH), 3.68 (m, 2H, N-CH₂), 3.49 (m, 2H, N-CH₂), 2.84 (m, 4H, P-CH), 1.47 (m, 12H, CHCH₃), 1.36 (t, *J* = 4.6 Hz, 1H, C(H)-Mn),

1.25 (m, 18H, CHCH₃, CH₂CH₃). ¹³C{¹H}-NMR (151 MHz, CD₂Cl₂, 20 °C): δ 221.8 (br, CO), 216.7 (t, *J* = 17.9 Hz, CO), 215.0 (t, *J* = 19.1 Hz, CO), 169.6 (t, *J* = 9.3 Hz, C-N), 141.4 (s, CH), 108.9 (t, *J* = 4.0 Hz, CH), 48.8 (s, C_{ipso}-Mn), 41.9 (s, CH₂), 33.6 (m, P-CH), 31.9 (m, P-CH), 18.8 (s, CHCH₃), 18.5 (s, CHCH₃), 18.2 (t, *J* = 4.1 Hz, CHCH₃), 18.0 (t, *J* = 2.7 Hz, CHCH₃), 12.9 (s, CH₂CH₃). ³¹P{¹H}-NMR (243 MHz, CD₂Cl₂, 20 °C): 148.7 (s, P). **HR-MS** (ESI⁺, CH₃CN/MeOH + 1% H₂O): *m/z* calcd for C₂₅H₄₂MnN₂O₃P₂ [M]⁺ 535.2046, found 535.2042. **IR** (ATR, cm⁻¹): 1942 (ν_{CO}), 1899 (ν_{CO}), 1880 (ν_{CO}).

4.4 Synthesis of Cr PCP Pincer Complexes

trans-[Cr(PCP^{NEt}-*i*Pr)Cl₂(CH₃CN)] (18)

A suspension of Cr(CO)₆ (77 mg, 0.35 mmol) and **5** (150 mg, 0.35 mmol) in acetonitrile (3 mL) was placed in a 20 mL microwave vial and stirred for 3 h at 150 °C whereupon a clear solution developed. The reaction mixture was then allowed to cool to rt and the product was obtained as crystalline material which was redissolved in CH₂Cl₂ (2 mL) and precipitated with *n*-pentane (15 mL). The supernatant was removed and the solid was washed two times with *n*-pentane yielding 46 mg (47%) as red solid. The second formed species **19** could not be isolated in pure form. Anal. Calcd for C₂₄H₄₄Cl₂CrN₃P₂ (559.48): C, 51.52; H, 7.93; N, 7.51. Found: C, 51.34; H, 8.19; N, 8.21. μ_{eff} = 3.9(1) μ_B (CH₂Cl₂, Evans method). **IR** (ATR, cm⁻¹): 2207 (ν_{CN}).

trans-[Cr(PCP^{NEt}-*i*Pr)Cl₂(THF)] (20)

Method A: A suspension of Cr(CO)₆ (77 mg, 0.35 mmol) and **5** (150 mg, 0.35 mmol) in toluene (3 mL) was placed in a 20 mL microwave vial and stirred for 6 h at 150 °C whereupon a clear solution developed. The reaction mixture was then allowed to cool to rt and was filtered through a syringe filter (PTFE, 0.2 μm) in a Schlenk flask. All volatiles were removed and the crude product was redissolved in THF and recrystallised by *n*-pentane diffusion yielding 35 mg (34%) as orange crystals. The second formed species **19** could not be isolated in pure form. **Method B:** **5** (150 mg, 0.35 mmol) was dissolved in THF (5 mL) and *n*-BuLi (0.5 mL, 1.6 M in *n*-hexane, 0.8 mmol) was added in a drop-wise fashion at -70 °C and stirred for 20 min at this temperature. Then a solution of CrCl₃·3THF (131 mg, 0.35 mmol) in THF (5 mL) was added in a drop-wise fashion. The reaction mixture turned red and was stirred for 15 min at -70 °C then another 15 min at rt. Then all volatiles were removed and the red solid was redissolved in CH₂Cl₂ (3 mL) and filtered through a syringe filter (big, PTFE, 0.2 μm) to remove insoluble materials. Again all volatiles were removed and the formed precipitate was dried under reduced pressure yielding 138 mg (64%) as red solid. μ_{eff} = 3.8(1) μ_B (CH₂Cl₂, Evans method).

trans-[Cr(POCOP-*i*Pr)Br₂(CH₃CN)] (21)

This complex was prepared analogously to **18** with Cr(CO)₆ (78 mg, 0.36 mmol) and **7** (150 mg, 0.36 mmol) yielding 43 mg (41%) as red solid. The second formed species **22** could not be isolated in pure form. μ_{eff} = 4.0(1) μ_B (CH₂Cl₂, Evans method).

trans-[Cr(POCOP-*i*Pr)Br₂(THF)] (23)

This complex was prepared analogously to **20** method A with Cr(CO)₆ (78 mg, 0.36 mmol) and **7** (150 mg, 0.36 mmol) yielding 26 mg (24%) as orange crystals. The second formed

species **22** could not be isolated in pure form. Anal. Calcd for $C_{22}H_{39}Br_2CrO_3P_2$ (625.30): C, 42.26; H, 6.29. Found: C, 42.36; H, 6.18. $\mu_{\text{eff}} = 3.9(1) \mu_B$ (CH_2Cl_2 , Evans method).

trans-[Cr(POCOP-*i*Pr)Cl₂(THF)] (**24**)

This complex was prepared analogously to **20** method B with $CrCl_3 \cdot 3THF$ (448 mg, 1.20 mmol), *n*-BuLi (1.6 mL, 1.6 M in *n*-hexane, 2.6 mmol) and **7** (500 mg, 1.19 mmol) yielding 350 mg (56%) as red solid. $\mu_{\text{eff}} = 3.8(1) \mu_B$ (CH_2Cl_2 , Evans method).

cis-[Cr(POCOP-*i*Pr)I₂(CH₃CN)] (**25**)

A suspension of $Cr(CO)_6$ (71 mg, 0.32 mmol) and **8** (150 mg, 0.32 mmol) in toluene (3 mL) was placed in a 20 mL microwave vial and stirred for 18 h at 160 °C whereupon a clear solution developed. The reaction mixture was then allowed to cool to rt and the product was obtained as crystalline material which was redissolved in CH_2Cl_2 (2 mL) and precipitated with *n*-pentane (15 mL). The supernatant was removed and the solid washed two times with *n*-pentane yielding 46 mg (42%) as dark red solid. $\mu_{\text{eff}} = 3.9(1) \mu_B$ (CH_2Cl_2 , Evans method).

[Cr(POCOP-*t*Bu)Br] (**26**)

A mixture of **9** (100 mg, 0.21 mmol) and $Cr(CO)_6$ (47 mg, 0.21 mmol) in toluene (3 mL) was placed in a 20 mL microwave vial. The solution was stirred at 180 °C for 3 h turning intensive red and then cooled to rt without stirring. The pure product could be obtained directly from the reaction mixture as red crystals (which were suitable for X-ray diffraction measurements) yielding 84 mg (76%). Anal. Calcd for $C_{22}H_{39}BrCrO_2P_2$ (529.40): C, 49.91; H, 7.43. Found: C, 49.46; H, 7.28. $\mu_{\text{eff}} = 4.8(1) \mu_B$ (CH_2Cl_2 , Evans method).

[Cr(POCOP-*t*Bu)(BH₄)] (**27**)

To a solution of **26** (25 mg, 0.047 mmol) in THF (4 mL) $LiBH_4$ (2 mg, 0.09 mmol) was added and stirred at rt overnight. A color change could not be observed. All volatiles were removed under reduced pressure and the red/brown residue was redissolved in CH_2Cl_2 (2 mL) and filtered through a pad of Al_2O_3 (basic activated). The product was dried under vacuum and could be isolated as red solid with a yield of 19 mg (86%). Crystals suitable for X-ray diffraction measurement were obtained by *n*-pentane diffusion into a THF solution of **27**. Anal. Calcd for $C_{22}H_{43}BCrO_2P_2$ (464.34): C, 56.91; H, 9.33. Found: C, 56.53; H, 9.11. $\mu_{\text{eff}} = 4.9(1) \mu_B$ (CH_2Cl_2 , Evans method). **IR** (ATR, cm^{-1}): 2407 (ν_{BH}), 2068 (ν_{BH}).

[Cr(POCOP-*t*Bu)(NO)(BH₄)] (**28**)

Method A: A solution of **27** (20 mg, 0.043 mmol) in toluene (3 mL) was placed in a Schlenk flask and put under a NO gas atmosphere (1 bar). The colour changed immediately from red to dark red and the reaction mixture was stirred at rt for 15 min. Then all volatiles were removed under reduced pressure yielding 19 mg (88%) as brown solid. **Method B:** To a solution of **29** (20 mg, 0.036 mmol) in THF (4 mL) $LiBH_4$ (2 mg, 0.09 mmol) was added and stirred at rt overnight. The colour changed from black to dark dark red. All volatiles were removed under reduced pressure and the red/brown residue was redissolved in CH_2Cl_2 (2 mL) and filtered through a pad of Al_2O_3 (basic activated). The product was dried under vacuum and could be isolated as brown solid with a yield of 16 mg (91%). Crystals suitable for X-ray diffraction measurement could be obtained by evaporation of a

saturated *n*-pentane solution of **28** at -20 °C. Anal. Calcd for C₂₂H₄₃BCrNO₃P₂ (494.34): C, 53.45; H, 8.77; N, 2.83. Found: C, 53.65; H, 8.43; N, 3.00. $\mu_{\text{eff}} = 2.0(1) \mu_{\text{B}}$ (CH₂Cl₂, Evans method). **IR** (ATR, cm⁻¹): 2465 (ν_{BH}), 2427 (ν_{BH}), 2016 (ν_{BH}), 1654 (ν_{NO}).

[Cr(POCOP-*t*Bu)(NO)Br] (**29**)

A solution of **26** (25 mg, 0.047 mmol) in toluene (3 mL) was placed in a Schlenk flask and put under a NO gas atmosphere (1 bar) and stirred for 20 min at rt. The colour changed immediately from red to black. Then all volatiles were removed under reduced pressure yielding 25 mg (95%) as black solid. Crystals suitable for X-ray diffraction measurement were obtained by *n*-pentane diffusion into a THF solution of **29**. Anal. Calcd for C₂₂H₃₉BrCrNO₃P₂ (559.41): C, 47.24; H, 7.03; N, 2.5. Found: C, 47.49; H, 6.92; N, 2.68. $\mu_{\text{eff}} = 1.8(1) \mu_{\text{B}}$ (CH₂Cl₂, Evans method). **IR** (ATR, cm⁻¹): 1654 (ν_{NO}).

[Cr(POCOP-*t*Bu)(CH₂SiMe₃)] (**30**)

To a solution of **26** (115 mg, 0.217 mmol) in toluene (6 mL) Li(CH₂SiMe₃) (0.23 mL, 1 M, 0.23 mmol) was added and stirred at rt for 4 h. The colour changed from red to a darker more intensive red. Then all volatiles were removed under reduced pressure and dried for another 20 min at fine vacuum. The residue was redissolved in *n*-pentane (1 mL) and filtered through a syringe filter (PTFE, 0.2 μm) into a 4 mL glass vial and the filter was washed two times with *n*-pentane (0.5 mL). The saturated solution was put in the freezer (-20 °C) over night. The next day red crystals could be collected (which were suitable for X-ray diffraction measurements) with a yield of 67 mg (57%). Anal. Calcd for C₂₆H₅₀CrO₂P₂Si (536.71): C, 58.18; H, 9.39. Found: C, 58.27; H, 9.25. $\mu_{\text{eff}} = 4.8(1) \mu_{\text{B}}$ (C₆H₆, Evans method).

4.5 Synthesis of Mo PCP Pincer Complexes

[Mo(PCP^{NEt}-*i*Pr)(CO)₃Cl] (**31**)

A suspension of Mo(CO)₆ (92 mg, 0.35 mmol) and **5** (150 mg, 0.35 mmol) in CH₃CN (2.5 mL) was placed in a 20 mL microwave vial and stirred for 3 h at 130 °C. After reaching rt, the pure product could be obtained directly from the reaction mixture as orange crystals (which were suitable for X-ray diffraction measurements) yielding 175 mg (82%). Anal. Calcd. for C₂₅H₄₁ClMoN₂O₃P₂ (612.97): C, 49.15; H, 6.76; N, 4.59. Found: C, 49.88; H, 6.80; N, 4.62. **¹H-NMR** (600 MHz, CD₂Cl₂, 20 °C): δ 7.07 (m, 1H, CH), 6.27 (d, *J* = 8.1 Hz, 2H, CH), 3.59 (m, 2H, N-CH₂), 3.51 (m, 2H, N-CH₂), 2.86 (m, 2H, P-CH), 2.75 (m, 2H, P-CH), 1.36 (m, 18H, CHCH₃), 1.28 (t, *J* = 7.0 Hz, 6H, CH₂CH₃), 1.17 (dd, *J* = 15.1 Hz, *J* = 7.3 Hz, 6H, CHCH₃). **¹³C{¹H}-NMR** (151 MHz, CD₂Cl₂, 20 °C): δ 240.6 (br, CO), 228.7 (t, *J* = 14.5 Hz, CO), 157.4 (t, *J* = 12.2 Hz, C-N), 135.4 (t, *J* = 8.1 Hz, C-Mo), 104.6 (t, *J* = 5.2 Hz, CH), 41.4 (s, CH₂), 31.3 (t, *J* = 11.3 Hz, P-CH), 30.7 (t, *J* = 9.3 Hz, P-CH), 21.5 (s, CHCH₃), 20.5 (s, CHCH₃), 19.3 (s, CHCH₃), 19.2 (t, *J* = 2.0 Hz, CHCH₃), 13.9 (s, CH₂CH₃). **³¹P{¹H}-NMR** (243 MHz, CD₂Cl₂, 20 °C): δ 143.3 (s, P). **IR** (ATR, cm⁻¹): 2007 (ν_{CO}), 1921 (ν_{CO}), 1899 (ν_{CO}).

[K(THF)₂][Mo(PCP^{NEt}-*i*Pr)(CO)₃] (**33**)

To a solution of **31** (50 mg, 0.082 mmol) in THF (4 mL) K₂C₈ (43 mg, 0.32 mmol) was added and the reaction mixture was stirred for 2 days at 25 °C. The mixture was then filtered through a syringe filter (PTFE, 0.2 μm). Then all volatiles were removed under

reduced pressure and the product could be isolated yielding 59 mg (95%) as red solid. Crystals suitable for X-ray diffraction measurement were obtained by *n*-pentane diffusion into a THF solution of **33**. **¹H-NMR** (600 MHz, THF-*d*₈, 20 °C): δ 6.48 (t, *J* = 7.8 Hz, 1H, CH), 5.75 (d, *J* = 7.8 Hz, 2H, CH), 3.41 (m, 4H, N-CH₂), 2.27 (m, 4H, P-CH), 1.19 (m, 18H, CHCH₃, CH₂CH₃), 1.01 (dd, *J* = 13.0 Hz, *J* = 6.9 Hz, 12H, CHCH₃). **¹³C{¹H}-NMR** (151 MHz, THF-*d*₈, 20 °C): δ 239.6 (t, *J* = 4.5 Hz, CO), 227.1 (t, *J* = 10.9 Hz, CO), 159.2 (t, *J* = 15.7 Hz, C-N), 150.0 (t, *J* = 10.6 Hz, C-Mo), 122.7 (s, CH), 100.2 (t, *J* = 5.0 Hz, CH), 41.3 (s, CH₂), 33.7 (t, *J* = 7.7 Hz, P-CH), 20.9 (t, *J* = 6.3 Hz, CHCH₃), 20.3 (s, CHCH₃), 15.0 (s, C₂HCH₃). **³¹P{¹H}-NMR** (243 MHz, THF-*d*₈, 20 °C): δ 163.0 (s, P). **HR-MS** (ESI⁺, CH₃CN/MeOH + 1%H₂O): *m/z* calcd for C₂₂H₄₁MoN₂O₃P₂ [M-3(CO)+3O]⁺ 541.1646, found 541.1643, *m/z* calcd for C₂₂H₄₁MoN₂O₄P₂ [M-3(CO)+4O]⁺ 557.1596, found 557.1596, *m/z* calcd for C₂₂H₄₁MoN₂O₅P₂ [M-3(CO)+5O]⁺ 573.1545, found 573.1546. **IR** (ATR, cm⁻¹): 1908 (ν_{CO}), 1787 (ν_{CO}), 1744 (ν_{CO}).

[Mo(κ³P,CH,P-P(CH)P^{NEt}-*i*Pr)(CO)₃] (**35**)

MeOH (0.5 mL) was added to **33** (44 mg, 0.058 mmol). A clear solution was obtained and shortly after orange crystals were formed (which were suitable for X-ray diffraction measurements). The supernatant was removed and the solid was washed two times with MeOH yielding 32 mg (96%). Anal. Calcd for C₂₅H₄₂MoN₂O₃P₂ (576.53): C, 52.08; H, 7.34; N, 4.86. Found: C, 52.12; H, 7.24; N, 4.93. **¹H-NMR** (600 MHz, CD₂Cl₂, 20 °C): δ 7.22 (tt, *J* = 8.1 Hz, *J* = 1.2 Hz, 1H, CH), 6.31 (dd, *J* = 8.2 Hz, *J* = 1.9 Hz, 2H, CH), 3.59 (m, 2H, N-CH₂), 3.40 (m, 2H, N-CH₂), 2.46 (m, 2H, P-CH), 2.39 (m, 2H, P-CH), 1.61 (tt, *J* = 4.2 Hz, *J* = 1.9 Hz, 1H, C(H)-Mo), 1.31 (m, 12H, CHCH₃), 1.13 (m, 12H, CHCH₃, CH₂CH₃), 1.01 (dd, *J* = 14.2 Hz, *J* = 7.0 Hz, 6H, CHCH₃). **¹³C{¹H}-NMR** (151 MHz, CD₂Cl₂, 20 °C): δ 233.4 (t, *J* = 6.1 Hz, CO), 220.8 (t, *J* = 8.6 Hz, CO), 216.9 (t, *J* = 10.3 Hz, CO), 162.4 (t, *J* = 9.6 Hz, C-N), 133.3 (s, CH), 106.5 (t, *J* = 3.7 Hz, CH), 75.5 (t, *J* = 4.7 Hz, C(H)-Mo), 40.6 (s, CH₂), 33.5 (t, *J* = 6.7 Hz, P-CH), 32.1 (t, *J* = 11.0 Hz, P-CH), 19.9 (t, *J* = 7.6 Hz, CHCH₃), 19.3 (s, CHCH₃), 18.7 (s, CHCH₃), 18.4 (t, *J* = 5.5 Hz, CHCH₃), 13.3 (s, CH₂CH₃). **³¹P{¹H}-NMR** (243 MHz, CD₂Cl₂, 20 °C): δ 149.7 (s, P). **IR** (ATR, cm⁻¹): 1947 (ν_{CO}), 1838 (ν_{CO}), 1814 (ν_{CO}).

[Mo(OCO^{NEt}-OP*i*Pr)(O₂)Cl] (**37**)

A solution of **31** (50 mg, 0.082 mmol) in THF (4 ml) was exposed to air (dried over a column filled with phosphorous pentoxide) and stirred for 3 h at rt. A colour change from green to orange could be observed. Then all volatiles were removed and the product could be isolated yielding 45 mg (93%) as orange solid. Crystals suitable for X-ray diffraction measurement were obtained by *n*-pentane diffusion into a THF solution of **37**. **¹H-NMR** (250 MHz, CD₂Cl₂, 20 °C): δ 7.29 (m, 1H, CH), 7.06 (d, *J* = 7.8 Hz, 2H, CH), 3.86 (m, 2H, N-CH₂), 3.55 (m, 2H, N-CH₂), 2.75 (m, 2H, P-CH), 2.08 (m, 2H, P-CH), 1.61 (dd, *J* = 15.3 Hz, *J* = 7.2 Hz, 6H, CHCH₃), 1.42 (dd, *J* = 16.7 Hz, *J* = 7.1 Hz, 6H, CHCH₃), 1.16 (t, *J* = 7.0 Hz, 6H, CH₂CH₃), 1.05 (dd, *J* = 17.1 Hz, *J* = 7.3 Hz, 6H, CHCH₃), 0.81 (dd, *J* = 16.2 Hz, *J* = 7.3 Hz, 6H, CHCH₃). **¹³C{¹H}-NMR** (101 MHz, CD₂Cl₂, 20 °C): δ 174.7 (s, C-N), 145.3 (s, C-Mo), 129.0 (s, CH), 117.9 (d, *J* = 4.7 Hz, CH), 42.6 (d, *J* = 4.4 Hz, CH₂), 28.9 (s, P-CH), 28.1 (s, P-CH), 25.5 (s, P-CH), 24.7 (s, P-CH), 17.7 (s, CHCH₃), 17.2 (d, *J* = 4.9 Hz, CHCH₃), 16.3 (d, *J* = 1.6 Hz, CHCH₃), 16.1 (d, *J* = 3.6 Hz, CHCH₃), 14.0 (d, *J* = 3.4 Hz, CH₂CH₃). **³¹P{¹H}-NMR** (162 MHz, CD₂Cl₂, 20 °C): δ 65.8 (s, *i*Pr₂PO). **HR-MS** (ESI⁺, CH₃CN/MeOH + 1%H₂O): *m/z* calcd for C₂₂H₄₁MoN₂O₄P₂ [M-Cl]⁺ 557.1590, found 557.1581.

[Mo(POCOP-*t*Bu)(CO)₂Br] (38)

A solution of **9** (40 mg, 0.084 mmol) and Mo(CO)₆ (22 mg, 0.083 mmol) in toluene (3 mL) was placed in a 8 mL microwave vial and stirred at 180 °C for 4 h. The solution turned blue and after cooling to rt all volatiles were removed under reduced pressure. Then redissolved in *n*-pentane and filtered through a syringe filter (PTFE, 0.2 μm). The product was dried under vacuum and could be isolated with a yield of 49 mg (93%) as blue solid. Single crystals for X-ray diffraction measurement could be obtained by slow evaporation of a saturated *n*-pentane solution of **38** at rt. **¹H-NMR** (600 MHz, CD₂Cl₂, 20 °C): δ 7.18 (t, *J* = 7.9, 1H, CH), 6.82 (d, *J* = 7.9, 2H, CH), 1.40 (d, *J* = 14.0, 18H, CH₃), 1.31 (d, *J* = 13.7, 18H, CH₃). **¹³C{¹H}-NMR** (151 MHz, CD₂Cl₂, 20 °C): δ 245.0 (t, *J* = 9.1 Hz, CO), 244.7 (t, *J* = 12.1 Hz, CO), 166.4 (t, *J* = 6.8 Hz, C-N), 148.4 (t, *J* = 10.6 Hz, C-Mo), 130.9 (s, CH), 107.9 (d, *J* = 9.6 Hz, CH), 42.9 (d, *J* = 16.2 Hz, P-C), 42.2 (s, P-C), 29.5 (s, CH₃), 29.0 (s, CH₃). **³¹P{¹H}-NMR** (243 MHz, CD₂Cl₂, 20 °C): δ 214.2 (s, P). **HR-MS** (ESI⁺, CH₃CN/MeOH + 1% H₂O): *m/z* calcd for C₂₄H₃₉MoO₄P₂ [M-Br]⁺ 551.1372, found 551.1364. **IR** (ATR, cm⁻¹): 1954 (ν_{CO}), 1873 (ν_{CO}).

4.6 Synthesis of W PCP Pincer Complexes**[W(PCP^{NEt}-*i*Pr)(CO)₃Cl] (32)**

This complex was prepared analogously to the Mo complex **31** with W(CO)₆ (122 mg, 0.35 mmol) and **5** (150 mg, 0.35 mmol) as starting materials at 170 °C and for 3 h. The pure product could be obtained directly from the reaction mixture as yellow crystals (which were suitable for X-ray diffraction measurements) yielding 196 mg (81%). Anal. Calcd for C₂₅H₄₁ClN₂O₃P₂W (698.85): C, 42.97; H, 5.91; N, 4.01. Found: C, 42.83; H, 6.02; N, 4.12. **¹H-NMR** (600 MHz, CD₂Cl₂, 20 °C): δ 7.05 (tt, *J* = 8.1 Hz, *J* = 1.3 Hz, 1H, CH), 6.28 (d, *J* = 8.1 Hz, 2H, CH), 3.59 (m, 2H, N-CH₂), 3.49 (m, 2H, N-CH₂), 2.97 (m, 2H, P-CH), 2.78 (m, 2H, P-CH), 1.36 (m, 18H, CHCH₃), 1.28 (t, *J* = 7.0 Hz, 6H, CH₂CH₃), 1.17 (dd, *J* = 15.2 Hz, *J* = 7.4 Hz, CHCH₃). **¹³C{¹H}-NMR** (151 MHz, CD₂Cl₂, 20 °C): δ 236.8 (br, CO), 220.9 (t, *J* = 11.6 Hz, CO), 157.8 (t, *J* = 12.2 Hz, C-N), 136.6 (t, *J* = 8.3 Hz, C-W), 129.0 (s, CH), 104.3 (t, *J* = 5.0 Hz, CH), 41.4 (s, CH₂), 31.4 (t, *J* = 13.0 Hz, P-CH), 30.1 (t, *J* = 11.4 Hz, P-CH), 21.7 (s, CHCH₃), 21.1 (s, CHCH₃), 19.4 (s, CHCH₃), 19.2 (s, CHCH₃), 14.0 (s, CH₂CH₃). **³¹P{¹H}-NMR** (243 MHz, CD₂Cl₂, 20 °C): δ 124.0 (s, *J*_{PW} = 104.5 Hz). **HR-MS** (ESI⁺, CH₃CN/MeOH + 1% H₂O): *m/z* calcd for C₂₅H₄₁N₂O₃P₂W [M-Cl]⁺ 663.2096, found 663.2092. **IR** (ATR, cm⁻¹): 2002 (ν_{CO}), 1915 (ν_{CO}), 1878 (ν_{CO}).

[K(THF)₂][W(PCP^{NEt}-*i*Pr)(CO)₃] (34)

This complex was prepared analogously to the Mo complex **33** with **32** (68 mg, 0.097 mmol) and KC₈ (50 mg, 0.37 mmol) as starting materials. Yielding 76 mg (93%) as yellow solid. **¹H-NMR** (600 MHz, THF-*d*₈, 20 °C): δ 6.49 (t, *J* = 7.8 Hz, 1H, CH), 5.77 (d, *J* = 7.9 Hz, 2H, CH), 3.41 (m, 4H, N-CH₂), 2.27 (m, 4H, P-CH), 1.19 (m, 18H, CHCH₃, CH₂CH₃), 0.98 (dd, *J* = 13.3 Hz, *J* = 6.9 Hz, 12H, CHCH₃). **¹³C{¹H}-NMR** (151 MHz, THF-*d*₈, 20 °C): δ 233.4 (br, CO), 219.1 (t, *J* = 8.4 Hz, CO), 160.0 (t, *J* = 16.0 Hz, C-N), 143.7 (t, *J* = 8.7 Hz, C-W), 122.5 (s, CH), 100.3 (t, *J* = 5.4 Hz, CH), 41.3 (s, CH₂), 34.2 (t, *J* = 10.6 Hz, P-CH), 21.1 (t, *J* = 5.5 Hz, CHCH₃), 20.2 (s, CHCH₃), 14.7 (s, C₂HCH₃). **³¹P{¹H}-NMR** (243 MHz, THF-*d*₈, 20 °C): δ 142.8 (s, *J*_{PW} = 160.4 Hz, P). **HR-MS** (ESI⁺, CH₃CN/MeOH + 1% H₂O): *m/z* calcd for C₂₂H₄₁N₂O₃P₂W [M-3(CO)+3O]⁺ 627.2096, found 627.2083. **IR** (ATR, cm⁻¹): 1904 (ν_{CO}), 1774 (ν_{CO}), 1740 (ν_{CO}).

Chapter 5

References

- (1) Lawrence, M. A.; Green, K.-A.; Nelson, P. N.; Lorraine, S. C. *Polyhedron* **2018**, *143*, 11–27.
- (2) Gunanathan, C.; Milstein, D. *Chemical Reviews* **2014**, *114*, 12024–12087.
- (3) Murugesan, S.; Kirchner, K. *Dalton Trans.* **2016**, *45*, 416–439.
- (4) Asay, M.; Morales-Morales, D. *Dalton Trans.* **2015**, *44*, 17432–17447.
- (5) Morales-Morales, D., *Pincer Compounds Chemistry and Application*; Elsevier: 2018.
- (6) Szabo, K. J.; Wendt, O. F., *Pincer and pincer-type complexes: applications in organic synthesis and catalysis*; John Wiley & Sons: 2014.
- (7) Garbe, M.; Junge, K.; Beller, M. *European Journal of Organic Chemistry* **2017**, *2017*, 4344–4362.
- (8) Chakraborty, S.; Bhattacharya, P.; Dai, H.; Guan, H. *Accounts of Chemical Research* **2015**, *48*, 1995–2003.
- (9) Gorgas, N.; Kirchner, K. *Accounts of Chemical Research* **2018**, *51*, 1558–1569.
- (10) Gorgas, N.; Stöger, B.; Veiros, L. F.; Kirchner, K. *ACS Catalysis* **2016**, *6*, 2664–2672.
- (11) Glatz, M.; Stöger, B.; Himmelbauer, D.; Veiros, L. F.; Kirchner, K. *ACS catalysis* **2018**, *8*, 4009–4016.
- (12) Himmelbauer, D.; Mastalir, M.; Stöger, B.; Veiros, L. F.; Pignitter, M.; Somoza, V.; Kirchner, K. *Inorganic Chemistry* **2018**, *57*, 7925–7931.
- (13) Himmelbauer, D.; Stöger, B.; Veiros, L. F.; Kirchner, K. *Organometallics* **2018**, *37*, 3475–3479.
- (14) Moulton, C. J.; Shaw, B. L. *J. Chem. Soc., Dalton Trans.* **1976**, 1020–1024.
- (15) Creaser, C. S.; Kaska, W. C. *Inorganica Chimica Acta* **1978**, *30*, L325–L326.
- (16) Gandeepan, P.; Ackermann, L. *Chem* **2018**, *4*, 199–222.
- (17) Crabtree, R. H. *Journal of Organometallic Chemistry* **2004**, *689*, 4083–4091.
- (18) Benito-Garagorri, D.; Bocokić, V.; Mereiter, K.; Kirchner, K. *Organometallics* **2006**, *25*, 3817–3823.
- (19) Gwynne, E. A.; Stephan, D. W. *Organometallics* **2011**, *30*, 4128–4135.
- (20) Shaikh, Y.; Albahily, K.; Sutcliffe, M.; Fomitcheva, V.; Gambarotta, S.; Korobkov, I.; Duchateau, R. *Angewandte Chemie International Edition* **2012**, *51*, 1366–1369.
- (21) Pandarus, V.; Zargarian, D. *Organometallics* **2007**, *26*, 4321–4334.
- (22) Castonguay, A.; Beauchamp, A. L.; Zargarian, D. *Organometallics* **2008**, *27*, 5723–5732.
- (23) Gusev, D. G.; Lough, A. J. *Organometallics* **2002**, *21*, 5091–5099.
- (24) Kumar, A.; Zhou, T.; Emge, T. J.; Mironov, O.; Saxton, R. J.; Krogh-Jespersen, K.; Goldman, A. S. *Journal of the American Chemical Society* **2015**, *137*, 9894–9911.

- (25) Vabre, B.; Lindeperg, F.; Zargarian, D. *Green Chem.* **2013**, *15*, 3188–3194.
- (26) Shih, W.-C.; Ozerov, O. V. *Organometallics* **2015**, *34*, 4591–4597.
- (27) Xu, G.; Sun, H.; Li, X. *Organometallics* **2009**, *28*, 6090–6095.
- (28) Albrecht, M.; Spek, A. L.; van Koten, G. *Journal of the American Chemical Society* **2001**, *123*, 7233–7246.
- (29) Bhattacharya, P.; Krause, J. A.; Guan, H. *Organometallics* **2011**, *30*, 4720–4729.
- (30) Bhattacharya, P.; Krause, J. A.; Guan, H. *Organometallics* **2014**, *33*, 6113–6121.
- (31) Bhattacharya, P.; Krause, J. A.; Guan, H. *Journal of the American Chemical Society* **2014**, *136*, 11153–11161.
- (32) Benito-Garagorri, D.; Alves, L. G.; Veiros, L. F.; Standfest-Hauser, C. M.; Tanaka, S.; Mereiter, K.; Kirchner, K. *Organometallics* **2010**, *29*, 4932–4942.
- (33) Zhu, G.; Li, X.; Xu, G.; Wang, L.; Sun, H. *Dalton Trans.* **2014**, *43*, 8595–8598.
- (34) Zhao, H.; Sun, H.; Li, X. *Organometallics* **2014**, *33*, 3535–3539.
- (35) Huang, S.; Zhao, H.; Li, X.; Wang, L.; Sun, H. *RSC Adv.* **2015**, *5*, 15660–15667.
- (36) Jiang, S.; Quintero-Duque, S.; Roisnel, T.; Dorcet, V.; Grellier, M.; Sabo-Etienne, S.; Darcel, C.; Sortais, J.-B. *Dalton Trans.* **2016**, *45*, 11101–11108.
- (37) Van der Boom, M. E.; Liou, S.-Y.; Shimon, L. J.; Ben-David, Y.; Milstein, D. *Inorganica Chimica Acta* **2004**, *357*, 4015–4023.
- (38) Enthaler, S.; Junge, K.; Beller, M. *Angewandte Chemie International Edition* **2008**, *47*, 3317–3321.
- (39) Misal Castro, L. C.; Li, H.; Sortais, J.-B.; Darcel, C. *Green Chem.* **2015**, *17*, 2283–2303.
- (40) Bauer, G.; Hu, X. *Inorg. Chem. Front.* **2016**, *3*, 741–765.
- (41) Kallmeier, F.; Kempe, R. *Angewandte Chemie International Edition* **2018**, *57*, 46–60.
- (42) Nguyen, D. H.; Trivelli, X.; Capet, F.; Paul, J.-F.; Dumeignil, F.; Gauvin, R. M. *ACS Catalysis* **2017**, *7*, 2022–2032.
- (43) Kumar, A.; Daw, P.; Espinosa-Jalapa, N. A.; Leitus, G.; Shimon, L. J. W.; Ben-David, Y.; Milstein, D. *Dalton Trans.* **2019**, *48*, 14580–14584.
- (44) Daw, P.; Kumar, A.; Espinosa-Jalapa, N. A.; Ben-David, Y.; Milstein, D. *Journal of the American Chemical Society* **2019**, *141*, 12202–12206.
- (45) Borghs, J. C.; Tran, M. A.; Sklyaruk, J.; Rueping, M.; El-Sepelgy, O. *The Journal of Organic Chemistry* **2019**, *84*, 7927–7935.
- (46) Anderson, N. H.; Boncella, J.; Tondreau, A. M. *Chemistry – A European Journal* **2019**, *25*, 10557–10560.
- (47) Mastalir, M.; Pittenauer, E.; Allmaier, G.; Kirchner, K. *Journal of the American Chemical Society* **2017**, *139*, 8812–8815.
- (48) Bertini, F.; Glatz, M.; Stöger, B.; Peruzzini, M.; Veiros, L. F.; Kirchner, K.; Gonsalvi, L. *ACS Catalysis* **2019**, *9*, 632–639.
- (49) Xia, T.; Spiegelberg, B.; Wei, Z.; Jiao, H.; Tin, S.; Hinze, S.; de Vries, J. G. *Catal. Sci. Technol.* **2019**, *9*, 6327–6334.
- (50) De Aguiar, S. R. M. M.; Stöger, B.; Pittenauer, E.; Allmaier, G.; Veiros, L. F.; Kirchner, K. *Organometallics* **2016**, *35*, 3032–3039.
- (51) Tomsu, G.; Mastalir, M.; Pittenauer, E.; Stöger, B.; Allmaier, G.; Kirchner, K. *Organometallics* **2018**, *37*, 1919–1926.
- (52) Bistoni, G.; Rampino, S.; Scafuri, N.; Ciancaleoni, G.; Zuccaccia, D.; Belpassi, L.; Tarantelli, F. *Chem. Sci.* **2016**, *7*, 1174–1184.

-
- (53) Crabtree, R. H., *The Organometallic Chemistry of the Transition Metals*, 6th ed.; Jhon Wiley and Sons, Inc.: Hoboken, New Jersey, 2014.
- (54) Calderazzo, F. *Angewandte Chemie International Edition in English* **1977**, *16*, 299–311.
- (55) Jones, J. H. *Platinum Metals Review* **2000**, *44*, 94–105.
- (56) Sunley, G. J.; Watson, D. J. *Catalysis Today* **2000**, *58*, 293–307.
- (57) Xia, Y.; Zhang, Y.; Wang, J. *ACS Catalysis* **2013**, *3*, 2586–2598.
- (58) Thompson, C. V.; Arman, H. D.; Tonzetich, Z. J. *Organometallics* **2017**, *36*, 1795–1802.
- (59) Thompson, C. V.; Davis, I.; DeGayner, J. A.; Arman, H. D.; Tonzetich, Z. J. *Organometallics* **2017**, *36*, 4928–4935.
- (60) Hayton, T. W.; Legzdins, P.; Sharp, W. B. *Chemical reviews* **2002**, *102*, 935–992.
- (61) Mingos, D. M. P., *Nitrosyl Complexes in Inorganic Chemistry, Biochemistry and Medicine I*; Springer: 2014; Vol. 153.
- (62) Jiang, Y.; Schirmer, B.; Blacque, O.; Fox, T.; Grimme, S.; Berke, H. *Journal of the American Chemical Society* **2013**, *135*, 4088–4102.
- (63) Fogler, E.; Iron, M. A.; Zhang, J.; Ben-David, Y.; Diskin-Posner, Y.; Leitus, G.; Shimon, L. J.; Milstein, D. *Inorganic chemistry* **2013**, *52*, 11469–11479.
- (64) Gaviglio, C.; Ben-David, Y.; Shimon, L. J.; Doctorovich, F.; Milstein, D. *Organometallics* **2009**, *28*, 1917–1926.
- (65) De La Cruz, C.; Sheppard, N. *Spectrochimica Acta Part A: Molecular and Biomolecular Spectroscopy* **2011**, *78*, 7–28.
- (66) Enemark, J.; Feltham, R. *Coordination Chemistry Reviews* **1974**, *13*, 339–406.
- (67) Van der Boom, M. E.; Milstein, D. *Chemical reviews* **2003**, *103*, 1759–1792.
- (68) Tolman, C. A. *Chemical Reviews* **1977**, *77*, 313–348.
- (69) Wiedner, E. S.; Chambers, M. B.; Pitman, C. L.; Bullock, R. M.; Miller, A. J.; Appel, A. M. *Chemical reviews* **2016**, *116*, 8655–8692.
- (70) Gorgas, N.; Alves, L. G.; Stöger, B.; Martins, A. M.; Veiros, L. F.; Kirchner, K. *Journal of the American Chemical Society* **2017**, *139*, 8130–8133.
- (71) Bornschein, C.; Werkmeister, S.; Wendt, B.; Jiao, H.; Alberico, E.; Baumann, W.; Junge, H.; Junge, K.; Beller, M. *Nature Communications* **2014**, *5*.
- (72) Werkmeister, S.; Neumann, J.; Junge, K.; Beller, M. *Chemistry—A European Journal* **2015**, *21*, 12226–12250.
- (73) Goswami, M.; Chirila, A.; Rebreyend, C.; de Bruin, B. *Topics in Catalysis* **2015**, *58*, 719–750.
- (74) Rieger, A. L.; Rieger, P. H. *Organometallics* **2004**, *23*, 154–162.
- (75) Weil, J. A.; Bolton, J. R., *Electron paramagnetic resonance: elementary theory and practical applications*; John Wiley & Sons: 2007.
- (76) Roessler, M. M.; Salvadori, E. *Chemical Society Reviews* **2018**, *47*, 2534–2553.
- (77) Stoll, S. In *Encyclopedia of Biophysics*, Roberts, G. C. K., Ed.; Springer Berlin Heidelberg: Berlin, Heidelberg, 2013, pp 2316–2319.
- (78) Brustolon, M.; Giamello, E., *Electron Paramagnetic Resonance: A Practitioners Toolkit*; John Wiley & Sons: 2009.
- (79) Ehrlich, N.; Kreye, M.; Baabe, D.; Schweyen, P.; Freytag, M.; Jones, P. G.; Walter, M. D. *Inorganic chemistry* **2017**, *56*, 8415–8422.
- (80) Tondreau, A. M.; Milsmann, C.; Lobkovsky, E.; Chirik, P. J. *Inorganic chemistry* **2011**, *50*, 9888–9895.

- (81) Pecak, J.; Stöger, B.; Mastalir, M.; Veiros, L. F.; Ferreira, L. P.; Pignitter, M.; Linert, W.; Kirchner, K. *Inorganic Chemistry* **2019**, *58*, 4641–4646.
- (82) Glatz, M.; Stöger, B.; Bichler, B.; Bauer, G.; Veiros, L. F.; Pignitter, M.; Kirchner, K. *European Journal of Inorganic Chemistry* **2019**, in press.
- (83) Kupper, C.; Schober, A.; Demeshko, S.; Bergner, M.; Meyer, F. *Inorganic Chemistry* **2015**, *54*, 3096–3098.
- (84) Kuriyama, S.; Arashiba, K.; Nakajima, K.; Matsuo, Y.; Tanaka, H.; Ishii, K.; Yoshizawa, K.; Nishibayashi, Y. *Nature communications* **2016**, *7*, 12181.
- (85) Ohki, Y.; Hoshino, R.; Tatsumi, K. *Organometallics* **2016**, *35*, 1368–1375.
- (86) Evans, D. F. *J. Chem. Soc.* **1959**, 2003–2005.
- (87) Schubert, E. M. *Journal of Chemical Education* **1992**, *69*, 62.
- (88) Himmelbauer, D.; Mastalir, M.; Stöger, B.; Veiros, L. F.; Kirchner, K. *Organometallics* **2018**, *37*, 3631–3638.
- (89) Himmelbauer, D.; Stöger, B.; Veiros, L. F.; Pignitter, M.; Kirchner, K. *Organometallics* **2019**, *38*, 4669–4678.
- (90) Hebden, T. J.; Schrock, R. R.; Takase, M. K.; Müller, P. *Chem. Commun.* **2012**, *48*, 1851–1853.
- (91) Hebden, T. J.; St. John, A. J.; Gusev, D. G.; Kaminsky, W.; Goldberg, K. I.; Heinekey, D. M. *Angewandte Chemie International Edition* **2011**, *50*, 1873–1876.
- (92) Chen, X.-M.; Tong, M.-L. *Accounts of chemical research* **2007**, *40*, 162–170.
- (93) Mastalir, M.; De Aguiar, S. R.; Glatz, M.; Stöger, B.; Kirchner, K. *Organometallics* **2016**, *35*, 229–232.
- (94) Gunstone, F. D.; Tucker, H. S. *Organic Syntheses* **1952**, *32*, 23.
- (95) Weimar, M.; Dürner, G.; Bats, J. W.; Göbel, M. W. *The Journal of organic chemistry* **2010**, *75*, 2718–2721.
- (96) Eder, W. Base Metal Complexes with PCP Pincer Ligands., master thesis, Vienna University of Technology, 2018.
- (97) Pape, A.; Lutz, M.; Müller, G. *Angewandte Chemie* **1994**, *106*, 2375–2377.
- (98) ConnellyáRobinson, S. et al. *Chemical Communications* **2017**, *53*, 669–676.
- (99) Weigert, F. J.; Roberts, J. D. *Journal of the American Chemical Society* **1969**, *91*, 4940–4941.
- (100) Van der Boom, M. E.; Iron, M. A.; Atasoylu, O.; Shimon, L. J.; Rozenberg, H.; Ben-David, Y.; Konstantinovski, L.; Martin, J. M.; Milstein, D. *Inorganica Chimica Acta* **2004**, *357*, 1854–1864.
- (101) Vigalok, A.; Uzan, O.; Shimon, L. J. W.; Ben-David, Y.; Martin, J. M. L.; Milstein, D. *Journal of the American Chemical Society* **1998**, *120*, 12539–12544.
- (102) Montag, M.; Schwartsburd, L.; Cohen, R.; Leituss, G.; Ben-David, Y.; Martin, J. M. L.; Milstein, D. *Angewandte Chemie International Edition* **2007**, *46*, 1901–1904.
- (103) Murugesan, S.; Stöger, B.; Pittenauer, E.; Allmaier, G.; Veiros, L. F.; Kirchner, K. *Angewandte Chemie International Edition* **2016**, *55*, 3045–3048.
- (104) Berke, H.; Jiang, Y.; Lewandowska, H.; Mingos, D., *Nitrosyl Complexes in Inorganic Chemistry, Biochemistry and Medicine I*; Structure and Bonding 153; Springer: Berlin Heidelberg, 2014.
- (105) Tondreau, A. M.; Boncella, J. M. *Polyhedron* **2016**, *116*, 96–104.
- (106) Dani, P.; Toorneman, M. A. M.; van Klink, G. P. M.; van Koten, G. *Organometallics* **2000**, *19*, 5287–5296.

-
- (107) McLoughlin, M. A.; Flesher, R. J.; Kaska, W. C.; Mayer, H. A. *Organometallics* **1994**, *13*, 3816–3822.
- (108) Gusev, D. G.; Madott, M.; Dolgushin, F. M.; Lyssenko, K. A.; Antipin, M. Y. *Organometallics* **2000**, *19*, 1734–1739.
- (109) De Aguiar, S. R. M.; Stöger, B.; Pittenauer, E.; Puchberger, M.; Allmaier, G.; Veiros, L. F.; Kirchner, K. *Journal of Organometallic Chemistry* **2014**, *760*, 74–83.
- (110) Benito-Garagorri, D.; Becker, E.; Wiedermann, J.; Lackner, W.; Pollak, M.; Mereiter, K.; Kisala, J.; Kirchner, K. *Organometallics* **2006**, *25*, 1900–1913.
- (111) Eder, W.; Stöger, B.; Kirchner, K. *Monatshefte für Chemie - Chemical Monthly* **2019**, *150*, 1235–1240.
- (112) McGowan, K. P.; Abboud, K. A.; Veige, A. S. *Organometallics* **2011**, *30*, 4949–4957.
- (113) Alzamy, A.; Gambarotta, S.; Korobkov, I. *Organometallics* **2013**, *32*, 7204–7212.
- (114) Alzamy, A.; Gambarotta, S.; Korobkov, I. *Organometallics* **2013**, *32*, 7107–7115.
- (115) Mastalir, M.; Glatz, M.; Stöger, B.; Weil, M.; Pittenauer, E.; Allmaier, G.; Kirchner, K. *Inorganica Chimica Acta* **2017**, *455*, 707–714.
- (116) Sutton, A. D.; Ngyuen, T.; Fettingner, J. C.; Olmstead, M. M.; Long, G. J.; Power, P. P. *Inorganic chemistry* **2007**, *46*, 4809–4814.
- (117) Liu, Z.; Gao, W.; Liu, X.; Luo, X.; Cui, D.; Mu, Y. *Organometallics* **2011**, *30*, 752–759.
- (118) Smith, J. M.; Lachicotte, R. J.; Holland, P. L. *Organometallics* **2002**, *21*, 4808–4814.
- (119) Dionne, M.; Hao, S.; Gambarotta, S. *Canadian journal of chemistry* **1995**, *73*, 1126–1134.
- (120) Barron, A. R.; Salt, J. E.; Wilkinson, G.; Motevalli, M.; Hursthouse, M. B. *Polyhedron* **1986**, *5*, 1833–1837.
- (121) Murugesan, S.; Stöger, B.; Weil, M.; Veiros, L. F.; Kirchner, K. *Organometallics* **2015**, *34*, 1364–1372.
- (122) Seo, J.; Cabelof, A. C.; Chen, C.-H.; Caulton, K. G. *Chem. Sci.* **2019**, *10*, 475–479.
- (123) Simler, T.; Braunstein, P.; Danopoulos, A. A. *Organometallics* **2016**, *35*, 4044–4049.
- (124) Schiwiek, C. H.; Vasilenko, V.; Wadepohl, H.; Gade, L. H. *Chem. Commun.* **2018**, *54*, 9139–9142.
- (125) Dilsky, S. *Journal of Organometallic Chemistry* **2007**, *692*, 2887–2896.
- (126) Curtis, M. D.; Shiu, K. B. *Inorganic Chemistry* **1985**, *24*, 1213–1218.
- (127) Orrell, K. G.; Osborne, A. G.; Sik, V.; da Silva, M. W. *Polyhedron* **1995**, *14*, 2797–2802.
- (128) Smith, J. D.; Logan, J. R.; Doyle, L. E.; Burford, R. J.; Sugawara, S.; Ohnita, C.; Yamamoto, Y.; Piers, W. E.; Spasyuk, D. M.; Borau-Garcia, J. *Dalton Trans.* **2016**, *45*, 12669–12679.
- (129) Grotjahn, D. B.; Bikzhanova, G. A.; Collins, L. S. B.; Concolino, T.; Lam, K.-C.; Rheingold, A. L. *Journal of the American Chemical Society* **2000**, *122*, 5222–5223.
- (130) Lee, H. M.; Yao, J.; Jia, G. *Organometallics* **1997**, *16*, 3927–3933.
- (131) Freitag, F.; Irrgang, T.; Kempe, R. *Journal of the American Chemical Society* **2019**, *141*, 11677–11685.
- (132) Deegan, M. M.; Peters, J. C. *Journal of the American Chemical Society* **2017**, *139*, 2561–2564.
- (133) De Aguiar, S. R. M. M.; Öztöpcü, Ö.; Troiani, A.; de Petris, G.; Weil, M.; Stöger, B.; Pittenauer, E.; Allmaier, G.; Veiros, L. F.; Kirchner, K. *European Journal of Inorganic Chemistry* **2018**, *2018*, 876–884.
- (134) Coucouvanis, D.; Hadjikyriacou, A.; Toupadakis, A.; Koo, S. M.; Ileperuma, O.; Draganjac, M.; Salifoglou, A. *Inorganic Chemistry* **1991**, *30*, 754–767.

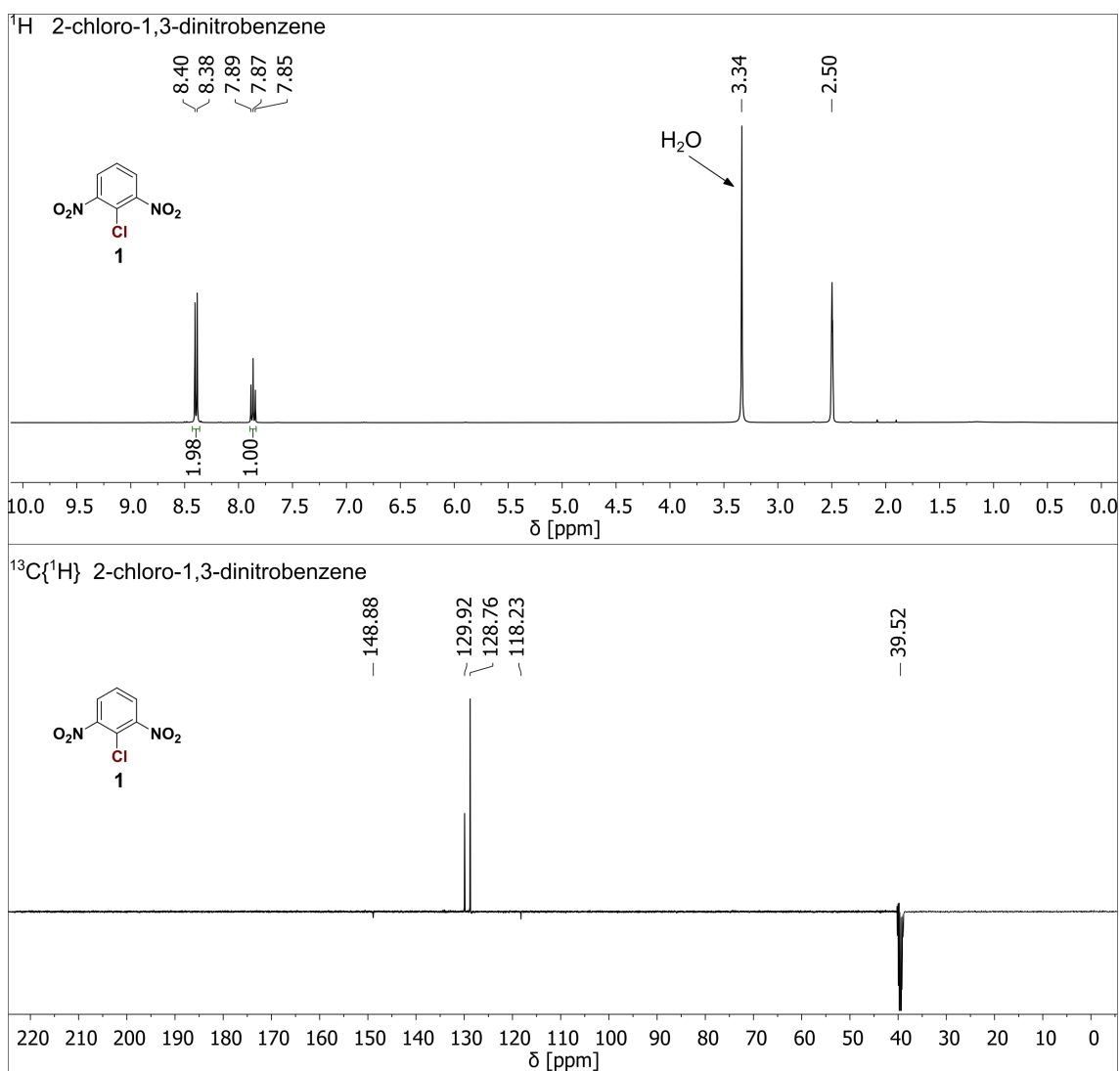
CHAPTER 5. REFERENCES

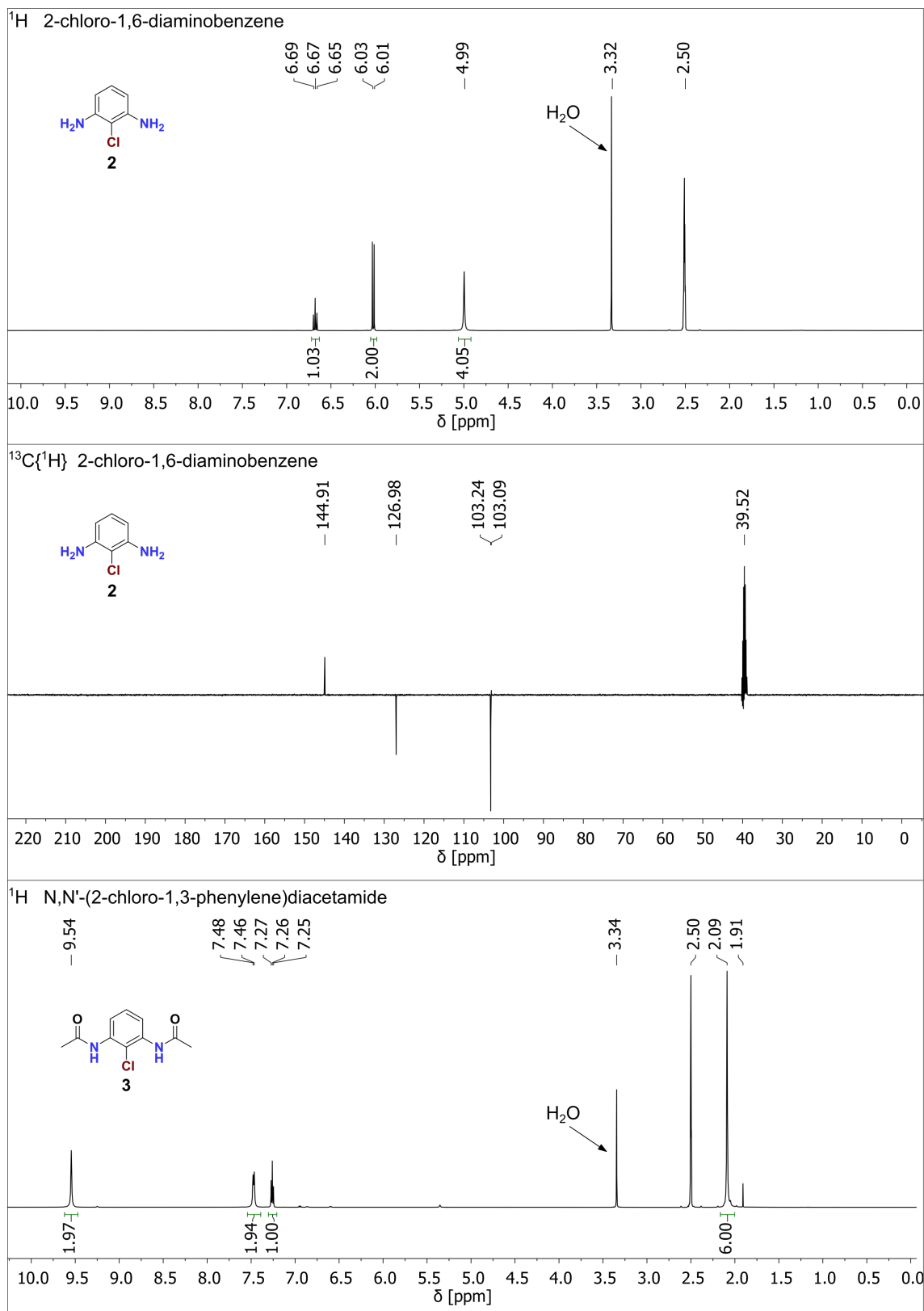
- (135) Donahue, J. P.; Goldsmith, C. R.; Nadiminti, U.; Holm, R. H. *Journal of the American Chemical Society* **1998**, *120*, 12869–12881.
- (136) Baba, K.; Okamura, T.-a.; Suzuki, C.; Yamamoto, H.; Yamamoto, T.; Ohama, M.; Ueyama, N. *Inorganic Chemistry* **2006**, *45*, 894–901.
- (137) Sugimoto, H.; Harihara, M.; Shiro, M.; Sugimoto, K.; Tanaka, K.; Miyake, H.; Tsukube, H. *Inorganic Chemistry* **2005**, *44*, 6386–6392.
- (138) Perin, D. D.; Amerego, W. L. F., *Purification of Laboratory Chemicals*, 3rd ed.; Pergamon: New York, 1988.
- (139) Bruker, A. Inc., Madison, Wisconsin, USA, © 2005, COSMO (Version 1.48), SAINT (Version 7.06 A).
- (140) Sheldrick, G. M. *Acta Crystallographica Section A* **2008**, *64*, 112–122.

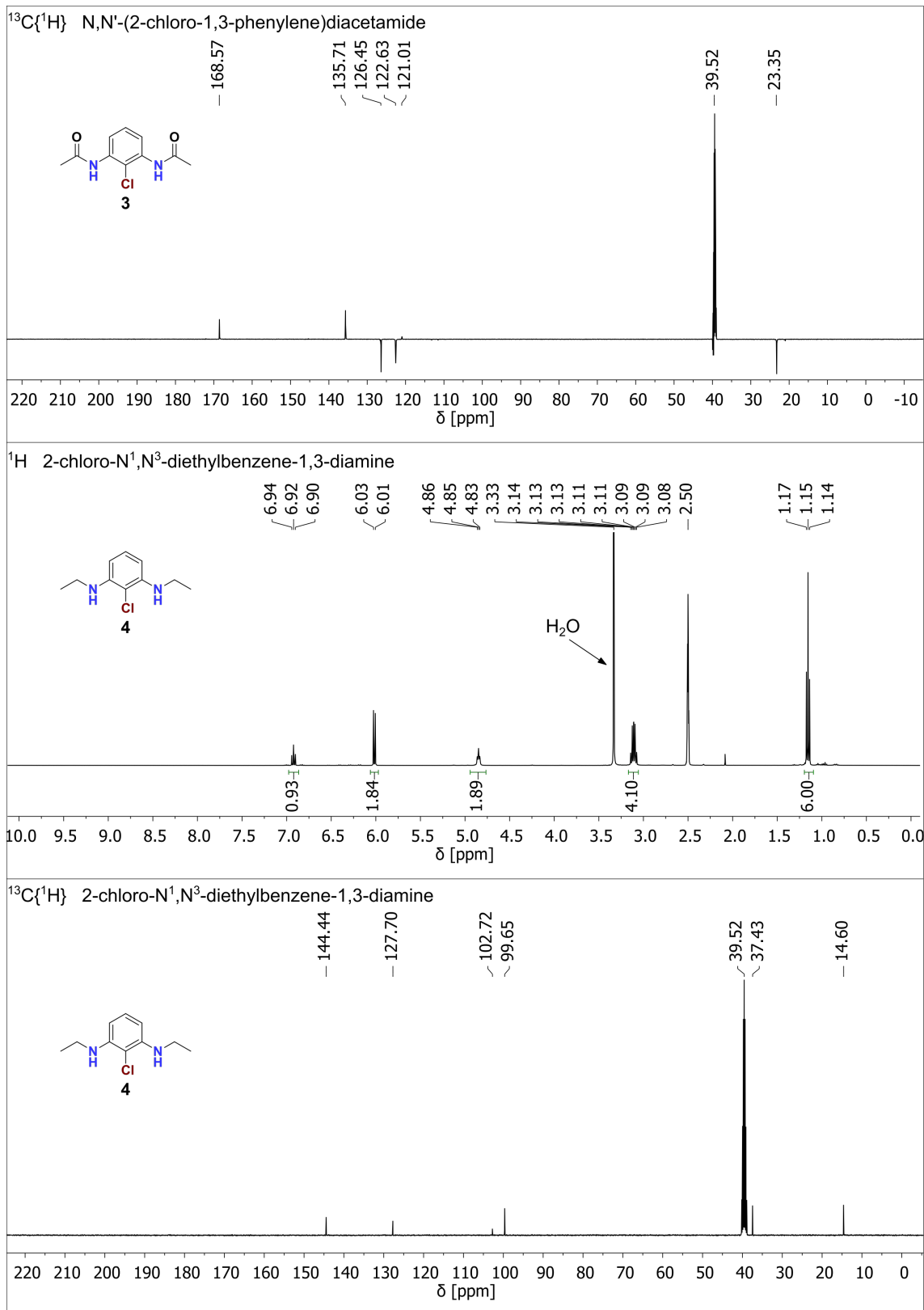
Chapter 6

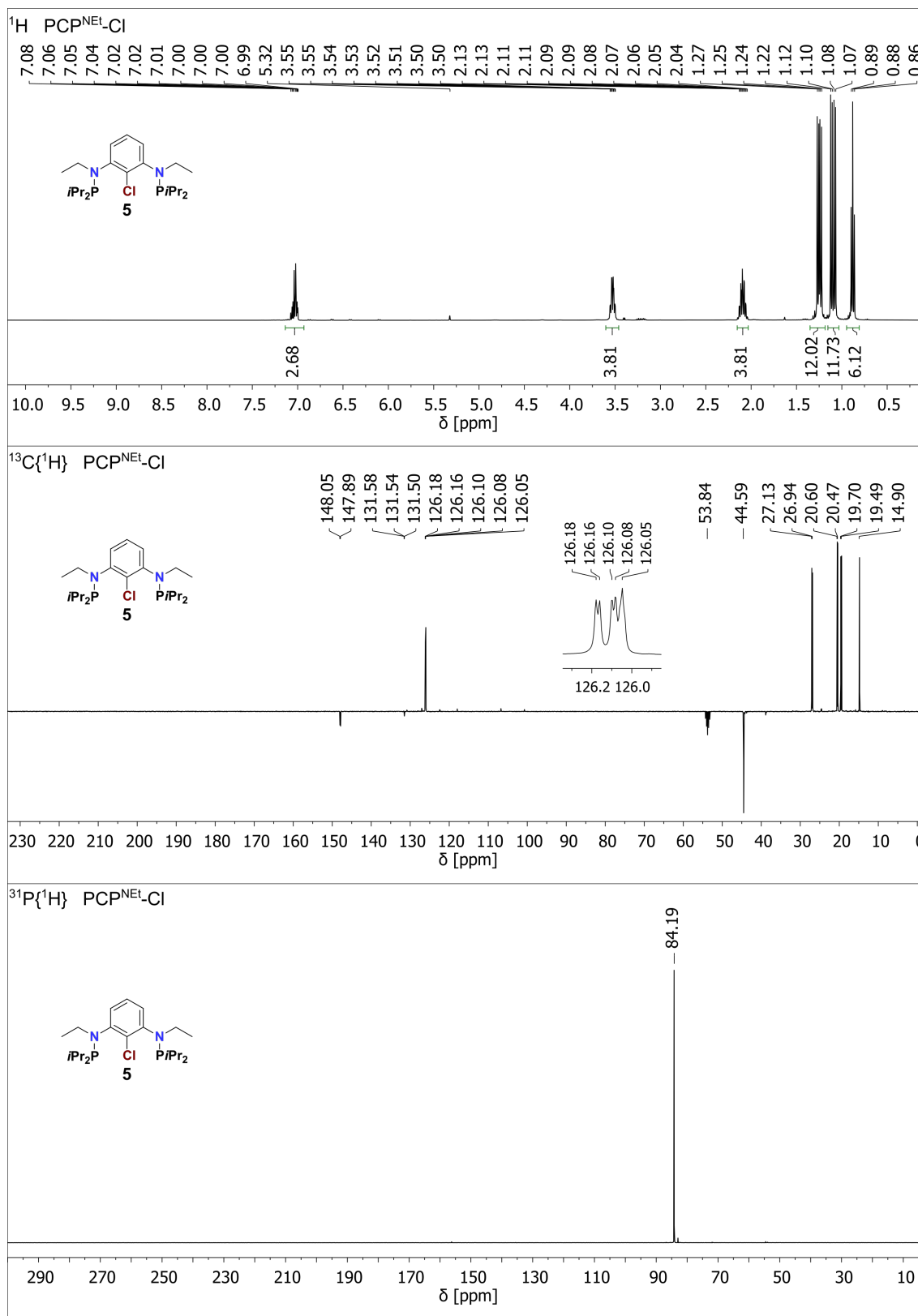
Appendix

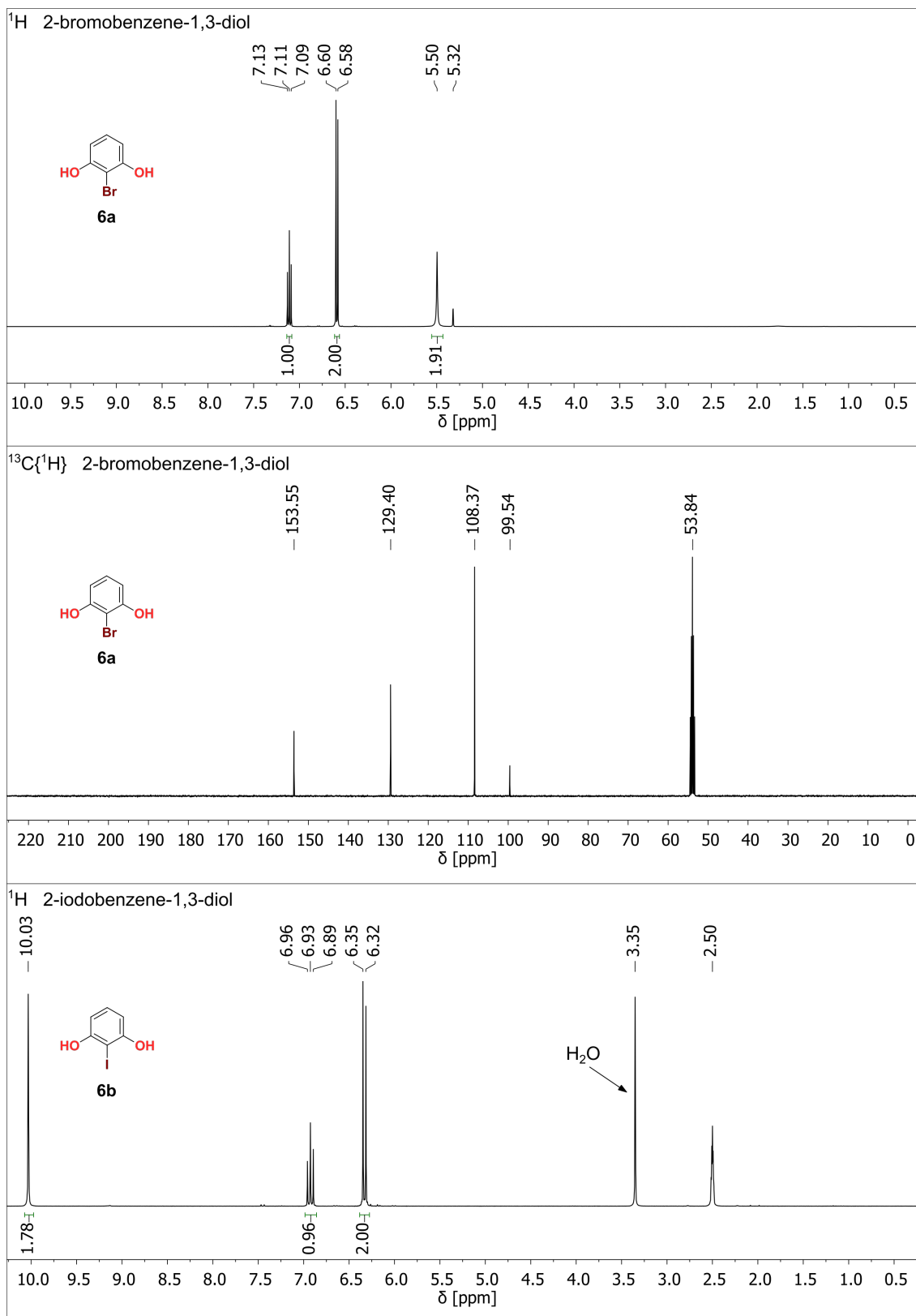
6.1 NMR Spectra

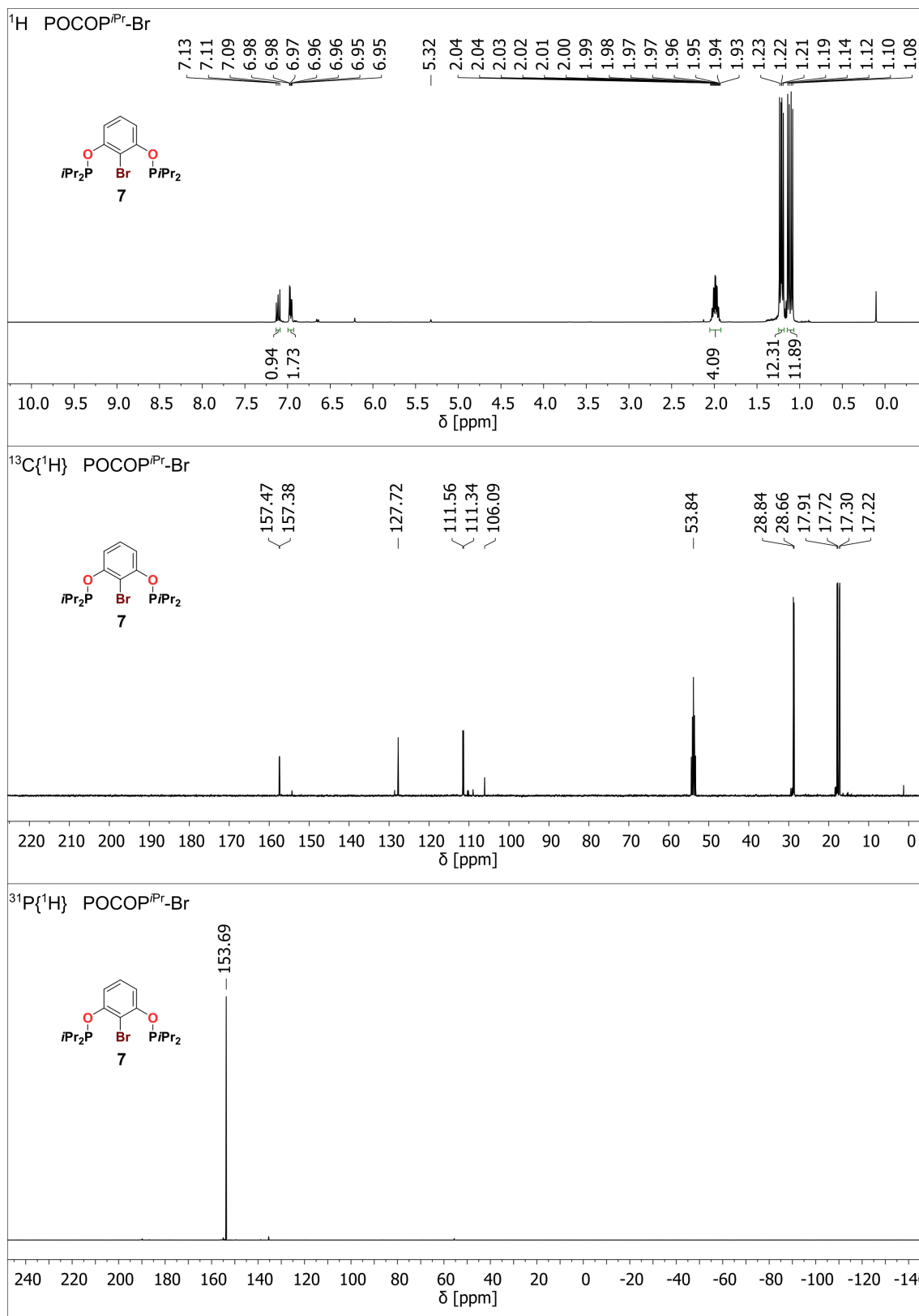


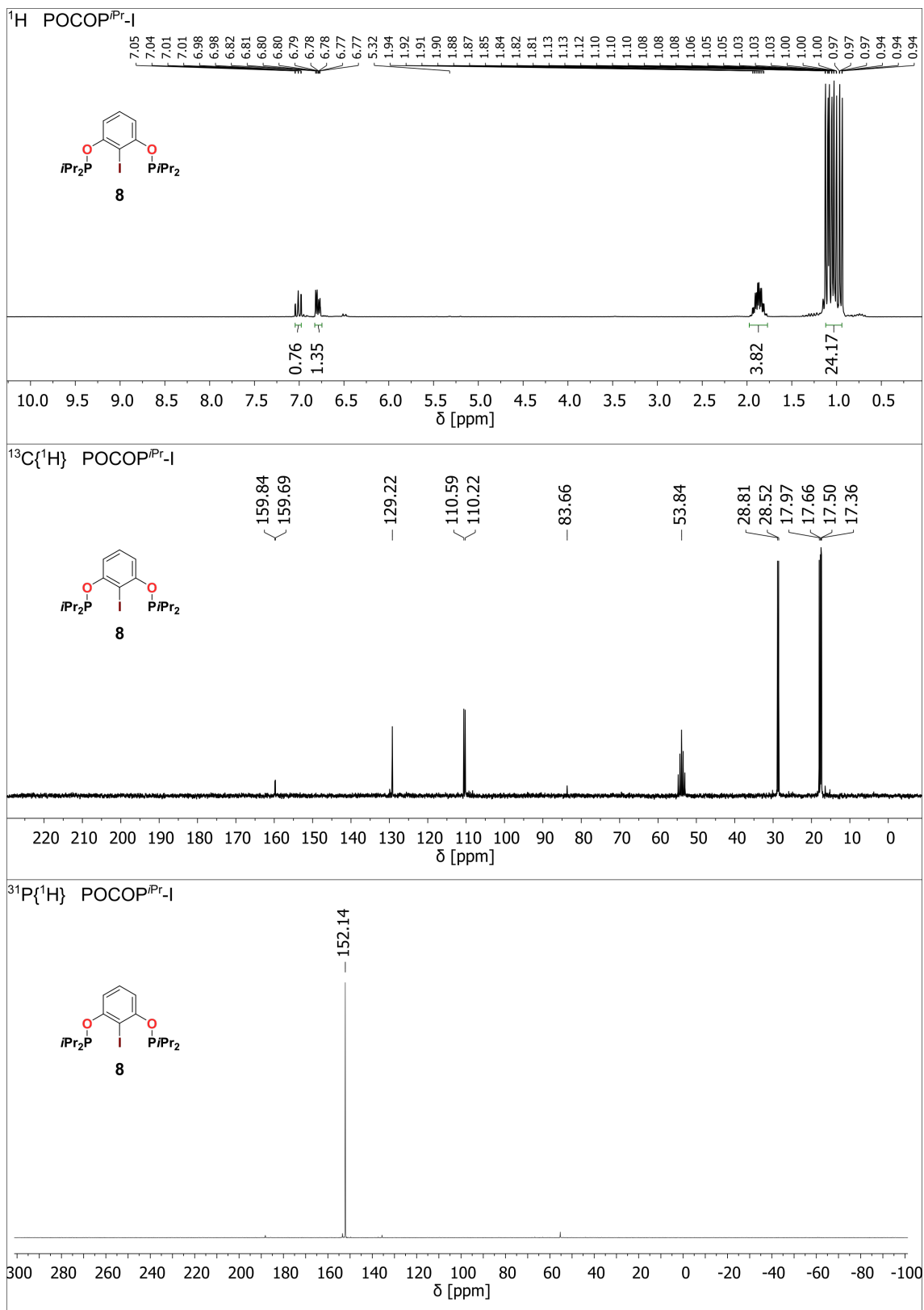


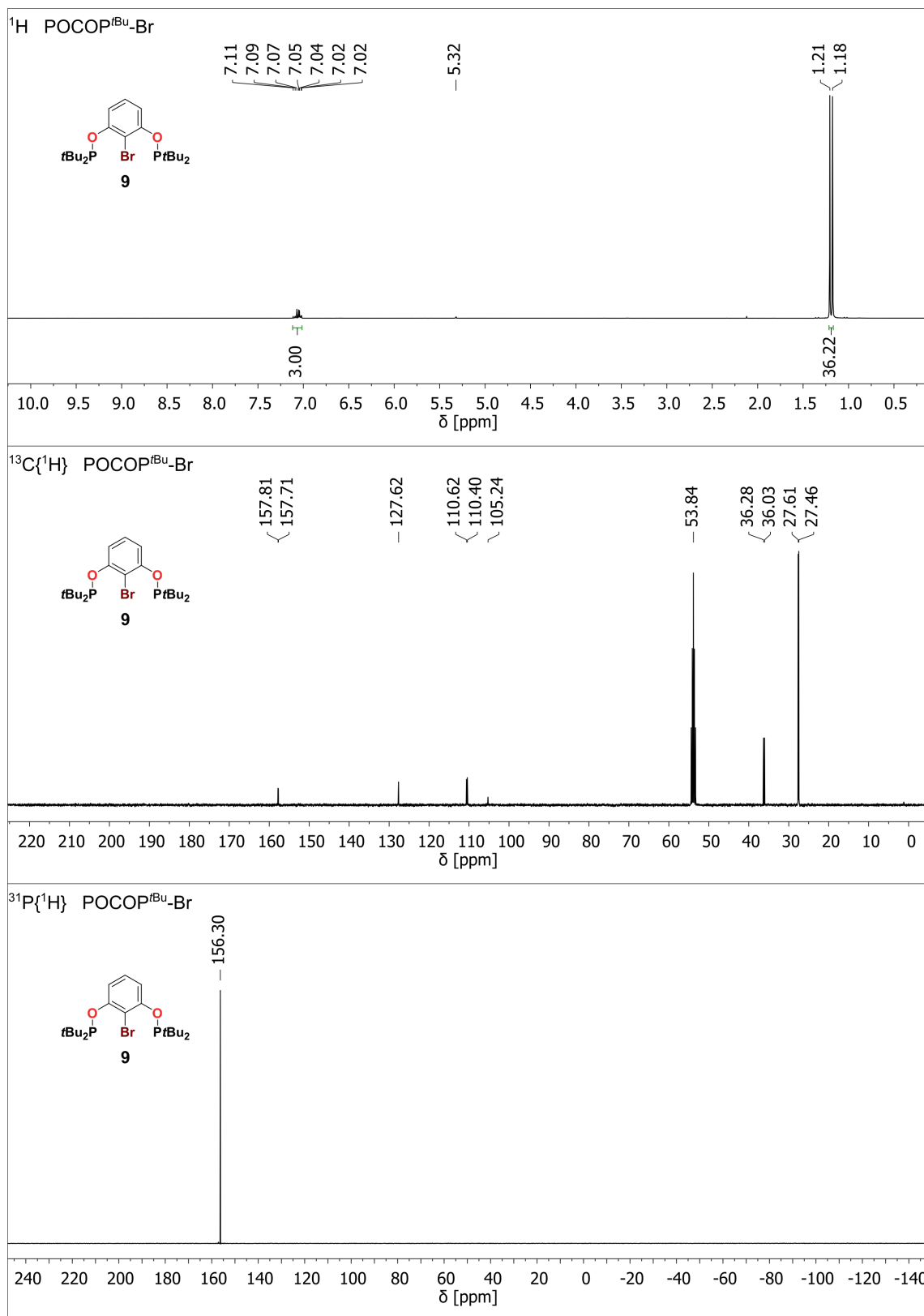


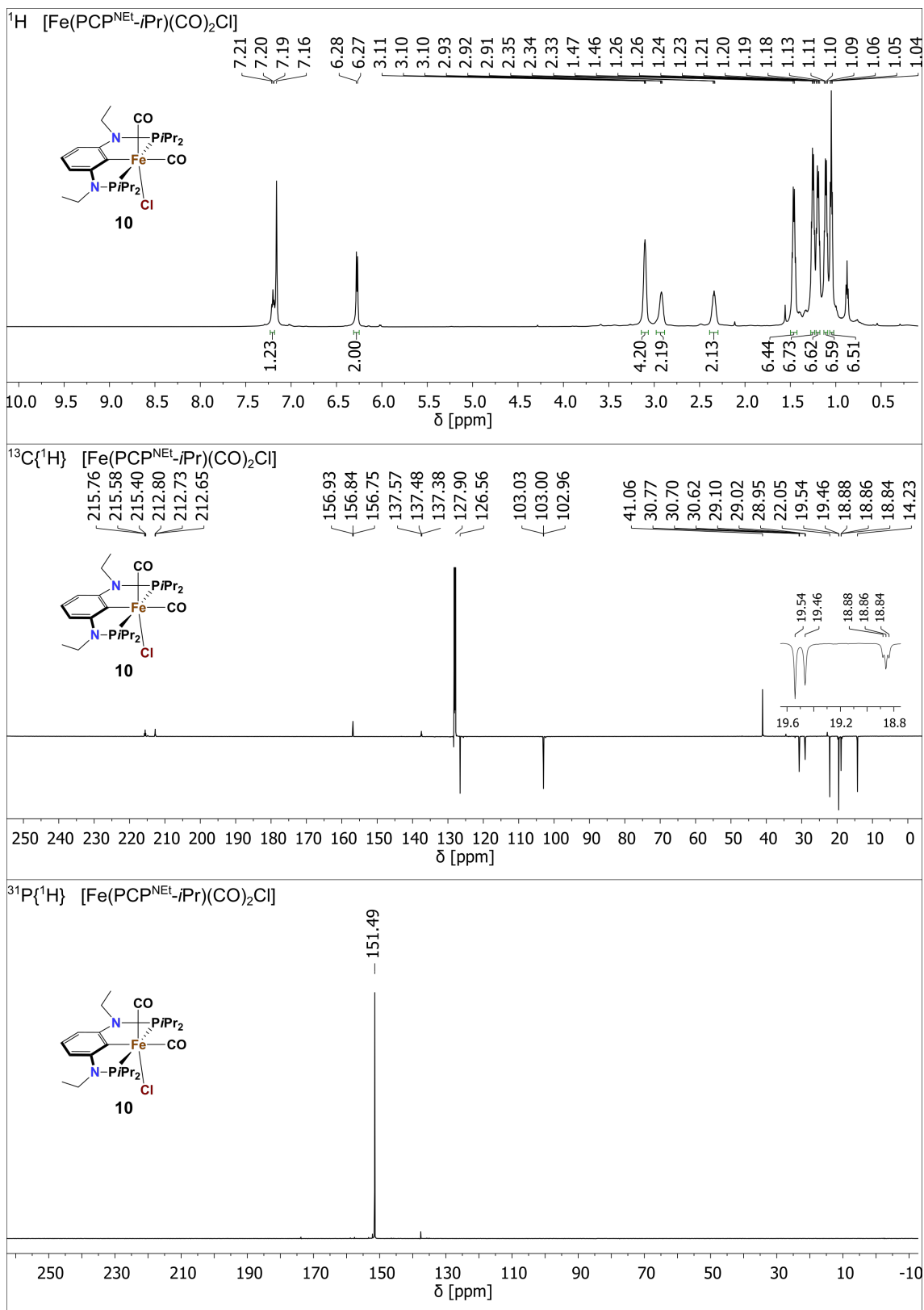


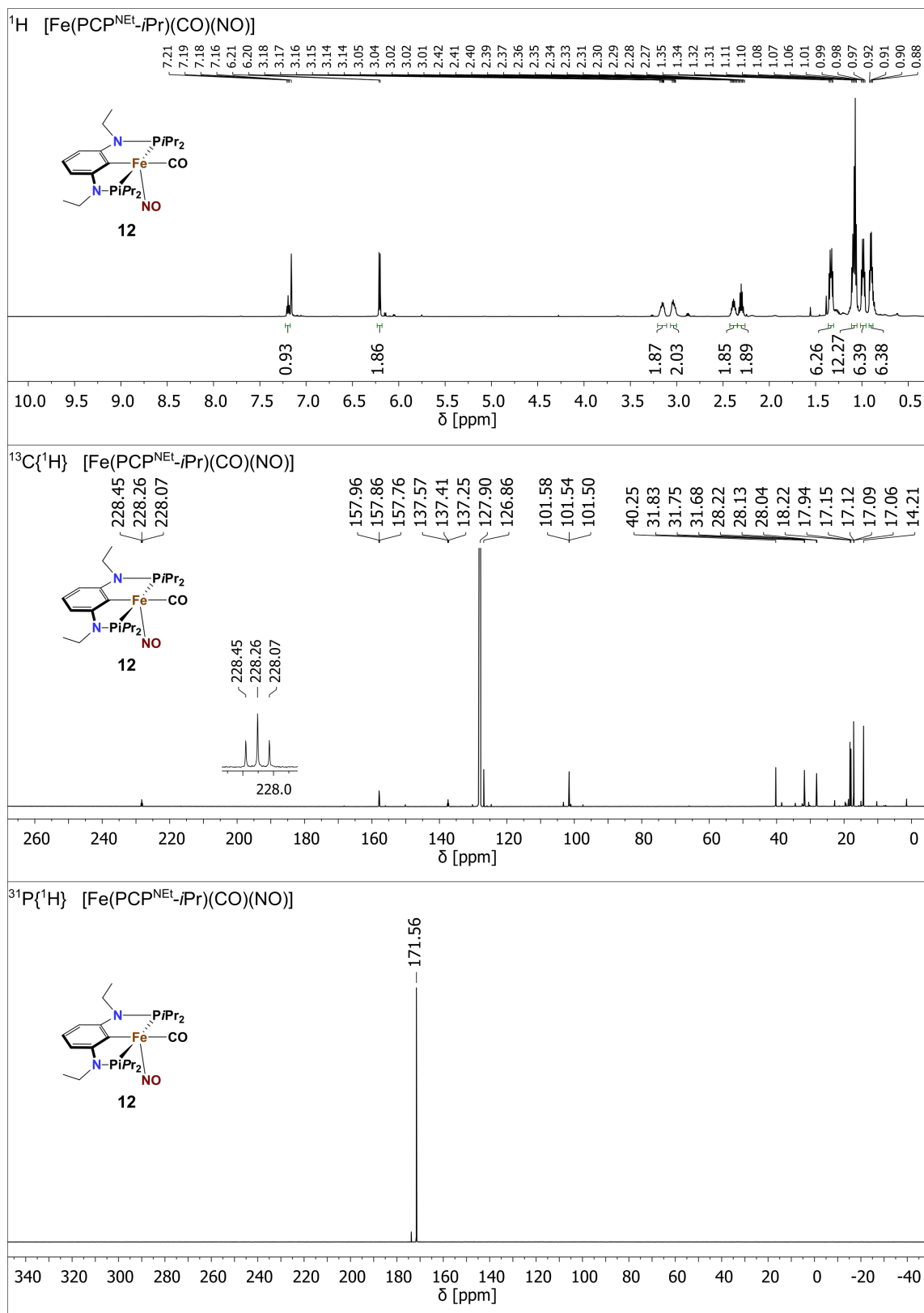


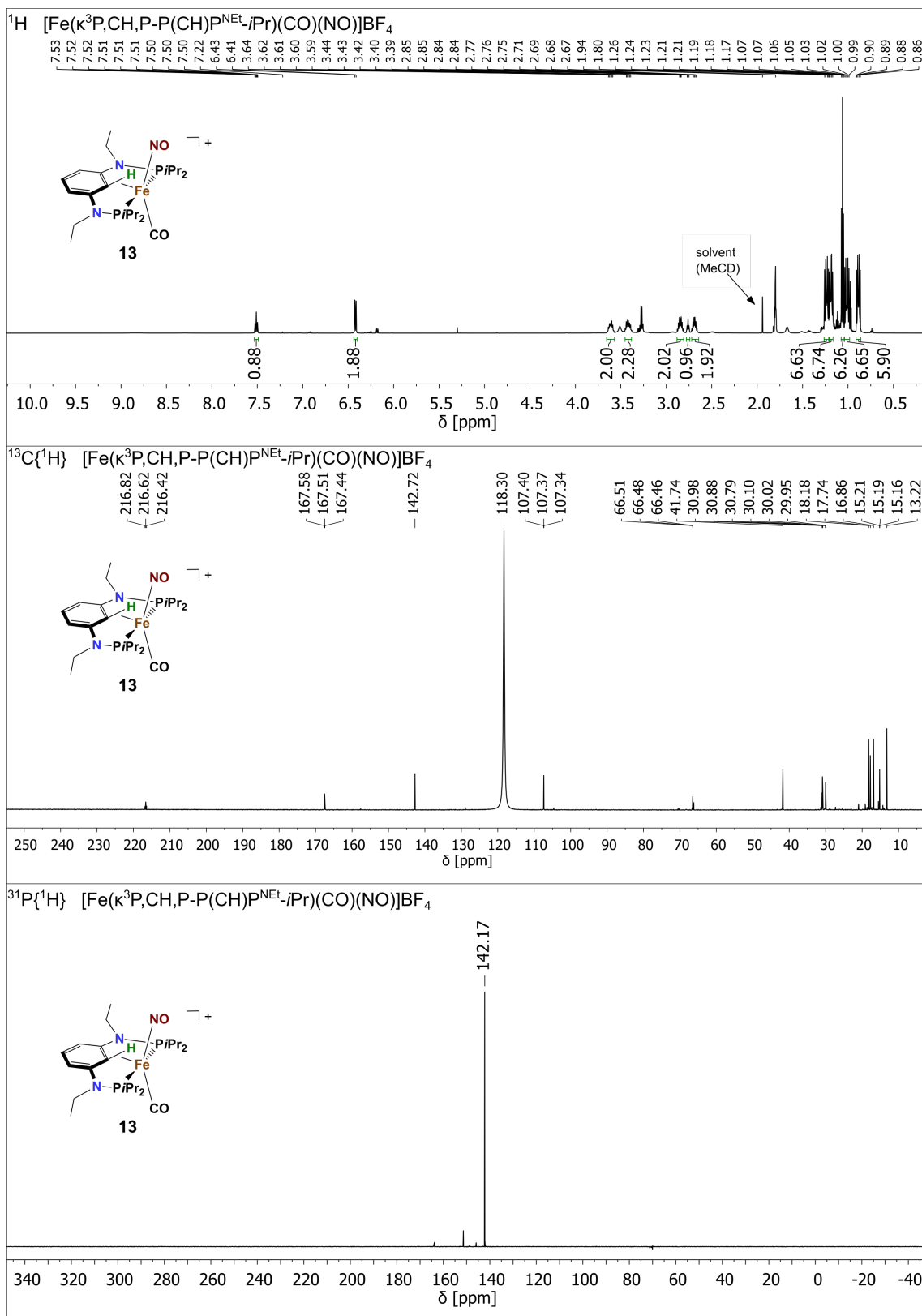


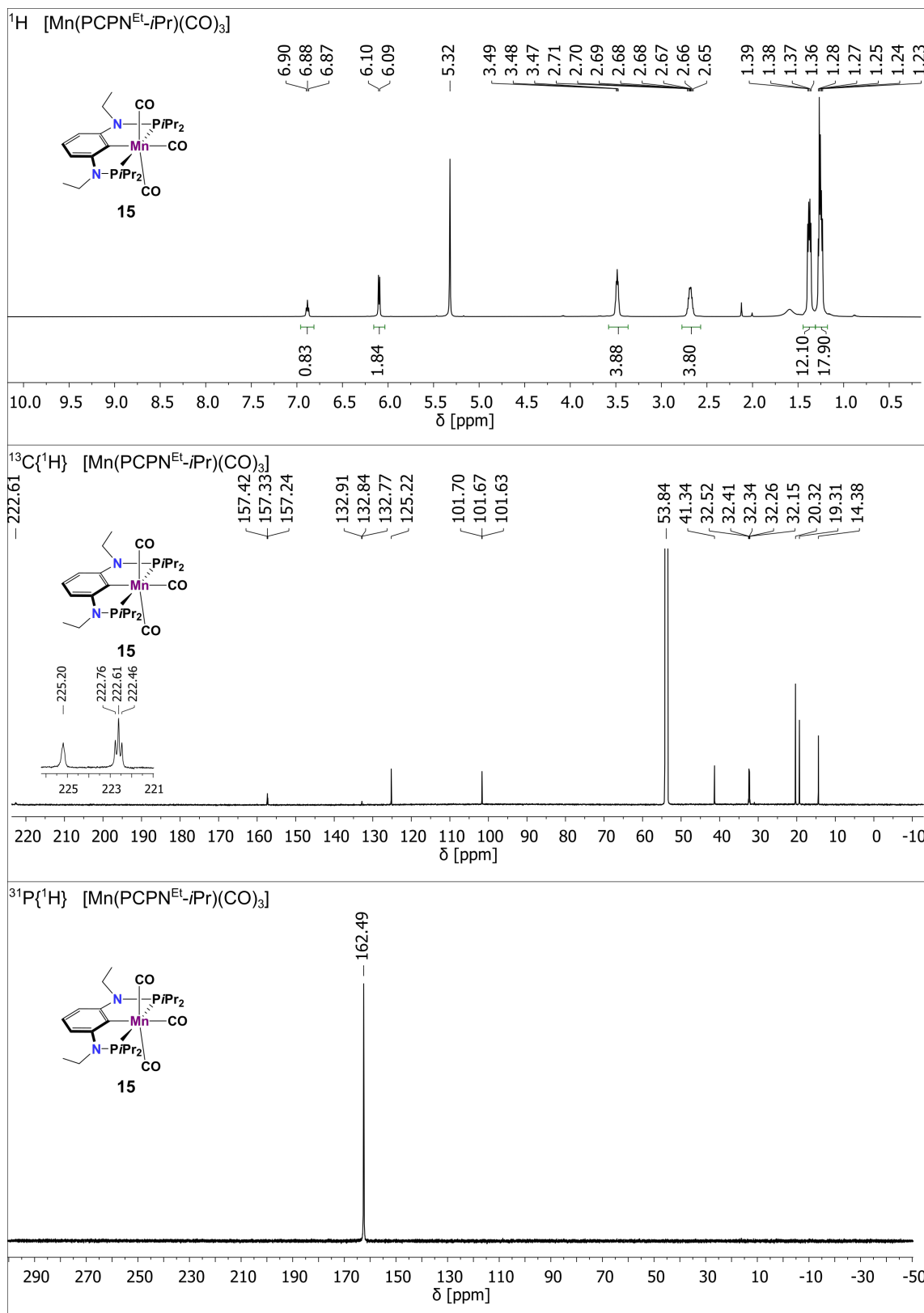


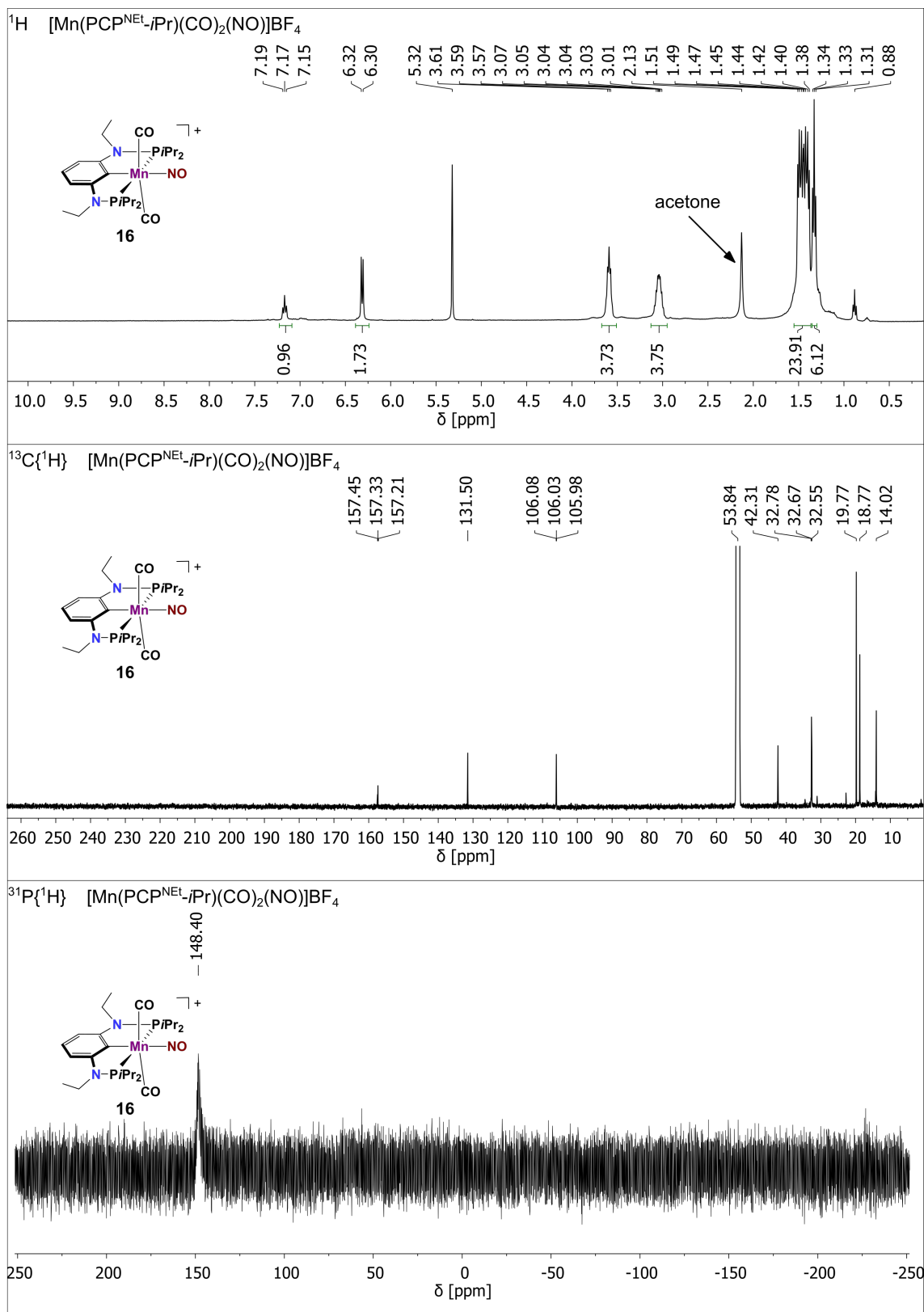


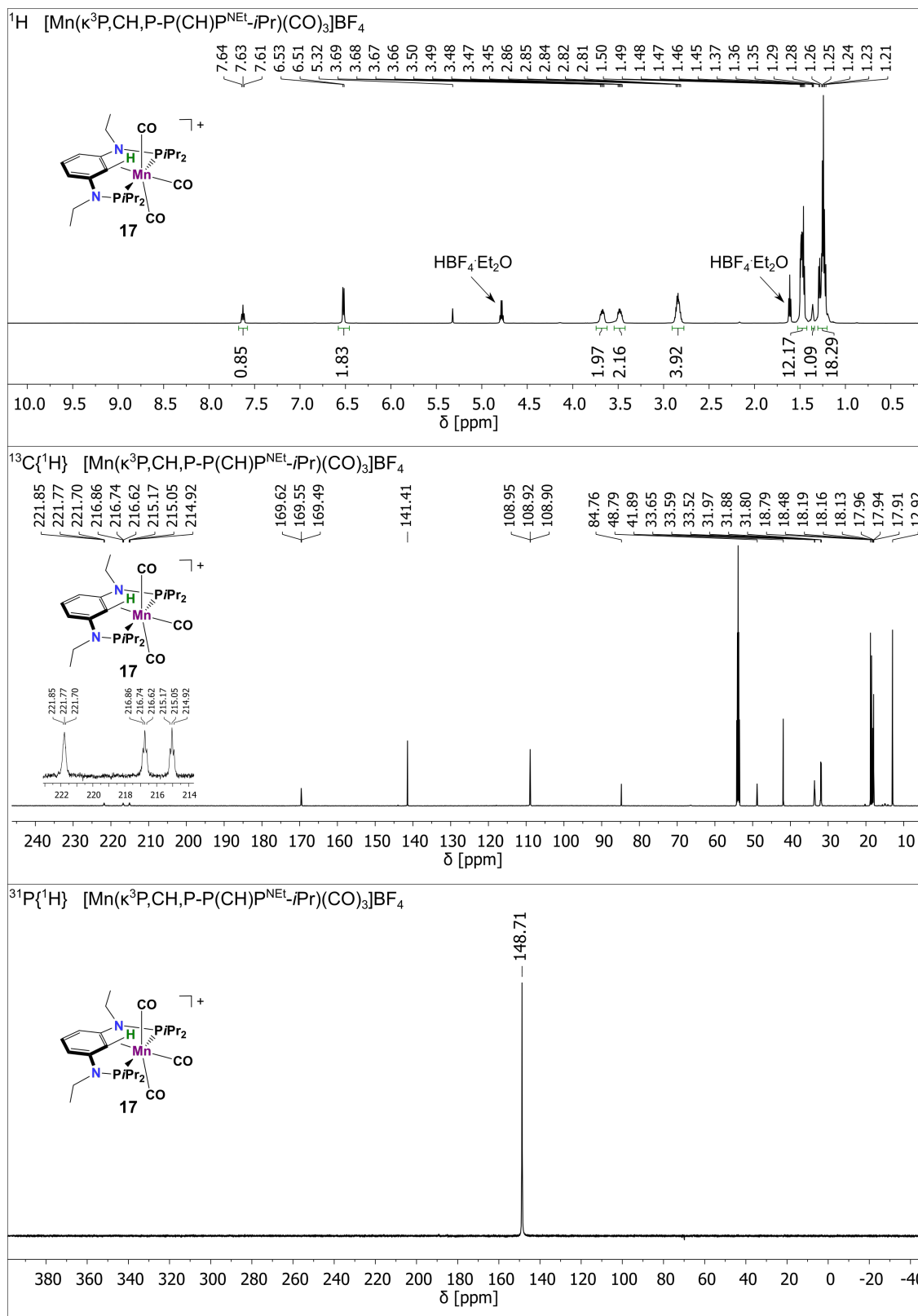


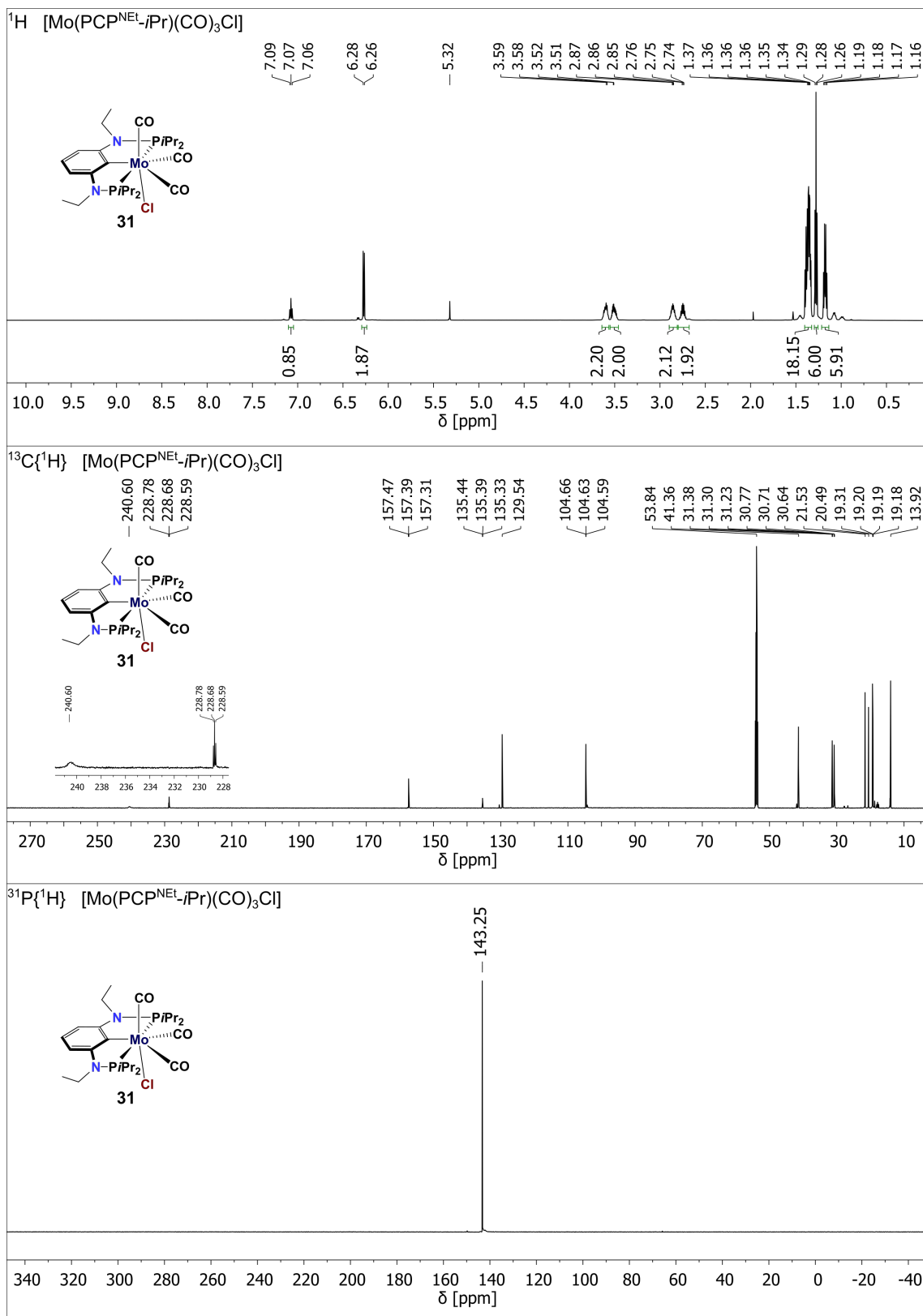


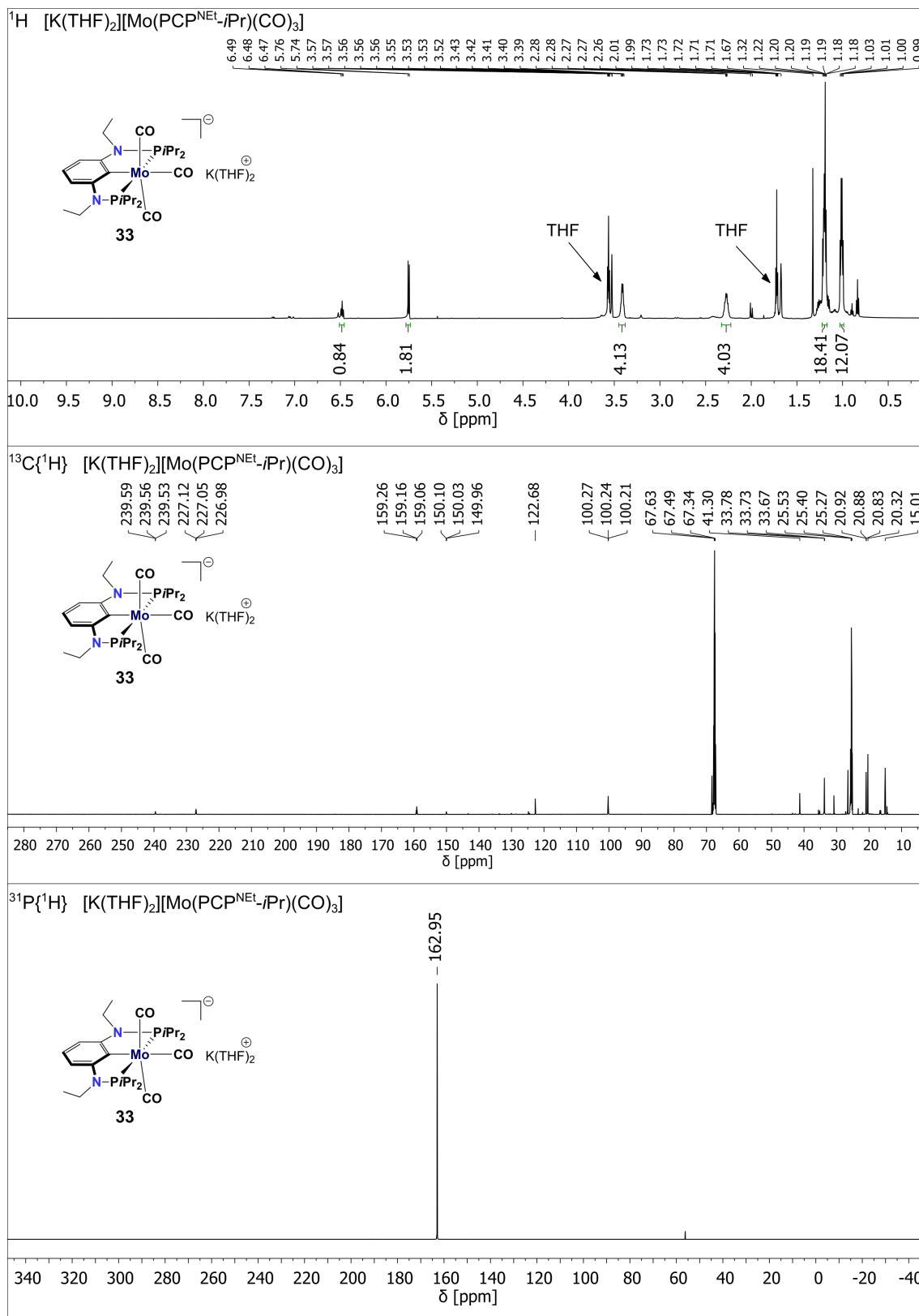


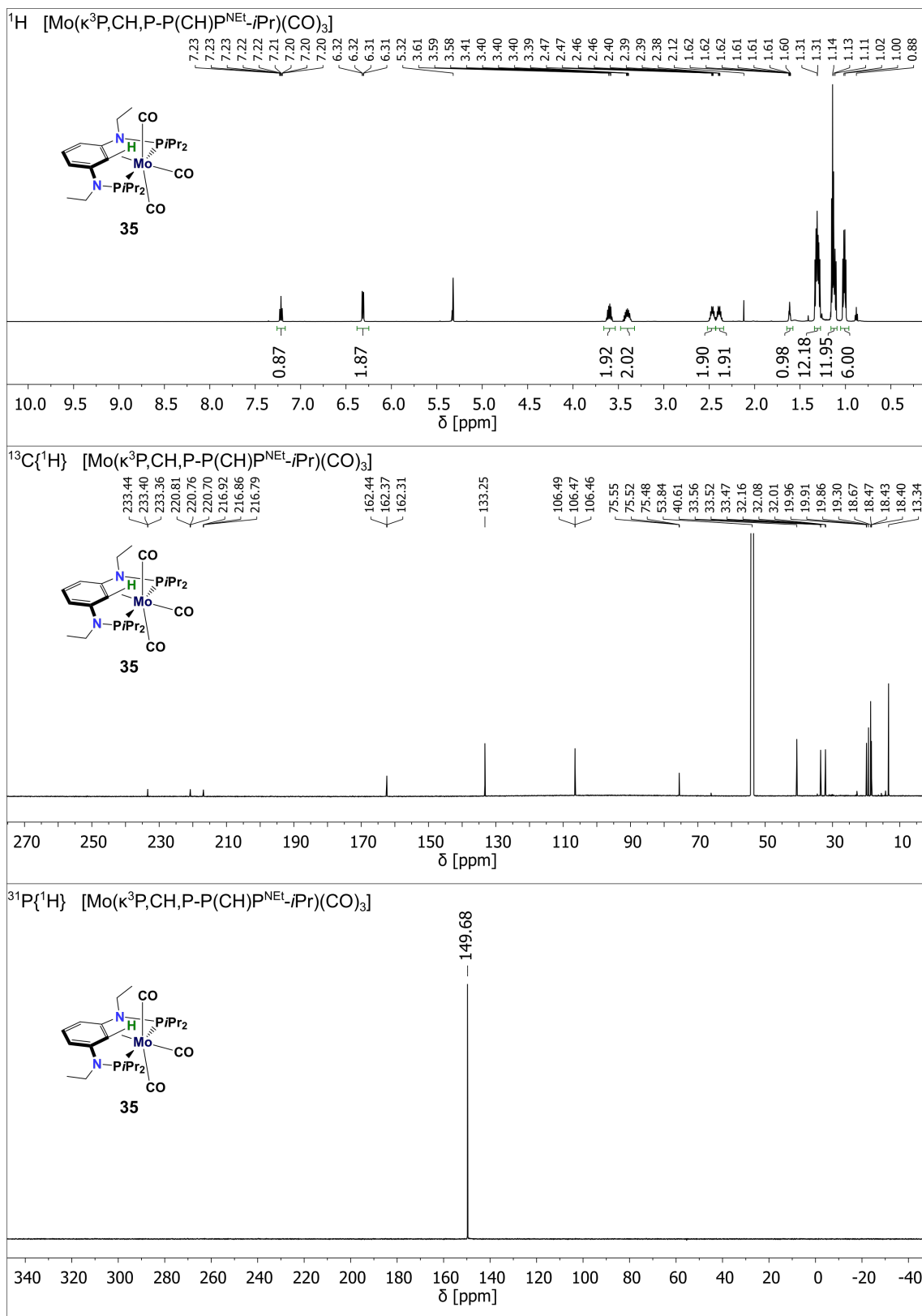


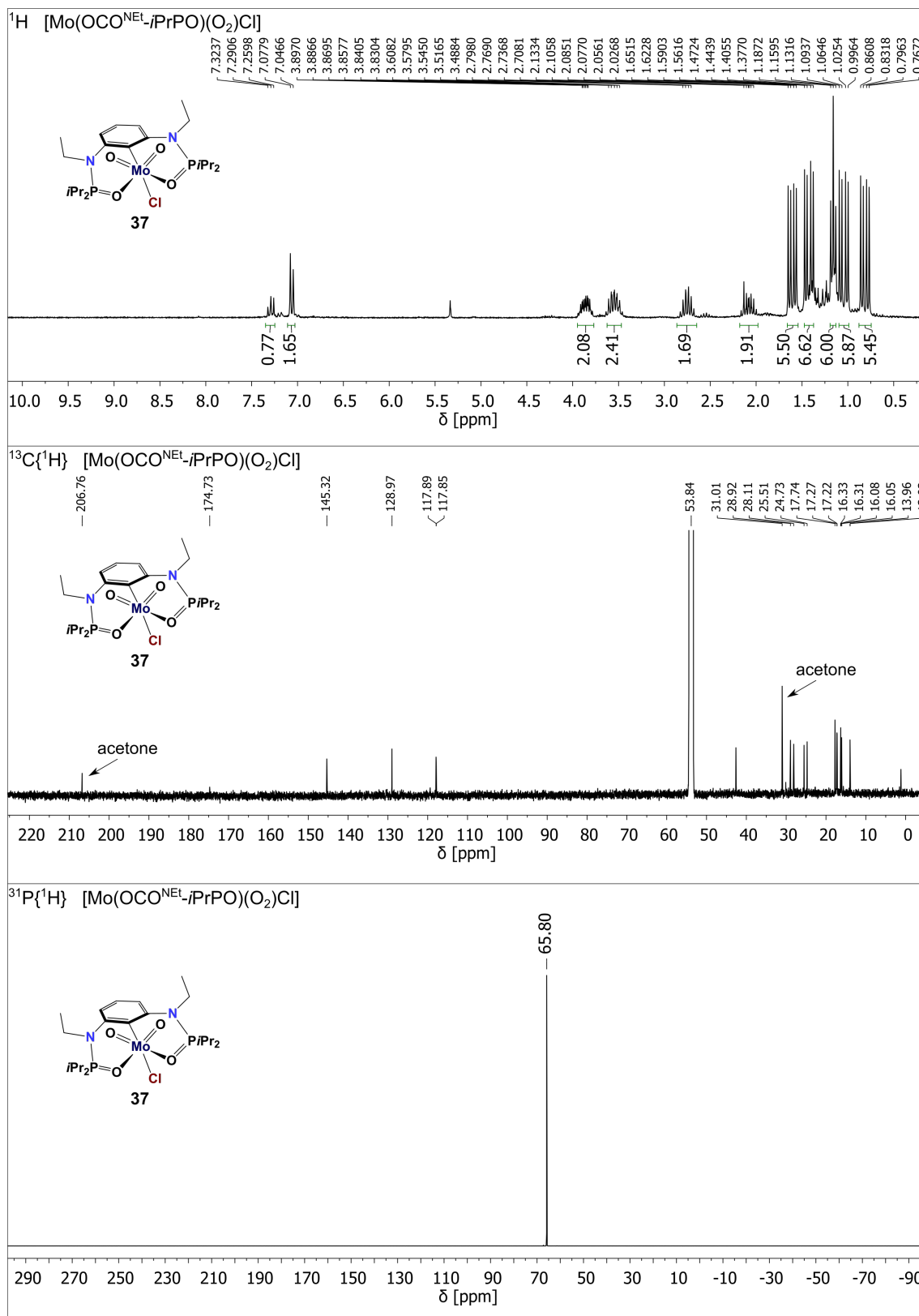


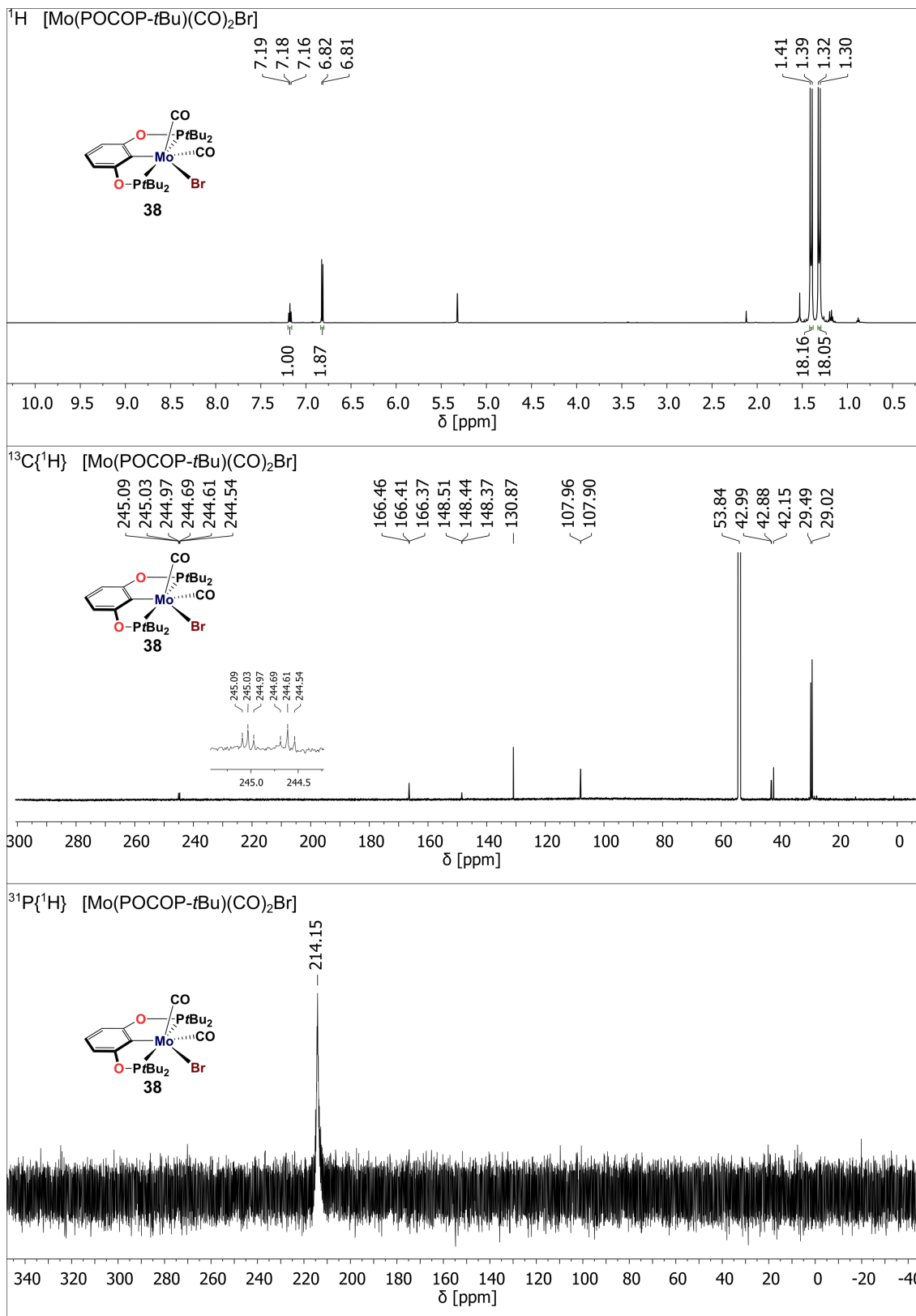


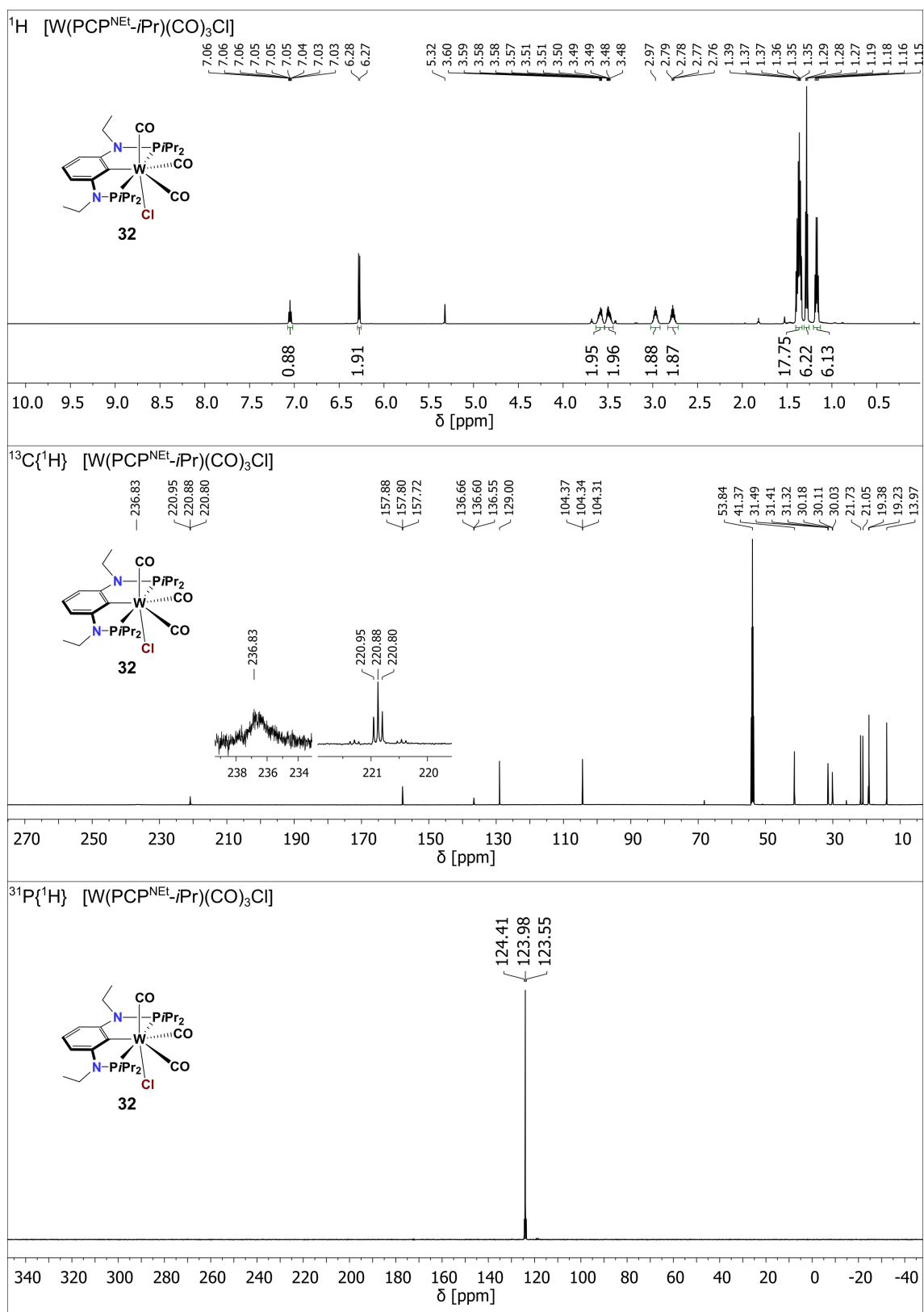


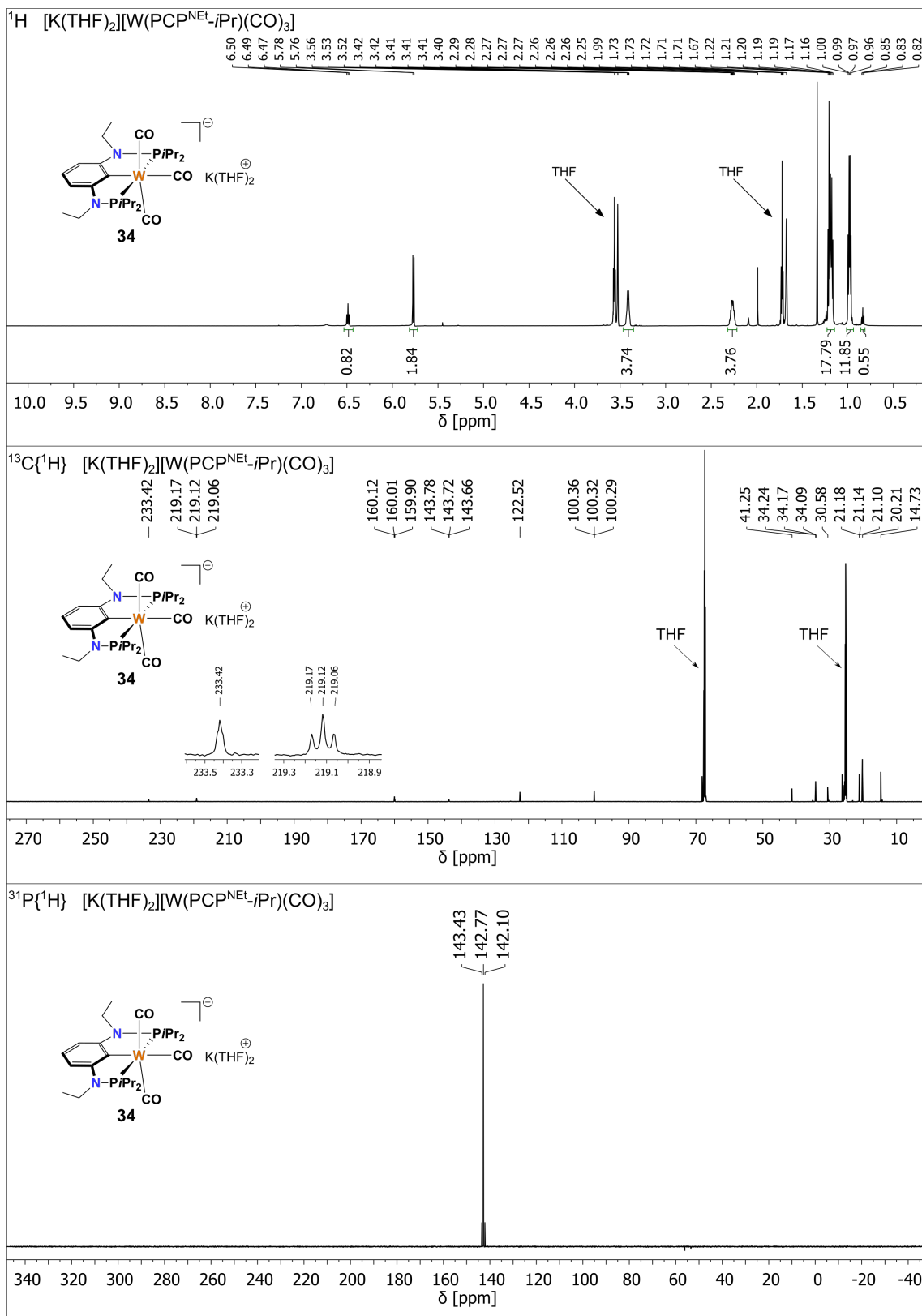












6.2 Crystallographic Data

complex	[Fe(PCP ^{NEt} - <i>i</i> Pr) (CO) ₂ Cl] (10)	[Fe(PCP ^{NEt} - <i>i</i> Pr) (CO) ₂] (11)	[Fe(κ^3 P,CH,P-P(CH)P ^{NEt} - <i>i</i> Pr)(CO)(NO)]BF ₄ (13)	[Fe(POCOP- <i>t</i> Bu) (CO) ₂] (14)
empirical formula	C ₂₄ H ₄₁ ClFeN ₂ O ₂ P ₂	C ₂₄ H ₄₁ FeN ₂ O ₂ P ₂	C ₂₃ H ₄₂ BF ₄ FeN ₃ O ₂ P ₂	C ₂₄ H ₃₉ FeO ₄ P ₂
MW [g/mol]	542.83	507.38	597.19	509.34
crystal size [mm]	0.42 x 0.23 x 0.04	0.42 x 0.10 x 0.08	0.32 x 0.20 x 0.09	0.35 x 0.25 x 0.16
colour, shape	orange, plate	violet, rod	red, plate	green, brick
crystal system	triclinic	orthorhombic	monoclinic	triclinic
space group	P -1	P b c a	P 21/n	P -1
a [Å]	8.2228(14)	16.2844(11)	8.2856(12)	13.4933(18)
b [Å]	18.285(3)	11.1540(8)	15.533(2)	25.671(3)
c [Å]	18.392(3)	29.0498(19)	22.355(3)	38.134(5)
α [°]	88.728(5)	90	90	86.404(5)
β [°]	79.844(5)	90	93.543(4)	87.601(4)
γ [°]	80.161(5)	90	90	79.813(4)
V [Å ³]	2681.8(8)	5276.5(6)	2871.6(7)	12969(3)
Z	4	8	4	20
ρ_{calc} [g/cm ³]	1.344	1.277	1.381	1.304
T [K]	100	100	100	100
μ [mm ⁻¹]	0.804	0.715	0.688	0.731
F (0 0 0)	1152	2168	1256	5420
Θ_{min} [°]	1.125	1.879	1.825	1.071
Θ_{max} [°]	30.134	27.194	36.361	30.168
No. of reflns. measd.	72730	39790	58063	332470
No. of unique reflns.	15785	5847	13902	75997
No. of reflns. I > 2 σ	10810	3138	10407	27731
No. of params.	709	294	348	2931
R ₁ (all data)	0.0933	0.1090	0.0609	0.1698
wR ₂ (all data)	0.1070	0.0876	0.0909	0.1994
GooF	1.005	0.877	1.021	0.996
complex	[Mn(PCP ^{NEt} - <i>i</i> Pr) (CO) ₃] (15)	[Mn(PCP ^{NEt} - <i>i</i> Pr) (CO) ₂ (NO)]BF ₄ (16)	[Mn(κ^3 P,CH,P-P(CH)P ^{NEt} - <i>i</i> Pr)(CO) ₃]BF ₄ (17)	<i>trans</i> -[Cr(PCP ^{NEt} - <i>i</i> Pr) Cl ₂ (CH ₃ CN)] (18)
empirical formula	C ₂₅ H ₄₁ MnN ₂ O ₃ P ₂	C ₂₄ H ₄₁ BF ₄ MnN ₃ O ₃ P ₂	C ₂₅ H ₄₂ BF ₄ MnN ₂ O ₃ P ₂	C ₂₄ H ₄₄ Cl ₂ CrN ₃ P ₂
MW [g/mol]	534.48	623.29	622.29	559.46
crystal size [mm]	0.39 x 0.38 x 0.21	0.15 x 0.12 x 0.05	0.42 x 0.41 x 0.31	0.41 x 0.20 x 0.18
colour, shape	colourless, block	red, plate	yellow, block	orange, block
crystal system	monoclinic	monoclinic	monoclinic	monoclinic
space group	P 21	P 21/n	P 21/c	P 21/c
a [Å]	12.3427(6)	15.286(3)	8.4565(16)	9.0641(4)
b [Å]	14.5018(8)	8.0602(16)	21.917(5)	12.0142(6)
c [Å]	15.7246(8)	24.201(5)	16.318(3)	26.2548(14)
α [°]	90	90	90	90
β [°]	106.4910(10)	105.895(6)	104.121(5)	95.9170(10)
γ [°]	90	90	90	90
V [Å ³]	2698.8(2)	2867.9(10)	2933.0(10)	2843.9(2)
Z	4	4	4	4
ρ_{calc} [g/cm ³]	1.315	1.444	1.409	1.307
T [K]	100	100	100	100
μ [mm ⁻¹]	0.636	0.629	0.614	0.720
F (0 0 0)	1136	1304	1304	1188
Θ_{min} [°]	1.862	1.421	1.587	2.259
Θ_{max} [°]	32.712	30.541	31.569	32.648
No. of reflns. measd.	45904	41110	41945	51392
No. of unique reflns.	19724	8774	9780	10387
No. of reflns. I > 2 σ	16315	5774	7270	8133
No. of params.	616	358	357	300
R ₁ (all data)	0.0599	0.1013	0.0747	0.0519
wR ₂ (all data)	0.0798	0.1083	0.1353	0.0855
GooF	0.997	1.012	1.039	1.012

6.2. CRYSTALLOGRAPHIC DATA

complex	<i>trans</i> -[Cr(PCP ^{Nt} - <i>i</i> Pr) Cl ₂ (THF)] (20)	<i>trans</i> -[Cr(POCOP- <i>i</i> Pr) Br ₂ (THF)] (23)	<i>cis</i> -[Cr(POCOP- <i>i</i> Pr) I ₂ (MeCN)] (25)	[Cr(POCOP- <i>t</i> Bu)Br] (26)
empirical formula	C ₂₆ H ₄₉ Cl ₂ CrN ₂ O ₂ P ₂	C ₂₂ H ₃₉ Br ₂ CrO ₃ P ₂	C ₂₀ H ₃₄ CrI ₂ NO ₂ P ₂	C ₂₂ H ₃₉ BrCrO ₂ P ₂
MW [g/mol]	591.26	625.29	688.22	529.4
crystal size [mm]	0.39 x 0.24 x 0.22	0.15 x 0.08 x 0.05	0.50 x 0.36 x 0.32	0.28 x 0.20 x 0.16
colour, shape	brown, block	orange, block	red, block	orange, block
crystal system	monoclinic	monoclinic	monoclinic	triclinic
space group	P 21/c	C 2/c	P 21/c	P -1
a [Å]	9.2077(4)	12.0083(7)	17.539(4)	14.8897(14)
b [Å]	26.9791(13)	17.4319(11)	9.663(2)	13.1977(14)
c [Å]	12.5048(6)	13.7498(10)	15.698(3)	8.231(4)
α [°]	90	90	90	114.35(3)
β [°]	104.0360(10)	114.793(2)	103.925(5)	117.0963
γ [°]	90	90	90	89.544(5)
V [Å ³]	3013.6(2)	2612.9(3)	2582.5(10)	1279.2(7)
Z	4	4	4	2
ρ _{calc} [g/cm ³]	1.303	1.590	1.770	1.3745
T [K]	100	100	100	100
μ [mm ⁻¹]	0.685	3.640	2.973	2.149
F (0 0 0)	1261	1276	1348	600
Θ _{min} [°]	2.258	2.203	2.393	1.74
Θ _{max} [°]	27.911	30.631	35.047	33.3
No. of refls. measd.	49820	7763	48908	38635
No. of unique refls.	7171	3520	11328	9831
No. of refls. I > 2σ	5432	2322	9694	7126
No. of params.	346	142	267	299
R ₁ (all data)	0.0581	0.0885	0.0382	0.0730
wR ₂ (all data)	0.0866	0.1114	0.0670	0.1354
Goof	1.003	0.987	1.085	
complex	[Cr(POCOP- <i>t</i> Bu)BH ₄] (27)	[Cr(POCOP- <i>t</i> Bu)(NO)(BH ₄)] (28)	[Cr(POCOP- <i>t</i> Bu)(NO)Br] (29)	[Cr(POCOP- <i>t</i> Bu) (CH ₂ SiMe ₃)] (30)
empirical formula	C ₂₂ H ₄₂ BCrO ₂ P ₂	C ₂₂ H ₄₃ BCrNO ₃ P ₂	C ₂₂ H ₃₉ BrCrNO ₃ P ₂	C ₂₆ H ₅₀ CrO ₂ P ₂ Si
MW [g/mol]	467.6	494.32	559.4	536.69
crystal size [mm]	0.27 x 0.25 x 0.20	0.24 x 0.21 x 0.03	0.45 x 0.35 x 0.20	0.33 x 0.16 x 0.10
colour, shape	orange, polyhedron	orange, plate	black, block	orange, block
crystal system	triclinic	orthorhombic	triclinic	triclinic
space group	P -1	P b c a	P -1	P -1
a [Å]	15.0410(14)	12.3504(8)	8.2437(12)	8.4361(17)
b [Å]	13.2429(12)	15.0602(11)	12.5482(18)	11.212(2)
c [Å]	8.2490(7)	28.272(2)	13.3342(19)	17.429(4)
α [°]	114.537(3)	90	99.005(4)	87.209(5)
β [°]	117.497(3)	90	95.805(4)	79.112(5)
γ [°]	89.512(3)	90	104.587(4)	70.079(5)
V [Å ³]	1291.2(2)	5258.6(7)	1304.1(3)	1521.8(5)
Z	2	8	2	2
ρ _{calc} [g/cm ³]	1.2027	1.249	1.4246	1.171
T [K]	100	100	100	100
μ [mm ⁻¹]	0.658	0.579	2.116	0.540
F (0 0 0)	503	2120	582	580
Θ _{min} [°]	1.74	1.441	1.71	2.287
Θ _{max} [°]	32.61	27.876	31.56	30.794
No. of refls. measd.	55542	25982	31850	34737
No. of unique refls.	9414	6244	8684	9449
No. of refls. I > 2σ	7564	3650	6284	6173
No. of params.	279	371	431	304
R ₁ (all data)	0.0325	0.1276	0.0696	0.0937
wR ₂ (all data)	0.0852	0.1375	0.1814	0.1149
Goof	1.35	0.1375	1.53	0.936

complex	[Mo(PCP ^{NET} - <i>i</i> Pr)(CO) ₃ Cl] (31)	[W(PCP ^{NET} - <i>i</i> Pr)(CO) ₃ Cl] (32)	[Mo(PCP ^{NET} - <i>i</i> Pr)(CO) ₂ Cl] (31-CO)	[K(THF) ₂][Mo(PCP ^{NET} - <i>i</i> Pr)(CO) ₃] (33)
empirical formula	C ₂₅ H ₄₁ MoN ₂ O ₃ P ₂	C ₂₇ H ₄₄ ClN ₃ O ₃ P ₂ W	C ₂₄ H ₄₁ ClMoN ₂ O ₂ P ₂	C ₃₃ H ₅₇ KMoN ₂ O ₅ P ₂
MW [g/mol]	610.93	739.89	582.96	758.78
crystal size [mm]	0.59 x 0.54 x 0.05	0.41 x 0.28 x 0.05	0.34 x 0.29 x 0.21	0.57 x 0.47 x 0.15
colour, shape	orange, plate	yellow, plate	green, block	red, plate
crystal system	monoclinic	monoclinic	monoclinic	orthorhombic
space group	C 2/c	P 21/n	P 21/n	P b c n
a [Å]	31.784(4)	14.483(3)	15.3894(12)	21.3927(12)
b [Å]	14.2474(19)	12.834(3)	12.6372(10)	18.5758(11)
c [Å]	12.5415(17)	17.178(4)	28.942(2)	19.0610(12)
α [°]	90	90	90	90
β [°]	94.894(4)	103.939(7)	102.042(2)	90
γ [°]	90	90	90	90
V [Å ³]	5658.6(13)	3099.1(11)	5504.7(8)	7574.6(8)
Z	8	4	8	8
ρ _{calc} [g/cm ³]	1.434	1.586	1.317	1.331
T [K]	100	100	100	100
μ [mm ⁻¹]	0.700	3.949	0.704	0.579
F (0 0 0)	2544	1488	2208	3200
Θ _{min} [°]	1.567	2.002	1.394	1.452
Θ _{max} [°]	35.046	31.658	30.651	29.756
No. of refls. measd.	56905	38492	89471	63730
No. of unique refls.	12470	10408	16849	10722
No. of refls. I > 2σ	10532	6690	11091	5998
No. of params.	331	345	623	536
R ₁ (all data)	0.0482	0.0930	0.1086	0.1150
wR ₂ (all data)	0.0788	0.0946	0.1945	0.1384
Goof	1.122	0.982	1.137	1.035
complex	[K(THF) ₂][W(PCP ^{NET} - <i>i</i> Pr)(CO) ₃] (34)	[Mo(OCO ^{NET} -OP <i>i</i> Pr)(O) ₂ Cl] (37)	[Mo(POCOP- <i>t</i> Bu)(CO) ₂ Br] (38)	
empirical formula	C ₃₃ H ₅₂ KN ₂ O ₅ P ₂ W	C ₂₂ H ₄₁ ClMoN ₂ O ₄ P ₂	C ₂₄ H ₃₉ BrMoO ₄ P ₂	
MW [g/mol]	841.65	590.94	629.34	
crystal size [mm]	0.62 x 0.10 x 0.08	0.49 x 0.32 x 0.28	0.32 x 0.30 x 0.03	
colour, shape	yellow, needle	orange, block	blue, plate	
crystal system	monoclinic	monoclinic	orthorhombic	
space group	P 21/c	P 21/c	P c a 21	
a [Å]	9.6424(13)	18.9924(10)	16.065(4)	
b [Å]	12.3069(17)	16.5046(8)	17.167(4)	
c [Å]	31.848(5)	18.9924(10)	19.972(4)	
α [°]	90	90	90	
β [°]	90.714(2)	116.21	90	
γ [°]	90	90	90	
V [Å ³]	3779.0(9)	5341.4(5)	5508(2)	
Z	4	8	8	
ρ _{calc} [g/cm ³]	1.479	1.468	1.518	
T [K]	100	100	100	
μ [mm ⁻¹]	3.290	0.741	2.070	
F (0 0 0)	1708	2461	2576	
Θ _{min} [°]	0.639	1.195	1.736	
Θ _{max} [°]	28.021	32.482	30.708	
No. of refls. measd.	43588	40937	123698	
No. of unique refls.	9132	14025	17108	
No. of refls. I > 2σ	7901	8141	15029	
No. of params.	419	8141	602	
R ₁ (all data)	0.0499	0.0973	0.0468	
wR ₂ (all data)	0.1066	0.1159	0.0768	
Goof	1.214	0.900	1.001	

Chapter 7

Curriculum Vitae

DI Daniel Himmelbauer

*Seitenberggasse 63/7/736
A-Vienna 1160
0660 38 36 159
daniel.himmelb@gmail.com*

Personnel Information

Name: Daniel
Last name: Himmelbauer
Nationality: Austria
Date of birth: 09.08.1991

Education

- 11.2016 - 02.2020 **Ph.D in Organometallic Chemistry and Catalysis**
Vienna University of Technology, Institute of Applied Synthetic Chemistry, research group Prof. Karl Kirchner
Getreidemarkt 9/163, A-1060 Vienna, Austria
Development, synthesis and characterisation of PCP pincer complexes, in respect to the first row transition elements as well as investigation of their chemical properties and possible catalytic applications.
- 10.2012 - 08.2016 **M.Sc. in Technical Chemistry - Synthesis**
Vienna University of Technology
Karlsplatz 13, A-1040 Vienna
The master thesis was done in cooperation with Sandoz GmbH (*Biochemiestraße 10, A-6250 Kundl*) and investigated the development of new synthetic paths for the beta-lactamase inhibitor Avibactam[®].
- 09.2011 - 05.2012 **B.Sc. in Medicinal Chemistry and Pharmaceutical Science**
Dublin Institute of Technology
Kevin Street, Dublin 2
- 09.2005 - 06.2010 **HTL Rosensteingasse (chemistry-focused secondary school)**
Rosensteingasse 79, A-1170 Vienna

Experience

- since 11.2016 **Project assistant (FWF)**
Vienna University of Technology, Institute of Applied Synthetic Chemistry
Getreidemarkt 9/163, A-1060 Vienna, Austria
- 10.2015 - 03.2016 **Tutor for the master-workman school of technical chemistry and environmental engineering**
Economic Development Institute of the economic chamber Tirol
Egger-Lienz-Straße 116, A-6020 Innsbruck
- summer 2015 **Internship at the chemical development center of Sandoz GmbH**
Biochemistraße 10, A-6250 Kundl
- 03.2015 - 06.2015 **Tutor at the fundamentals of chemistry lab course**
Vienna University of Technology, Institute of Applied Synthetic Chemistry
Getreidemarkt 9/163, A-1060 Vienna, Austria
- summer 2014 **Internship at OMV Refining GmbH and Sandoz GmbH**
Lobgrundstraße 2, 1220 Vienna and Biochemistraße 10, A-6250 Kundl

Achievements**Publications:**

- Himmelbauer, D.; Stöger, B.; Veiros, L. F.; Pignitter, M.; Kirchner, K. Cr(II) and Cr(I) PCP Pincer Complexes: Synthesis, Structure, and Catalytic Reactivity. *Organometallics* **2019**, *38*, 4669-4678.
- Himmelbauer, D.; Mastalir, M.; Stöger, B.; Veiros, L. F.; Kirchner, K. Synthesis and Reactivity of Group Six Metal PCP Pincer Complexes: Reversible CO Addition Across the Metal-C_{aryl} Bond. *Organometallics* **2018**, *37*, 3631-3638.
- Himmelbauer, D.; Mastalir, M.; Stöger, B.; Veiros, L. F.; Pignitter, M.; Somoza, V.; Kirchner, K. Iron PCP Pincer Complexes in Three Oxidation States: Reversible Ligand Protonation To Afford an Fe(0) Complex with an Agostic C-H Arene Bond. *Inorganic Chemistry* **2018**, *57*, 7925-7931.
- Himmelbauer, D.; Stöger, B.; Veiros, L. F.; Kirchner, K. Reversible Ligand Protonation of a Mn(I) PCP Pincer Complex To Afford a Complex with an η²-C_{aryl}-H Agostic Bond. *Organometallics* **2018**, *37*, 3475-3479.
- Glatz, M.; Stöger, B.; Himmelbauer, D.; Veiros, L. F.; Kirchner, K. Chemoselective Hydrogenation of Aldehydes under Mild, Base-Free Conditions: Manganese Outperforms Rhenium. *ACS catalysis* **2018**, *8*, 4009-4016.

Oral Presentations:

- 18th Chemical Days Linz 2019
- 18th International Seminar of PhD Students on Organometallic and Coordination Chemistry Poland 2018
- 28th International Conference of Organometallic Chemistry Florence 2018
- 10th Workshop Inorganic Chemistry Austria Graz 2018

Poster Presentation:

- 17th Chemical Days Salzburg 2017

Technical Skills

Laboratory: Working under air and water free conditions using Schlenk technique and glove box, handling of various gases (CO, NO, H₂, etc.) in combination with autoclaves.

Analytical methods: Chromatography (thin layer, ion exchange, exclusion, HPLC, GC), sound theoretical knowledge and interpretation of most analysis techniques (NMR, MS, EPR, XRD, ATR IR).

Computer Skills

LaTeX (document preparation system for high-quality typesetting)

Inkscape (professional quality vector graphics software)

MNova and Topspin (NMR data processing and presentation package)

Mercury (Crystal Structure Visualisation software)

European Computer Driving Licence Core

Other Skills

Teaching: Assisting bachelor and master students under the supervision of Prof. Karl Kirchner.

Language: German (native) and english.

Communication: Excellent proficiency in communication/presentation of data in a clearly and confidently fashion to small and large groups (in english).